The entanglement Hamiltonian for cMERA states

Quinten Mortier

Supervisors: Prof. dr. Karel Van Acoleyen, Prof. dr. Jutho Haegeman

Master's dissertation submitted in order to obtain the academic degree of
Master of Science in Physics and Astronomy

Department of Physics and Astronomy
Chair: Prof. dr. Dirk Ryckbosch

Faculty of Sciences
Academic year 2017-2018

This work has been performed at the Quantum Theory group of Prof. dr. Verstraete and Prof. dr. Haegeman at the Faculty of Sciences of Ghent University.

Preface

Already during my first chemistry lesson ever, I was mesmerized by the fact that science could describe tiny systems like atoms and molecules. Starting my first year at Ghent University as an engineering student, I was therefore convinced that one day, I would graduate as a chemical engineer. It did not take long however, until I realized that my true interests lay in physics. Encountering subjects like the Lagrangian and Hamiltonian vision on classical mechanics, quantum mechanics and Einsteins theory of general relativity, I became captivated by the rich world of theoretical physics. It was this undeniable passion that led to numerous elective courses starting with the word "quantum" and/or ending with the word "theory", an additional master in physics and astronomy and eventually this master thesis discussing the entanglement Hamiltonian for cMERA states. Hoping this work can make a useful contribution to research, I would like to express my gratitude to the people involved in its realization.

First, I would like to thank my supervisor Prof. dr. Karel Van Acoleyen not only for giving me the opportunity to work on this interesting and relevant topic but also for your input, experience and ideas, especially during those afternoon brainstorm sessions. I also would like to thank my co-supervisor Prof. dr. Jutho Haegeman for his contribution to this work and for helping me tackle the various encountered problems. Finally, thank you both for helping me compose my doctoral applications. I hope one of these is accepted so that I can continue researching the topics this thesis gave me an introduction to.

Of course, working on this project had to be interspersed with the necessary amount of relaxation. Therefore, I would like to say a word of thanks to my friends. The dances, drinks and laughs we shared during the past six years here in Ghent and especially during those legendary Yucca Wednesday nights, made my student days into the time of my life. I cannot thank you enough for that.

Finally, none of this would have been possible without the support of my family. More specifically, I would like to thank my dad for the multiple spell checks of this "integral infested nonsense" and for giving me the opportunity to study under the best possible conditions. Thank you Eva for putting up with me during the (sometimes) stressful realization of this thesis and for borrowing me that iPod Touch a million times. And of course, thank you mom for your unwavering and relentless support. I could never have wished for a better number one fan.

Quinten Mortier
June 1, 2018

Copyright Agreement

Quinten Mortier
June 1, 2018

The entanglement Hamiltonian for cMERA states

by Quinten Mortier

Supervisors: Prof. dr. Karel Van Acoleyen, Prof. dr. Jutho Haegeman

Master's dissertation submitted in order to obtain the academic degree of
Master of Science in Physics and Astronomy

Department of Physics and Astronomy
Chair: Prof. dr. Dirk Ryckbosch

Faculty of Sciences
Academic year 2017-2018

Abstract

In this work, the entanglement structure of cMERA states for free quantum field theories is studied. To this end, the (Rényi) entanglement entropies and the entanglement Hamiltonian were determined for cMERA states of both bosonic Klein-Gordon and fermionic Dirac theories in (1+1) dimensions. Where the entanglement entropies could be calculated directly, the determination of the entanglement Hamiltonian was more challenging as it diverges for cMERA states. However, by implementing an additional regularization, a non-divergent version of the entanglement Hamiltonian was derived. Both for this regularized entanglement Hamiltonian and the entanglement entropy a satisfactory agreement with theoretical predictions was obtained.

Keywords

Quantum Field Theory, Quantum Entanglement, Renormalization Group Theory,
Tensor Network States, cMERA

English Summary

The main objective of this project is to understand the entanglement structure of the continuous multi-scale entanglement renormalization ansatz (cMERA) for free quantum field theories. More specifically, entanglement measures like the (Rényi) entanglement entropies and the entanglement Hamiltonian are determined for cMERA states of both bosonic Klein-Gordon and fermionic Dirac field theories in (1+1) dimensions. In order to do this, the so-called discretization method is put forward. Herein, quantum fields are restricted to an equidistant lattice, after which a Gaussian state on this lattice is defined by cMERA-based two-point correlators. Within the resulting discretized framework it is then possible to determine entanglement properties by solving matrix eigenvalue problems. Finally letting the lattice spacing shrink to zero, the continuous entanglement properties are obtained. Applying the discretization method to calculate (Rényi) entanglement entropies, analytical predictions like the logarithmic scaling law for large energy cut-offs were reproduced to a good degree. Also the damping influence of a mass on the entropy profiles was retrieved. For the entanglement Hamiltonian, the situation is more involved as this quantity is expected to diverge. Indeed, on small length scales cMERA states behave like product states and as the entanglement Hamiltonian for a product state is completely divergent, a similar divergence is also expected for cMERAs. Studying the divergences more accurately, it was found that the various parts of the entanglement Hamiltonian (e.g. local and non-local) display a different scaling behavior as function of the lattice spacing. As a result, differently scaling parts can be separated to yield a complete description of how and why the entanglement Hamiltonian diverges. However, this scaling-based decomposition requires substantial computational resources as the encountered matrix eigenvalue problems require an elevated spectral resolution. Therefore, an alternative was proposed in the form of the regularized discretization method. Herein, the small unentangled length scales are artificially removed. In this way, the product state part of the cMERA state is removed as well, resulting in a non-divergent entanglement Hamiltonian. This regularized version of the entanglement Hamiltonian contains, just like the original, all kinds of contributions with a different scaling behavior. In the CFT limit, this ensures that the contribution responsible for the strongest divergences overpowers the others, so that only this contribution can be compared to theoretical CFT predictions. Both in the bosonic and the fermionic case, an almost exact reproduction was obtained. Sub-dominant parts of the theoretical CFT prediction were however not yet reproduced as these require the scaling-based decomposition.

Dutch Summary

Het hoofddoel van dit project bestaat erin de verstrengelingsstructuur van de continuous multiscale entanglement renormalization ansatz (cMERA) beter te begrijpen voor vrije kwantumveldentheorien. Meer specifiek worden verstrengelingseigenschappen zoals de (Rényi) verstrengelingsentropieën en de verstrengelingshamiltoniaan bepaald voor cMERA toestanden van zowel bosonische Klein-Gordon als fermionische Dirac veldentheorien in (1+1) dimensies. Om dit te doen, wordt de zogenaamde discretisatiemethode ingevoerd. Hierin worden de kwantumvelden gerestringeerd tot een equidistant rooster waarna een Gaussische toestand op dit rooster gedefinieerd wordt op basis van cMERA geïnspireerde tweepuntsfuncties. Binnen het resulterende discrete framework kunnen dan verstrengelingseigenschappen voor deze toestand bepaald worden door middel van matrix eigenwaardeproblemen. Wanneer men de roosterafstand naar nul laat krimpen, komen de berekende verstrengelingseigenschappen overeen met hun continue varianten. In eerste instantie werd de discretisatiemethode gebruikt om de (Rényi) verstrengelingsentropieën van cMERA toestanden te bepalen. Deze reproduceren allerlei analytische resultaten zoals de logaritmische schaalwet voor grote cut-off energieën en bevestigen ook dat een massa een dempende invloed heeft op de verstrengelingsentropie. De bepaling van de verstrengelingshamiltoniaan daarentegen vormt een grotere uitdaging omdat deze grootheid verwacht wordt te divergeren. Inderdaad, voor kleine lengteschalen gedraagt een cMERA toestand zich zoals een product toestand. Aangezien de verstrengelingshamiltoniaan hiervan divergeert, wordt een gelijkaardige divergentie ook verwacht voor de cMERA toestanden. We vonden echter dat verschillende contributies tot de verstrengelingshamiltoniaan (bijvoorbeeld locaal en niet-locaal) een verschillend schaalgedrag vertonen in functie van de roosterlengte. Door contributies met een verschillend schaalgedrag van elkaar te scheiden kan men dus heel precies bepalen hoe en waarom de verstrengelingshamiltoniaan divergeert. De voorgenoemde ontbinding resulteert echter in zware computationele berekeningen. Daarom werd er een alternatief bedacht: de geregulariseerde discretisatiemethode. Hierin worden kleine ongecorreleerde lengteschalen kunstmatig verwijderd zodat ook het product toestand gedeelte van de cMERA toestand eveneens wordt verwijderd. Bijgevolg blijft een niet-divergerende verstrengelingshamiltoniaan over. Deze geregulariseerde versie van de verstrengelingshamiltoniaan bevat net zoals de originele allerlei contributies met een verschillend schaalgedrag. In de CFT limiet zorgt dit ervoor dat het stuk verantwoordelijk voor de sterkste divergenties de andere overtreft. Bijgevolg kan ook enkel dit stuk met theoretische CFT voorspellingen vergeleken worden, hetgeen een bevredigende overeenkomst opleverede voor zowel de Klein-Gordon als de Dirac theorie. Om de andere, sub-dominante contributies terug te vinden (en zo bijvoorbeeld de invloed van een massa te onderzoeken) is een volledige schaaldecompositie noodzakelijk.

Table of Contents

List of Abbreviations

RG	Renormalization Group
TNS	Tensor Network States
QFT	Quantum Field Theory
QED	Quantum Electrodynamics
DMRG	Density Matrix Renormalization Group
SVD	Singular Value Decomposition
MPS	Matrix Product States
AKLT	Affleck-Lieb-Kennedy-Tasaki
PEPS	Projected Entangled Pair States
MERA	Multi-scale Entanglement Renormalization Ansatz
CFT	Conformal Field Theory
AdS	Anti-de Sitter
cMERA	Continuous Multi-scale Entanglement Renormalization Ansatz

Chapter 1

Introduction

As is almost exclusively the case in science and especially in theoretical physics, the goals and ideas of this project are rooted in previous research. Therefore, this introductory chapter will mainly attempt to illustrate the relevant concepts and methods that gave rise to this work and will be frequented throughout it. Emphasizing their general importance as well as their applicability to this thesis, the renormalization group (RG), tensor network states (TNS) and quantum entanglement will be covered. The treatment of these topics is however far from complete and the reader will hence be referred to more comprehensive works on a regular basis. At the end of the chapter, the global structure of this project will be discussed.

1.1 Renormalization Group

An astronomer wishing to describe the orbit of a planet around its host star, does not have to worry about the motion of the individual molecules making up this planet, to obtain a reliable model for the planet's motion. Even the possible influence of moons and other satellites on the orbit can be neglected at first and added perturbatively later on. Unfortunately, not all physics problems have such a decoupling of distance scales. Quantum field theories (QFTs) and quantum many body systems (especially with strong interactions) are two examples of systems where all (or a large range of) distance scales are equally important. Modeling these systems is therefore far more complicated. Indeed, where for the aforementioned planetary system the large-scale motion of the planet around its star is treated first, after which the small-scale influence of moons etc. is added perturbatively, this approach is not applicable for strongly coupled quantum systems where all distance scales are equally important and should be treated simultaneously. Renormalization group theory aims to provide a framework describing the interplay of large and small-scale degrees of freedom (or equivalently low and high-energy degrees of freedom) in extended quantum systems.

Renormalization first appeared in the perturbative treatment of quantum field theory and more specifically in quantum electrodynamics (QED) where including all self-energy corrections in Feynman diagrams led to infinities due to the lack of an UV cut-off in the underlying theory.[1] The traditional way to treat these UV divergences is to absorb them in the physical parameters governing the theory. *I.e.* the measured value for physical parameters (like mass and electric

charge) is said to consist of a so-called "bare" contribution and a contribution due to self-interaction loops. In this way, the infinities in the theory can safely be circumvented when the measured effective values for the parameters are used. While yielding impressive results (e.g. the QED value for the Lamb shift[2]) and introducing the notion of parameters "flowing" with the energy scale, this method always had an air of black magic to it, especially because it is not applicable to all field theories but only to the so-called renormalizable field theories. Also the meaning of the bare parameters remained unclear (e.g. they diverge when all energy scales are considered). Later on, this was understood as the theory only being valid up to a certain energy cut-off while for higher energy scales (and corresponding smaller length scales) a more fundamental theory should be used.

In the original perturbative renormalization method, fluctuations are treated equally on all scales. Wilson however realized that fluctuations on a certain scale are strongly coupled only to those at neighboring scales;[3–5] a picture that reduces to the original perturbative treatment when fluctuation couplings are weak for all scales (as is the case for QED). Wilson's findings led to the renormalization group theory, describing for instance that certain features of a more fundamental theory at small scales fade out in the UV limit making place for an effective theory with parameters depending on the energy scale with which the theory is probed. Kadanoff came to a similar conclusion in his work studying the scaling behavior of the Ising model.[6] The Wilsonian RG picture also introduced the concepts of marginal, relevant and irrelevant operators, distinguishing different types of RG flow and making clear why the Standard Model is renormalizable: the irrelevant (non-renormalizable) operators fade away under the RG flow from the UV free field fixed point.[1] Another interesting feature of Wilsonian RG are universality classes. These are groups of (possibly very different) microscopic Hamiltonians that have a common critical IR fixed point and therefore exhibit the same behavior at large distance scales.

Not only does RG form a theoretical framework describing the interplay between degrees of freedom at different scales, it also has many numerical applications with Wilson's solution of the Kondo problem as one of the most famous examples.[5] Many present-day numerical methods are also based on Wilsonian RG, e.g. the Density Matrix Renormalization Group (DMRG)[7] and the exact renormalization group approach.[8] The Schrieffer-Wolff transformation[9,10] on the other hand is a method that compresses the relevant low energy part of the Hamiltonian into a Hilbert space that is numerically tractable, thus clearly RG ideas to reduce a problem's complexity. A similar approach is followed in the truncated spectrum approach (see e.g.[11–14]) that recently gained a lot of attention.

1.2 Quantum Entanglement

The main objective of this work is to apply RG inspired recipes to extended quantum systems. More specifically cMERA states for QFTs (discussed in the next section) will be studied, focussing on one of the most striking properties of quantum systems, their ability to be entangled. The concept of quantum entanglement is most easily introduced when considering a bipartite system C built up by the disjoint subsystems A and B. Standard quantum mechanics learns

that the Hilbert space corresponding to C, $\mathbb{H}_C$, is given by the tensor product of $\mathbb{H}_A$ and $\mathbb{H}_B$. Quantum mechanical states are described by positive operators acting on the Hilbert space with trace equal to one, the so-called density operators. Typically one distinguishes pure states and mixed states: a pure state can be written as $\rho = |\psi\rangle\langle\psi|$ while for mixed states this is not possible. For classical (or separable) states on the other hand, the density operator can be decomposed as:

$$\rho^C = \sum_j p_j \rho_j^A \otimes \rho_j^B \tag{1.1}$$

where the superscripts indicate the relevant Hilbert spaces and p_j clearly corresponds to a discrete probability distribution. This decomposition explicitly shows that the density operator ρ^C has separate parts corresponding to the A and B subsystems. Altering the A subsystem (e.g. by performing a measurement on A) therefore has no influence on the state of the B system. The density operator of a general quantum state however, cannot be decomposed as in (1.1). The states for which this is not possible are called non-separable or entangled and for these states influencing one subsystem necessarily influences the other. This strikingly non-classical property was first discovered by Schrödinger[15] and gives rise to other interesting quantum effects like quantum teleportation. However, entanglement also annoyed physicists like Einstein since it gave the impression that via entanglement, information could be passed faster than the speed of light, an effect he wrongfully attributed to "hidden variables".[16]

The interest in entangled states quickly led to the need for a quantity describing how much entanglement is present in a certain quantum state. A first step in this direction was taken by observing the connected correlation function of two non-trivial operators O^A and O^B, each only working on their corresponding subsystems:

$$\Gamma^{A,B} = \langle O^A \otimes O^B \rangle - \langle O^A \rangle \langle O^B \rangle \tag{1.2}$$

where $\langle ... \rangle$ stands for the expectation value. The usual way to calculate these expectation values proceeds via the partial traces of the density operator ρ^C (the reduced density operators of ρ^C) defined by:

$$\begin{aligned} \rho^A &= \mathrm{tr}_B\, \rho^C \\ \rho^B &= \mathrm{tr}_A\, \rho^C \end{aligned} \tag{1.3}$$

where tr_X takes the traces over Hilbert space $\mathbb{H}_X$. The connected correlation function of O^A and O^B is then given by:

$$\Gamma^{A,B} = \mathrm{tr}_C \left(\rho^C O^A \otimes O^B\right) - \mathrm{tr}_A \left(\rho^A O^A\right) \mathrm{tr}_B \left(\rho^B O^B\right) \tag{1.4}$$

For classical states this quantity is bound by the Bell inequalities while entangled states can exceed these bounds.[17] Although connected correlation functions allow to discern classical from entangled states, a more workable entanglement measure, applicable for pure states, will be discussed in the next paragraph.

Consider finite dimensional Hilbert spaces for A, B and C so that $\dim \mathbb{H}_C = \dim \mathbb{H}_A \dim \mathbb{H}_B$ and define the bases $\{|i\rangle_A\}_{i=1,\ldots,\dim \mathbb{H}_A}$ for $\mathbb{H}_A$, $\{|j\rangle_B\}_{j=1,\ldots,\dim \mathbb{H}_B}$ for $\mathbb{H}_B$ and

$\{|i\rangle_A \otimes |j\rangle_B\}_{i=1,\ldots,\dim \mathbb{H}_A, j=1,\ldots,\dim \mathbb{H}_B}$ for $\mathbb{H}_C$. An arbitrary pure state $|\Psi\rangle$ in C is then given by:

$$|\Psi\rangle = \sum_{i,j} \psi_{ij} |i\rangle_A \otimes |j\rangle_B \tag{1.5}$$

with corresponding density operator:

$$\rho^C = |\Psi\rangle\langle\Psi| = \sum_{i,i',j,j'} \psi_{ij}\psi^*_{i'j'} |i\rangle_A\langle i'|_A \otimes |j\rangle_B\langle j'|_B \tag{1.6}$$

The only way this state is separable is if ψ_{ij} has rank one and hence decomposes as $u_i v_j$ yielding:

$$\rho^C = |u\rangle_A|v\rangle_B \otimes \langle u|_A\langle v|_B \qquad \Leftrightarrow \qquad |\Psi\rangle = |u\rangle_A|v\rangle_B \tag{1.7}$$

with $|u\rangle_A = \sum_i u_i|i\rangle_A$ and $|v\rangle_B = \sum_j v_j|j\rangle_B$. A pure state is thus separable if and only if it is a product state. For pure entangled states the coefficient matrix ψ has a rank higher than one and as a result one should resort to the singular value decomposition[18] (SVD) of ψ_{ij}:

$$\psi_{ij} = \sum_{k=1}^{\dim \mathbb{H}_A} \sum_{l=1}^{\dim \mathbb{H}_B} U_{ik}\Sigma_{kl}V^\dagger_{lj} \tag{1.8}$$

with U and V unitary matrices and Σ a $\dim \mathbb{H}_A \times \dim \mathbb{H}_B$ matrix only containing diagonal elements called the singular values of ψ. The singular values are positive and typically ordered in descending order in Σ. The squares of the non-zero singular values are the Schmidt values of $|\Psi\rangle$. Using the fact that the number of non-zero singular values is equal to the rank of their originating matrix, $|\Psi\rangle$ can be rewritten as:

$$|\Psi\rangle = \sum_{k=1}^{r} \sqrt{\lambda_k} |u_k\rangle_A \otimes |v_k\rangle_B \tag{1.9}$$

with λ_k the Schmidt values of $|\Psi\rangle$ (and thus $\sqrt{\lambda_k}$ the singular values), $|u_k\rangle_A = \sum_i U_{ik}|i\rangle_A$, $|v_k\rangle_B = \sum_j V^*_{jk}|j\rangle_B$ and r the rank of ψ. Since U and V were unitary, $\{|u_k\rangle_A\}$ and $\{|v_k\rangle_B\}$ form a basis for their Hilbert space. Taking the trace of ρ^C hence gives that $\sum_{k=1}^r \lambda_k = 1$ proving that the Schmidt values comprise a discrete probability distribution. This is also the case for the product state but for these states only one Schmidt value is different from zero. Based on this observation, the concept of (Von Neumann) entanglement entropy was defined as the Shannon entropy of the Schmidt value distribution function (also called the entanglement spectrum):

$$S^{A,B}(|\Psi\rangle) = -\sum_{k=1}^{r} \lambda_k \ln \lambda_k \tag{1.10}$$

This quantity is zero (and minimal) for product states, becomes higher than zero for entangled states and reaches a maximum for the so-called maximally entangled state where all Schmidt values are equal to $\frac{1}{r}$, clearly illustrating its significance as an entanglement measure. Making use of equation (1.9), an alternative definition is given by:

$$S^{A,B}(|\Psi\rangle) = -\mathrm{tr}_A(\rho^A \ln \rho^A) = -\mathrm{tr}_B(\rho^B \ln \rho^B) \tag{1.11}$$

where the second equality follows from the partial traces of ρ^C:

$$\begin{aligned} \rho^A &= \sum_{k=1}^{r} \lambda_k |u_k\rangle_A\langle u_k|_A \\ \rho^B &= \sum_{k=1}^{r} \lambda_k |v_k\rangle_B\langle v_k|_B \end{aligned} \tag{1.12}$$

Associated entanglement measures are the Rényi entropies defined by:

$$S_\beta^{A,B}(|\Psi\rangle) = \frac{1}{1-\beta}\ln\left[\sum_{k=1}^{r}\lambda_k^\beta\right] = \frac{1}{1-\beta}\ln\left[\mathrm{tr}_A(\rho^{A^\beta})\right] = \frac{1}{1-\beta}\ln\left[\mathrm{tr}_B(\rho^{B^\beta})\right] \tag{1.13}$$

where $\beta > 0$ and the Von Neumann entanglement entropy is reached when the limit $\beta \to 0$ is considered. Other frequently occurring variants are the collision entropy when $\beta = 2$ and the minimum entropy when $\beta = +\infty$. The latter owes its name to the fact the Rényi entropies are non-increasing as a function of β.

Even though the mentioned entropy measures were introduced for finite dimensional Hilbert spaces, they can safely be applied in infinite dimensional Hilbert spaces as well. In contrast to pure states, however, is finding an appropriate entanglement measure for mixed states more involved. Indeed, the spectra of the partial traces are no longer equal and defining a single entanglement spectrum is hence far from trivial. Fortunately, only pure states are considered in this work and the (Rényi) entanglement entropies can thus safely be applied.

Not particularly a measure of entanglement in the sense of the aforementioned entropies, but rather a more complete description of how a state is entangled is given by the so-called entanglement or modular Hamiltonian. This quantity was first introduced for quantum lattice models in the context of DMRG[19] but also appears in quantum field theory and can be defined as follows. Let ρ be the density operator describing the state of a quantum field or a quantum lattice theory and let ρ_V be the reduced density matrix corresponding to the spatial degrees of freedom inside a (hyper-)volume V (*i.e.* ρ with all degrees of freedom outside of V being traced out), then this reduced density matrix can typically be written as:

$$\rho_V = Ke^{-\mathcal{H}} \tag{1.14}$$

where $\mathcal{H}$ is the entanglement Hamiltonian and K is a normalization constant. For Gaussian states, the entanglement Hamiltonian typically has the following form:

$$\mathcal{H} = \sum_l \epsilon_l a_l^\dagger a_l \tag{1.15}$$

with ϵ_l the positive entanglement energies and $a_l^\dagger$ and a_l creation and annihilation operators linearly related to the original field operators and satisfying the canonical commutation relations $[a_l, a_{l'}^\dagger] = \delta_{ll'}$ for bosons and the canonical anticommutation relations $\{a_l, a_{l'}^\dagger\} = \delta_{ll'}$ for fermions.[20,21] Indeed, with this particular form for $\mathcal{H}$, one proves that the Wick property, characteristic for Gaussian states, holds for both bosons and fermions implying that all observables of the theory can be calculated by considering two-point correlators.[22,23]

One could ask for the reasons behind the interest in the entanglement Hamiltonian. These are essentially two-fold. On the one hand, the entanglement Hamiltonian offers one of the most complete pictures of how entanglement is organized in a state, allowing an almost direct calculation of other (less complete) entanglement measures like the (Rényi) entanglement entropies. Furthermore, this complete entanglement description also provides a versatile tool in the study

of universal behavior in extended quantum systems. Indeed, Casini *et al.*[24] for instance found that the entanglement Hamiltonian of QFT ground states contains a universal local contribution, being a reflection of the fact there exist local temperatures for these theories that carry some degree of universality. A second motive for our interest in the modular Hamiltonian is the holographic relation with a de Sitter geometry as suggested by de Boer *et al.*[25]

1.3 Tensor Network States

An immediate consequence of the tensor product structure of a composite system's Hilbert space, is that its dimensions grow exponentially with the number of subsystems N.[26] This exponential growth precludes a full simulation of the Hamiltonian already for relatively small N. However, via the variational optimization of an appropriate ansatz for low energy states one can find an approximation of the ground state (and some of the first excited states) in many cases. During the last decade tensor product states became very popular for these purposes. Indeed, tensor network state manifolds typically comprise only a small part of the complete Hilbert space, that corresponds to those states with the lowest energy. The way to make this sure is by keeping track of how correlations are distributed in low energy states, which is mostly locally, and using this knowledge to target the corresponding part of the Hilbert space. The relevant states typically obey an entropy/area law[27] corresponding to the fact that correlations between two regions are mainly concentrated near the boundary between both.

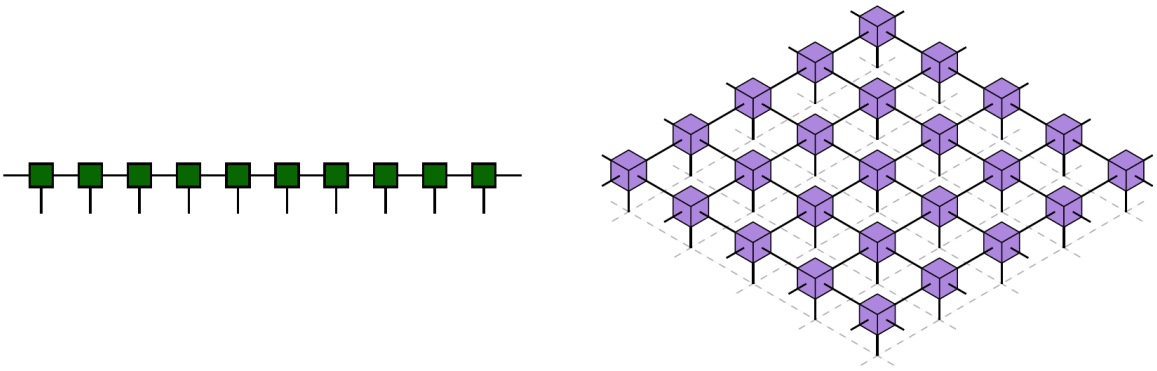

Figure 1.1: Illustration of the MPS (left) and PEPS (right) tensor networks.

Different types of TNS reflect both different physical geometries (e.g. 1d versus 2d lattices) and different entanglement structures (e.g. gapped versus critical systems). Some of the most well-known tensor product states are depicted in Figure 1.1. The leftmost corresponds to a so-called Matrix Product State (MPS).[27,28] This type of TNS, originally based on the 1d AKLT model,[29] is used to describe one-dimensional spin chains (represented by the open lines) via virtual (entanglement) degrees of freedom (represented by the closed lines). The link between both is given by local tensors (represented by the blocks). The precise form of the tensors is optimized variationally, a procedure that is very well understood and developed at present. In fact the initial success of DMRG was later understood as being related to the fact that it is a

particular variational method within the MPS manifold. On the right of Figure1.1, one finds the two-dimensional generalization of MPS, the Projected Entangled Pair States (PEPS).[30] Even though their definition is relatively straightforward, variational procedures within the PEPS manifold are far more complicated than for MPS. Yet during the last years several algorithms have been devised,[31,32] accurately simulating the ground state of certain frustrated spin systems and strongly correlated electron systems.[33,34]

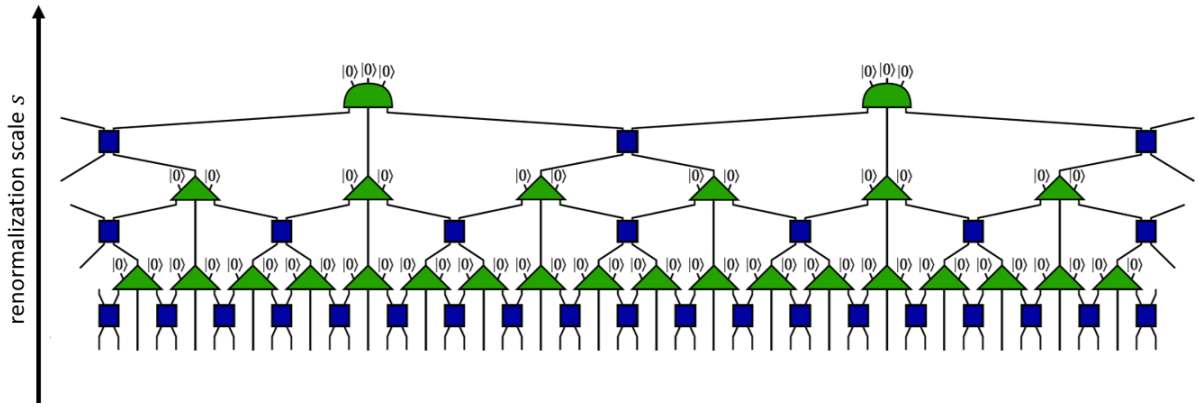

Figure 1.2: Illustration of the MERA tensor network.

A third type of TNS is depicted in Figure 1.2. This multi-scale entanglement renormalization ansatz or MERA tensor network[35] strongly differs from MPS and PEPS since its tensors have a manifestly different interpretation. Where MPS and PEPS can be seen as Wilsonian RG-like compressions of the Euclidean path integral for the ground state wavefunction,[36] MERA consists of multiple layers corresponding to the picture of a unitary RG-like flow. The specific structure of MERA has allowed it to model a wide variety of strongly interacting systems[37–39] while also confirming theoretical results like the logarithmic corrections to the entropy/area law in (1+1) dimensions.[40] In the traditional MERA tensor network, two different types of tensor layers are typically distinguished: scalers (green triangles in Figure 1.2) and disentanglers (blue blocks in Figure 1.2). All of these transformations are local unitaries. The goal of the scaling transformations is to reduce the information of multiple neighboring lattice sites (three in this case) to a single lattice site while producing two additional ancillae. This can indeed be interpreted as a scaling transformation, blurring out the information of the original finer lattice to a more coarse grid (identical to the coarse-graining operation in real-space renormalization). Note also that the top layer has slightly different blocks in Figure 1.2 as this layer exclusively produces ancillae. If only scaling transformations were present, the MERA would reduce to the so called tree renormalization scheme.[35] While tree renormalization can also be interpreted as a unitary RG flow scheme, small-scale correlations can accumulate in each layer keeping the Hilbert space of the state at the top of the MERA very large. This strongly reduces the applicability of the scheme in computational simulations. Also, correlations between lattice sites combined via two different scalers, are treated differently than correlations between lattice sites combined via a single scaler. This kind of asymmetry is unwanted for an RG flow. For these reasons, the MERA tensor network combines scalers with disentanglers. These are transfor-

mations that aim to remove local correlations in the lattice before the scaling transformations are applied, thus solving the aforementioned problems. Typically both scalers and entanglers differ in consecutive layers. However, for critical theories, the low-energy behavior corresponds to a conformal field theory (CFT) having scale invariance. As a result, the lower layers of the MERA will depend on the renormalization scale s, thus fixing the non-universal UV behavior, while the higher layers will be identical corresponding to the effective scale invariance in the IR regime. In computational simulations, MERA is typically used from the top to the bottom. One starts with a fiducial state consisting of ancillae on all positions and via consecutive application of entanglers (disentanglers upside down) and subsequent scaling transformations a final state is prepared with correlations up to any desired scale. Finally, MERA introduces an extra emergent vertical dimension in the network, corresponding to the RG scale. This suggests a connection with the holographic AdS/CFT framework. Especially the link between bulk geometry and entanglement[41,42] has led to an increased interest in MERA during the last few years.[43]

In many applications, quantum field theories are regulated to discrete lattices to study their properties. Tensor network states can then be applied to these discrete systems allowing computational simulations. However, the inverse procedure can be followed as well: formulating continuous versions of MPS[44] and of MERA[45] that operate directly on the continuous QFT Hilbert space. In the continuous analogue of MERA, called cMERA, the unitary quantum circuit of MERA is replaced by a continuous unitary RG flow that is generated by a Hamiltonian which is local up to the RG scale. Due to the Hamiltonian nature of the cMERA approach, many properties can now be studied that were previously inaccessible for the Euclidean path-integral[40] (suffering from the sign problem) like real-time dynamics and entanglement properties of low energy states (especially interesting for this work). Furthermore, the emergent RG dimension has drawn quite some attention, in particular from the AdS/CFT community.[46] However, a large drawback of cMERA is its current restriction to theories where the RG flow Hamiltonian only consists of purely quadratic terms (so-called Gaussian cMERAs), excluding its application to interacting QFTs.

1.4 Outline and Objectives of this Thesis

The main objective of this project is to understand the entanglement structure of the continuous multi-scale entanglement renormalization ansatz for quantum field theories. To do this, entanglement measures like the (Rényi) entanglement entropies and the modular Hamiltonian will be determined for cMERA states of both bosonic Klein-Gordon and fermionic Dirac field theories in (1+1) dimensions. Especially interesting will be the behavior of these quantities in function of relevant variables as mass, energy cut-off and system length. Also the reproduction of analytical results for cMERA limiting cases will be studied extensively. A great deal of work in this context was already performed by Vidal *et al.* who studied the Von Neumann entanglement entropy for cMERA states of CTFs.[47] Not only do we wish to reproduce these result, we also would like to elaborate on them by considering massive field theories and Rényi entropies other than the Von Neumann entropy (*i.e.* $\beta \neq 1$). Furthermore, the research of Vidal *et al.* was restricted to cMERAs with a Gaussian cut-off function (*cfr.* Chapter 2). In this work however,

also variants of cMERA with other cut-off functions will be studied. The entanglement Hamiltonian $\mathcal{H}$ was until now only well understood for CFT ground states. Indeed, for these states analytical expressions for $\mathcal{H}$ can be derived by exploiting the conformal symmetry. However, Casini *et al.* reviewed a general method to numerically derive the entanglement Hamiltonian from the two-point correlators of Gaussian states and applied this procedure successfully to the ground states of QFTs in (1+1) dimensions.[23,24] They were also able to reproduce the theoretically predicted profiles for CFTs. Therefore, these papers will serve as a starting point in our treatment of the modular Hamiltonian for cMERA states. Again we would like to reproduce the findings of Casini *et al.* but a complete description of the entanglement Hamiltonian for cMERA states is the ultimate goal of this thesis.

As cMERA finds itself at the core of this work, an elaborate review of its philosophy and construction for the two mentioned QFTs will be treated in **Chapter 2**. In **Chapter 3** the results of the second chapter will be used to calculate the entanglement properties of Klein-Gordon cMERA states, focusing on their (Rényi) entanglement entropies and modular Hamiltonian. Similarly, the entanglement properties of Dirac cMERAs will be treated in **Chapter 4**. In both cases an involved numerical procedure and additional regularizations are necessary to compute the desired quantities with subtle differences for bosons and fermions, originating from their different canonical transformation groups (symplectic for bosons and special-orthogonal for fermions). Finally, **Chapter 5** concludes the performed work in combination with a discussion of further research possibilities based on the obtained results.

Chapter 2

Continuous Multi-Scale Entanglement Renormalization Ansatz

As this thesis aims to study the entanglement properties of cMERA states, a proper knowledge of the philosophy behind and the construction of these states is indispensable. Therefore, this chapter will introduce the cMERA as a continuous generalization of the MERA tensor network, following the original cMERA paper.[45] Subsequently, the construction of cMERAs for Klein-Gordon and Dirac fields in (1+1) dimensions will be treated. Both sharp and Gaussian cut-off functions will be discussed as well as the characterization of the cMERA states (and other relevant Gaussian states) by means of a family of annihilation operators.

2.1 cMERA Generalities

In the introductory chapter, MERA was first introduced bottom-up. *I.e.* all correlations of the physical state were removed in a step-by-step procedure, consisting of scaling and disentangling operations, until a fiducial state was reached. It was also mentioned that for computational simulations, the top-down interpretation is preferred where correlations are added to a product state via the consecutive application of scalers and entanglers. cMERA will also be introduced according to the latter interpretation. Finding an appropriate reference state (typically called $|\Omega\rangle$) therefore is the first step in the cMERA construction. Once this reference/product state is found, the continuous analogue of the MERA quantum circuit should be a unitary evolution consisting of infinitesimal MERA-like layers. In order to define this evolution, the continuous RG scale coordinate s is introduced and in contrast to the original MERA philosophy, s increases when evolving from the product state (at $s = s_\xi$) to the final cMERA state (at $s = s_\epsilon$). For the infinitesimal MERA-like layers, the following form was proposed by Haegeman *et al.*:[45]

$$\exp(-iK(s)\delta s) \tag{2.1}$$

where δs is an infinitesimal step in the RG scale and where $K(s)$ is a local operator generating the infinitesimal transformations. Even though these transformations represent the continuous analogue of the combined effect of scaling and entangling layers in the discrete MERA tensor

network, they are simply (and sometimes confusingly) called entangling transformations. Correspondingly, $K(s)$ is called the entangling generator. The fact that this $K(s)$ is a local operator is expressed as:

$$K(s) = \int k(s,x)dx \tag{2.2}$$

where $k(s,x)$ is a local combination of field operators, their adjoints and their derivatives, whose precise form is determined variationally. For the discrete MERA tensor network, a natural UV cut-off is present in the form of the lattice spacing. *I.e.* there is a smallest length scale below which no correlations are introduced. For QFTs on the other hand, such a smallest length scale ϵ should be introduced explicitly so that $K(s)$ does not introduce entanglement below it. In the original cMERA construction this is done by imposing that $K(s)$ only affects those momentum degrees of freedom for which $k \lesssim \Lambda$ with $\Lambda \approx \epsilon^{-1}$ the momentum/energy cut-off corresponding to ϵ. In this way, $K(s)$ only generates correlations on length scales comparable to ϵ. However we would like the cMERA evolution to introduce fluctuations on all length scales going from ϵ to the correlation length ξ. Therefore, $K(s)$ is combined with an Hermitian operator L, generating a dilating transformation:

$$\exp(-iL\delta s) \tag{2.3}$$

To make the nomenclature even more ambiguous, this transformation is called the infinitesimal scaling transformation and L is the scaling generator. Note that L is independent of the RG coordinate. Furthermore, L is also local, implying that:

$$L = \int l(x)dx \tag{2.4}$$

with $l(x)$ again a local combination of field operators, their adjoints and their derivatives. In contrast to the entangling generators however, scaling transformations are completely determined by the dilating effect they incorporate and hence contain no variational freedom. As L simply increases all length scales, it dilates length scales that were previously inaccessible for the entangling transformation beyond ϵ so that they can be entangled in the next infinitesimal step of the cMERA process. In fact this is similar to a discrete MERA as in Figure 2.1 where after the application of the scalers (green triangles) the distance between the lines is restored so that the entanglers (pink squares) always act on the same length scale. For a proper scaling generator L, a length scale a will be dilated to $ae^{\delta s}$ by an infinitesimal scaling transformation. This dilating behavior implies that the correlations inserted on length scale ϵ in the first cMERA layer, are dilated to length scale $\epsilon e^{s_\epsilon - s_\xi}$ at the end of cMERA. One concludes that cMERA has both an IR and UV cut-off. The former corresponds to the maximal length scale for which correlations are introduced (*i.e.* the correlation length ξ), $\epsilon e^{s_\epsilon - s_\xi} \approx \xi$, while the latter corresponds to the minimal length scale for which correlations are introduced, ϵ.

Putting the infinitesimal transformations in equations (2.1) and (2.3) together and taking the limit $\delta s \to 0$, the cMERA state $|\Psi^\Lambda\rangle$ is found to be:

$$|\Psi^\Lambda\rangle = \mathcal{T} \exp\left[-i \int_{s_\xi}^{s_\epsilon} K(s) + L ds\right] |\Omega\rangle = U(s_\epsilon, s_\xi)|\Omega\rangle \tag{2.5}$$

with $\mathcal{T}$ the time-ordering operator (ordering s values). This unitary transformation has a clear interpretation in the light of the previous paragraphs: it consists of an alternation of infinitesimal scaling and entangling transformations systematically adding correlations at different length scales. This interpretation of cMERA as the continuous generalization of MERA is supported by Figure 2.1 where both are compared. The cMERA procedure can also be turned upside down (corresponding to the bottom-up interpretation of MERA). One then starts from the fully entangled state $|\Psi^\Lambda\rangle$ at s_ϵ and evolves down to the product state at s_ξ by systematically removing correlations. The need for a UV cut-off then becomes especially apparent when considering correlations over a certain length scale a (at $s = s_\epsilon$). First, scaling reduces the length scale of these fluctuations to approximately ϵ (when $ae^{s-s_\epsilon} \approx \epsilon$) and during this scaling, $K(s)$ systematically disentangles the correlations. Once $ae^{s-s_\epsilon} \lesssim \epsilon$, only further scaling transformations are applied, finally allowing an isometric projection onto the reference state for the considered length scales when s_ϵ is reached. When the reference state is chosen to be scale invariant (*i.e.* $e^{-i\delta s L}|\Omega\rangle = |\Omega\rangle$ or equivalently $L|\Omega\rangle = 0$), these further scaling operations have no influence and fluctuations below ϵ can simply be projected onto the reference state immediately after crossing ϵ. Another important remark is that for length scales above ϵ only the sum $K(s) + L$ has a physical importance. Indeed, altering $K(s)$ and L a little but keeping their combined effect to be the same, an identical cMERA state will be created. This allows for some freedom in the choice of L, a feature that will be used for the Klein-Gordon bosons in the following sections. Finally, inspecting equation (2.5), one observes that shifting the integration range (while simultaneously redefining $K(s)$) has no influence on the cMERA state. Only the difference $s_\epsilon - s_\xi$ is of physical importance. Therefore, s_ϵ is typically set equal to zero and the cMERA procedure should thus be applied from $s = s_\xi \approx -\ln \frac{\xi}{\epsilon}$ up to $s = 0$. For critical systems with an infinite range of correlations ($\xi = +\infty$), cMERA should be started from $s = -\infty$.

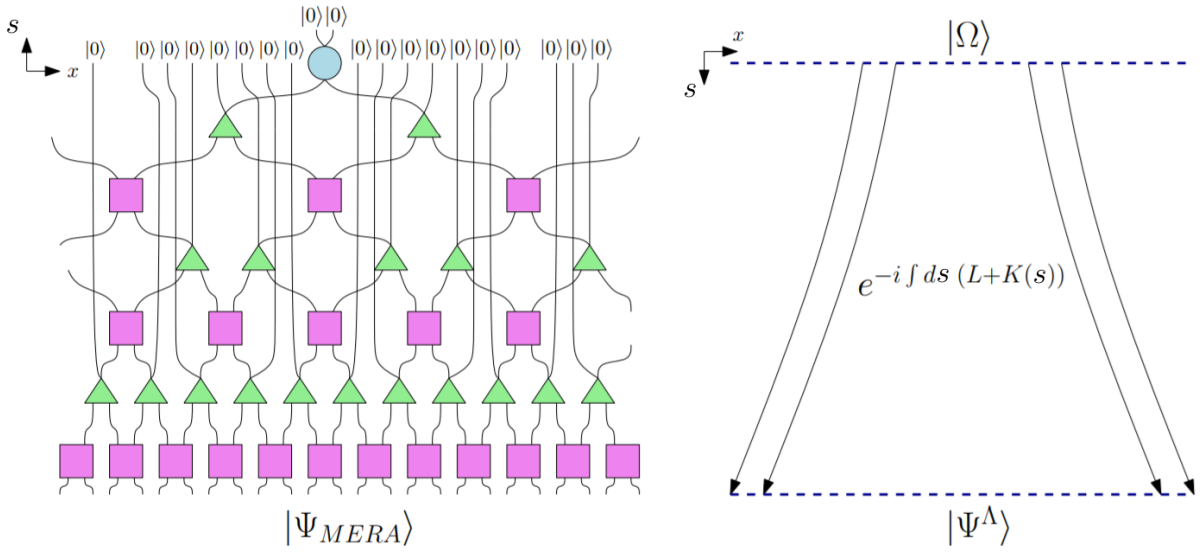

Figure 2.1: Comparison between the MERA tensor network (left) and the unitary evolution in cMERA, its continuous generalization (right).

The interpretation of cMERA discussed in the previous paragraph can also be compared to Wilson's momentum-shell renormalization group.[5] Indeed, in the latter high momentum degrees of freedom are integrated out in a shell out near cut-off Λ. Subsequent rescaling brings lower momenta into this shell, allowing their integration in a next step. In this way, high momenta are successively integrated out, making it possible to relate "bare" operators at the UV scale to "renormalized" operators at the IR scale. In fact, cMERA corresponds to a real-space version of this procedure but now modes near the cut-off are disentangled making it possible to isometrically project them onto the reference state. An important difference between both procedures is that cMERA constitutes a Hamiltonian method, making it possible to define an RG flow of operators under cMERA evolution. Indeed, consider the local operator $\mathcal{O}$ and its expectation value in a cMERA state $\langle\Psi^\Lambda|\mathcal{O}|\Psi^\Lambda\rangle$. By defining $\mathcal{O}(s) = U^\dagger(s_\epsilon, s)\mathcal{O}U(s_\epsilon, s)$, one obtains:

$$\frac{d\mathcal{O}}{ds}(s) = -i\left[K(s) + L, \mathcal{O}(s)\right] \tag{2.6}$$

The expectation value of $\mathcal{O}$ can then be calculated as $\langle\Omega|\mathcal{O}(s_\xi)|\Omega\rangle$ where $\mathcal{O}(s_\xi)$ is found by integrating this equation from s_ϵ down to s_ξ with $\mathcal{O}(s_\epsilon) = \mathcal{O}$. Thus, rather than the unitary evolution of the states, the evolution of the operators under cMERA is described by equation (2.6). Again, this evolution has a clear physical interpretation: at the UV level (s_ϵ) one has a "bare" operator $\mathcal{O}$ and as s decreases this $\mathcal{O}$ evolves to the "renormalized" $\mathcal{O}(s)$, where the degrees of freedom with momentum scales between Λ and Λe^{s-s_ϵ} are now disentangled.

In order to find a cMERA state for a QFT, one has to follow three steps: finding a reference state $|\Omega\rangle$ (typically scale invariant for the aforementioned reasons), deriving the scaling generator L and variationally determining the precise form of $K(s)$. At present, this process is only well understood for free QFTs. For these theories, it is possible to construct Gaussian cMERA states when a Gaussian reference state is used in combination with L and $K(s)$ operators, quadratic in the fields. Therefore, only Gaussian cMERA states will be constructed and applied in this work. Allowing variational freedom in the reference state does not improve the cMERA as every unitary relating the various reference states could be absorbed in the cMERA unitary. However, a variational $|\Omega\rangle$ can simplify calculations as will be demonstrated in the following sections. Finally, one of the main advantages of cMERA over MERA is the ability to choose Λ without imposing restrictions on the scalers. This facilitates the construction of translation invariant states in the continuous framework where a fine-tuning of the entanglers is necessary in the discrete case. An example of a manifestly translation invariant cMERA state is found when $k(s, x)$ does not depend on x and when a translation invariant reference state is utilized. Indeed, starting from a translation invariant reference state, scaling will leave this state translation invariant as will the application of $K(s)$ when $k(s, x)$ does not depend on x.

2.2 cMERA for Klein-Gordon Bosons

A first quantum field theory for which cMERA states will be derived is the real Klein-Gordon field in (1+1) dimensions describing relativistic, free, scalar and uncharged bosons with mass

m. The Hamiltonian of this theory is given by:

$$\begin{aligned} H &= \int dx \frac{1}{2}\left[\pi^2(x) + \left(\frac{d}{dx}\phi(x)\right)^2 + m^2\phi(x)^2\right] \\ &= \int dk \frac{1}{2}\left[\hat{\pi}(k)\hat{\pi}(-k) + (k^2+m^2)\hat{\phi}(k)\hat{\phi}(-k)\right] \end{aligned} \tag{2.7}$$

where the scalar field $\phi(x)$ and its conjugate momentum $\pi(x)$ satisfy the canonical commutation relation $[\phi(x), \pi(x')] = i\delta(x-x')$ (commutators between identical fields vanish). For the corresponding momentum-space operators, we have $[\hat{\phi}(k), \hat{\pi}(-k')] = i\delta(k-k')$ since $\hat{\phi}^\dagger(k) = \hat{\phi}(-k)$ and $\hat{\pi}^\dagger(k) = \hat{\pi}(-k)$ with the Fourier transform being defined by:

$$\hat{\phi}(k) = \frac{1}{\sqrt{2\pi}} \int_{-\infty}^{+\infty} e^{-ikx}\phi(x)dx \tag{2.8}$$

The first step in the cMERA construction process consists of finding a proper reference state. A general factorized Gaussian state with width Δ^{-1} can be defined via:

$$\left[\sqrt{\frac{\Delta}{2}}\phi(x) + i\sqrt{\frac{1}{2\Delta}}\pi(x)\right]|\Omega\rangle = 0 \qquad \forall x \in \mathbb{R} \tag{2.9}$$

The width of this state is left as a variational parameter and will be determined later on as described in the previous section. Next, the following form is proposed for the scaling transformation:

$$\begin{aligned} L &= -\frac{1}{2}\int dx \left[x\pi(x)\frac{d}{dx}\phi(x) + x\left(\frac{d}{dx}\phi(x)\right)\pi(x)\right] \\ &= \frac{1}{2}\int dk \left[k\hat{\pi}(-k)\frac{d}{dk}\hat{\phi}(k) + k\left(\frac{d}{dk}\hat{\phi}(k)\right)\hat{\pi}(-k) + \hat{\pi}(-k)\hat{\phi}(k) + \hat{\phi}(k)\hat{\pi}(-k)\right] \end{aligned} \tag{2.10}$$

One verifies that this yields correct scaling properties by considering the RG flow equations with $K(s) = 0$. Indeed, defining $\phi(x,s) = U(0,s)^\dagger\phi(x)U(0,s)$ and $\pi(x,s) = U(0,s)^\dagger\pi(x)U(0,s)$ while using that $L = U(0,s)^\dagger L U(0,s)$, the RG flow equation for the field $\phi(x,s)$ reduces to:

$$\begin{aligned} \frac{\partial}{\partial s}\phi(x,s) &= -i\left[L, \phi(x,s)\right] \\ &= \frac{i}{2}\int dx' \left[x'\pi(x',s)\frac{\partial}{\partial x'}\phi(x',s) + x'\left(\frac{\partial}{\partial x'}\phi(x',s)\right)\pi(x',s), \phi(x,s)\right] \\ &= \frac{i}{2}\int dx' \left(x'\pi(x',s)\left[\frac{\partial}{\partial x'}\phi(x',s), \phi(x,s)\right] + x'\left[\pi(x',s), \phi(x,s)\right]\frac{\partial}{\partial x'}\phi(x',s)\right) \\ &\quad + \frac{i}{2}\int dx' \left(x'\frac{\partial}{\partial x'}\phi(x',s)\left[\pi(x',s), \phi(x,s)\right] + x'\left[\frac{\partial}{\partial x'}\phi(x',s), \phi(x,s)\right]\pi(x',s)\right) \\ &= \frac{i}{2}\int dx'(-2ix')\frac{\partial}{\partial x'}\phi(x',s)\delta(x-x') \\ &= x\frac{\partial}{\partial x}\phi(x,s) \end{aligned} \tag{2.11}$$

Analogous calculations for the $\pi(x,s)$ field yield:

$$\frac{\partial}{\partial s}\pi(x,s) = \left(x\frac{\partial}{\partial x} + 1\right)\pi(x,s) \tag{2.12}$$

Together with the initial conditions that $\phi(x,0) = \phi(x)$ and $\pi(x,0) = \pi(x)$, these differential equations solve to:

$$\phi(x,s) = \phi(e^s x) \qquad \pi(x,s) = e^s \pi(e^s x) \tag{2.13}$$

In momentum-space, the corresponding scaling behavior is given by:

$$\hat{\phi}(k,s) = e^{-s}\hat{\phi}(e^{-s}k) \qquad \hat{\pi}(k,s) = \hat{\pi}(e^{-s}k) \tag{2.14}$$

confirming that both the fields and their arguments transform properly. However, if one uses this so-called relativistic scaling generator, the product state defined in equation (2.9) is not scale invariant. Indeed, applying a finite scaling transformation e^{-isL} again yields a factorized Gaussian state but with width $e^{-s}\Delta$ instead of Δ. The way to fix this is by using the relative freedom in the choice of L, redefining L as:

$$\begin{aligned} L &= -\frac{1}{2}\int dx \left[x\pi(x)\frac{d}{dx}\phi(x) + x\left(\frac{d}{dx}\phi(x)\right)\pi(x) + \frac{1}{2}\phi(x)\pi(x) + \frac{1}{2}\pi(x)\phi(x)\right] \\ &= \frac{1}{2}\int dk \left[k\hat{\pi}(-k)\frac{d}{dk}\hat{\phi}(k) + k\left(\frac{d}{dk}\hat{\phi}(k)\right)\hat{\pi}(-k) + \frac{1}{2}\hat{\pi}(-k)\hat{\phi}(k) + \frac{1}{2}\hat{\phi}(k)\hat{\pi}(-k)\right] \end{aligned} \tag{2.15}$$

The RG flow equations for the fields then reduce to:

$$\frac{\partial}{\partial s}\phi(x,s) = \left(x\frac{\partial}{\partial x} + \frac{1}{2}\right)\phi(x,s) \qquad \frac{\partial}{\partial s}\pi(x,s) = \left(x\frac{\partial}{\partial x} + \frac{1}{2}\right)\pi(x,s) \tag{2.16}$$

with the following solutions:

$$\phi(x,s) = e^{\frac{s}{2}}\phi(e^s x) \qquad \pi(x,s) = e^{\frac{s}{2}}\pi(e^s x) \tag{2.17}$$

In momentum-space, the corresponding scaling behavior is given by:

$$\hat{\phi}(k,s) = e^{-\frac{s}{2}}\hat{\phi}(e^{-s}k) \qquad \hat{\pi}(k,s) = e^{-\frac{s}{2}}\hat{\pi}(e^{-s}k) \tag{2.18}$$

The arguments are still scaled properly but the fields are attributed anomalous scale factors. However, only the sum of L and $K(s)$ is of physical importance for length scales above ϵ while for length scales below ϵ the scaling factors are irrelevant since the reference state is scale invariant there. The anomalous scaling factors hence pose no problem and one can safely use the so-called non-relativistic scaling generator in equation (2.15).

In order for the cMERA state to be Gaussian, its reference state should be Gaussian and both L and $K(s)$ should be quadratic in the field operators. This is clearly the case for the non-relativistic scaling generator. For the entangling generator, this has to be imposed explicitly. A possible way to do this, while safeguarding the significance of $K(s)$ as an operator generating entanglement, is by choosing $K(s)$ to be a generator of Bogoliubov transformations:

$$\begin{aligned} K(s) &= \frac{1}{2}\sum_{n=0}^{+\infty}\int dx \left[a_n(s)\frac{d^n\phi}{dx^n}(x)\pi(x) + \overline{a_n}(s)\frac{d^n\pi}{dx^n}(x)\phi(x)\right] \\ &= \frac{1}{2}\sum_{n=0}^{+\infty}\int dk \left[a_n(s)(ik)^n\hat{\phi}(k)\hat{\pi}(-k) + \overline{a_n}(s)(-ik)^n\hat{\pi}(-k)\hat{\phi}(k)\right] \\ &= \frac{1}{2}\int dk \left[g(k,s)\hat{\phi}(k)\hat{\pi}(-k) + \overline{g(k,s)}\hat{\pi}(-k)\hat{\phi}(k)\right] \end{aligned} \tag{2.19}$$

where $g(k,s)$ is analytical in its first argument. Again, the effect of this transformation on the fields is checked via the RG flow equations (now with $L=0$ and thus $K(s)=U(0,s)^\dagger K(s)U(0,s)$):

$$\begin{aligned}\frac{\partial}{\partial s}\hat{\phi}(k,s) &= -i\left[K(s),\hat{\phi}(k,s)\right] = -\frac{1}{2}\left(g(k,s)+\overline{g(k,s)}\right)\hat{\phi}(k,s)\\ \frac{\partial}{\partial s}\hat{\pi}(k,s) &= -i\left[K(s),\hat{\pi}(k,s)\right] = +\frac{1}{2}\left(g(k,s)+\overline{g(k,s)}\right)\hat{\pi}(k,s)\end{aligned} \tag{2.20}$$

yielding the following solutions:

$$\begin{aligned}\hat{\phi}(k,s) &= \exp\left[-s\frac{g(k,s)+\overline{g(k,s)}}{2}\right]\hat{\phi}(k)\\ \hat{\pi}(k,s) &= \exp\left[+s\frac{g(k,s)+\overline{g(k,s)}}{2}\right]\hat{\pi}(k)\end{aligned} \tag{2.21}$$

$K(s)$ thus clearly encodes a Bogoliubov transformation of the fields. However, in order for $K(s)$ to be local, the Taylor series defining $g(k,s)$ should be terminated at a finite order, reducing this function to a polynomial in k with s-dependent coefficients. Furthermore, $K(s)$ should only introduce entanglement for $|k| \lesssim \Lambda$. Therefore, $g(k,s)$ should incorporate a cut-off behavior near $|k|=\Lambda$. This is done by the following parametrization:

$$g(k,s) = \gamma(k,s)\Gamma(k) \tag{2.22}$$

with $\Gamma(k)$ a cut-off function and $\gamma(k,s)$ a polynomial function of k with s-dependent coefficients. Typically, the cut-off function adds a non-polynomial contribution to $g(k,s)$. As a result, $K(s)$ is only local up to $\mathcal{O}(\epsilon)$. As was mentioned in the original cMERA paper, this can also be interpreted as a purely local $K(s)$ acting on smoothed field operators with smoothing length ϵ. In this work, both Gaussian and sharp cut-off functions will be used:

$$\begin{aligned}\Gamma_{\text{sharp}}(k) &= \mathbb{H}\left(1-\frac{|k|}{\Lambda}\right)\\ \Gamma_{\text{Gaussian}}(k) &= e^{-\frac{k^2}{\Lambda^2}}\end{aligned} \tag{2.23}$$

with $\mathbb{H}$ the Heaviside function. The $g(k,s)$ function is also chosen to be real-valued. Odd terms then drop out in equation (2.19), yielding the following form for the entangling operator:

$$K(s) = \frac{1}{2}\int dk\gamma(k,s)\Gamma(k)\left[\hat{\phi}(k)\hat{\pi}(-k)+\hat{\pi}(-k)\hat{\phi}(k)\right] \tag{2.24}$$

Herein, $\gamma(k,s)$ is an even, real-valued polynomial function of k with s-dependent coefficients, that should be determined variationally. A quality cMERA state can already be found for the lowest order $\gamma(k,s)$ function (*i.e.* $\gamma(k,s)=\chi(s)$). Indeed, as will be demonstrated in the next paragraphs, increasing the order of $\gamma(k,s)$ introduces no new physics.

With the scaling and entangling generators defined in equation (2.15) and (2.24), one can now determine the influence of the full cMERA evolution on the field operators via the RG flow equations. Based on the results in equations (2.18) and (2.21), the following form is proposed for the fields:

$$\hat{\phi}(k,s) = e^{-f(k,s)}e^{-\frac{s}{2}}\hat{\phi}(e^{-s}k) \qquad \hat{\pi}(k,s) = e^{f(k,s)}e^{-\frac{s}{2}}\hat{\pi}(e^{-s}k) \tag{2.25}$$

where $f(k,s)$ is the so-called Bogoliubov angle. Substituting this in the RG equations (remembering that now neither $L = U(0,s)^\dagger L U(0,s)$ nor $K(s) = U(0,s)^\dagger K(s) U(0,s)$) yields:

$$\begin{aligned} & \frac{\partial}{\partial s}\hat{\phi}(k,s) = -i\left[L + K(s), \hat{\phi}(k,s)\right] \\ \iff & -\frac{\partial f}{\partial s}(k,s)\hat{\phi}(k,s) - \frac{1}{2}\hat{\phi}(k,s) - k e^{-\frac{s}{2}} e^{-f(k,s)} \frac{d\hat{\phi}}{dk}(e^{-s}k) \\ & = -\frac{1}{2}\hat{\phi}(k,s) - k e^{-\frac{s}{2}} e^{-f(k,s)} \frac{d\hat{\phi}}{dk}(e^{-s}k) - g(e^{-s}k, s)\hat{\phi}(k,s) \\ \iff & \frac{\partial f}{\partial s}(k,s) = g(e^{-s}k, s) \end{aligned} \tag{2.26}$$

Using that $f(k,0) = 0$, the Bogoliubov angle is obtained:

$$f(k,s) = \int_0^s g(e^{-w}k, w)dw = -\int_1^{e^{-s}} g(zk, -\ln z)\frac{1}{z}dz \tag{2.27}$$

Finally, all remaining freedom in $g(k,s)$ (or equivalently $f(k,s)$) is eliminated via a variational procedure, minimizing the energy in the cMERA state and thus approximating the ground state of the QFT. To do this, the energy functional is calculated making use of (2.25) and the definition of the product state:

$$\begin{aligned} E[f] &= \langle \Psi^\Lambda | H | \Psi^\Lambda \rangle = \langle \Omega | H(s_\xi) | \Omega \rangle \\ &= \int dk \frac{1}{4}\left[e^{2f(k)}\Delta + \frac{k^2+m^2}{\Delta}e^{-2f(k)}\right] e^{-s_\xi}\delta(e^{-s_\xi}k - e^{-s_\xi}k) \\ &= \int dx \int \frac{dk}{2\pi}\frac{1}{4}\left[e^{2f(k)}\Delta + \frac{k^2+m^2}{\Delta}e^{-2f(k)}\right] \end{aligned} \tag{2.28}$$

where $f(k) = f(k, s_\xi)$ and where the first factor is present due to the fact that energy is extensive. A better quantity to minimize, is the energy density $e[f]$ and the optimal cMERA state is then found by solving:

$$\frac{\delta}{\delta f}e[f] = \frac{\delta}{\delta f}\int \frac{dk}{2\pi}\frac{1}{4}\left[e^{2f(k)}\Delta + \frac{k^2+m^2}{\Delta}e^{-2f(k)}\right] = 0 \tag{2.29}$$

Below, cMERAs are explicitly derived for three specific cases.

2.2.1 Massless Bosons and Sharp Cut-off Function

If the free Klein-Gordon bosons, described previously, are massless, the corresponding field theory becomes conformal. The manifest scale-invariance present in CFTs like this, allows the $K(s)$ operator to be chosen s-independent. Combining this with the fact that $\gamma(k,s)$ can be reduced to its lowest order contribution (*i.e.* a single coefficient only depending on s), $g(k,s)$ simply becomes equal to a constant factor χ times the cut-off function and (almost) no variational optimization has to be performed. Indeed, for a sharp cut-off function, one obtains:

$$g(k,s) = \chi\mathbb{H}\left(1 - \frac{|k|}{\Lambda}\right) \quad \Rightarrow \quad f(k) = -\int_1^{+\infty}\frac{1}{z}\chi\mathbb{H}\left(1 - \frac{|zk|}{\Lambda}\right)dz = \begin{cases} \chi \ln\frac{|k|}{\Lambda} & |k| \leq \Lambda \\ 0 & |k| > \Lambda \end{cases} \tag{2.30}$$

where the limit $s_\xi \to -\infty$ was taken since the correlation length in a CFT is infinite. For massive theories, this limit can be taken as well since for these theories $g(k,s) \approx 0$ when $s > s_\xi$. Two

parameters are left to determine: Δ, specifying the reference state, and χ. The best way to do is, is by considering the annihilation operators of the important Gaussian states involved.[47,48] These are the reference state, the CFT ground state (also called the target state) and the cMERA state. Indeed, all of these are Gaussian states and can be specified unambiguously via a family of annihilation operators obeying the canonical commutation relations $[\hat{a}(k), \hat{a}^\dagger(q)] = \delta(k+q)$ in momentum-space. For the reference states, these are found by Fourier transforming (2.9), yielding:

$$\hat{a}(k)|\Omega\rangle = \left[\sqrt{\frac{\Delta}{2}}\hat{\phi}(k) + i\sqrt{\frac{1}{2\Delta}}\hat{\pi}(k)\right]|\Omega\rangle = 0 \qquad \forall k \in \mathbb{R} \tag{2.31}$$

while for the CFT ground state $|\Psi\rangle$ canonical quantization results in:

$$\hat{a}(k)|\Psi\rangle = \left[\sqrt{\frac{|k|}{2}}\hat{\phi}(k) + i\sqrt{\frac{1}{2|k|}}\hat{\pi}(k)\right]|\Psi\rangle = 0 \qquad \forall k \in \mathbb{R} \tag{2.32}$$

We thus recognize a similar form and propose the following for the cMERA state:

$$\hat{a}(k)|\Psi^\Lambda\rangle = \left[\sqrt{\frac{\alpha(k)}{2}}\hat{\phi}(k) + i\sqrt{\frac{1}{2\alpha(k)}}\hat{\pi}(k)\right]|\Psi^\Lambda\rangle = 0 \qquad \forall k \in \mathbb{R} \tag{2.33}$$

The $\alpha(k)$ function for the cMERA state is then determined via the RG flow equations:

$$\begin{aligned}
&\langle\Psi^\Lambda|\sqrt{\frac{\alpha(k)}{2}}\hat{\phi}(k) + i\sqrt{\frac{1}{2\alpha(k)}}\hat{\pi}(k)|\Psi^\Lambda\rangle \\
&= \langle\Omega|\sqrt{\frac{\alpha(k)}{2}}\hat{\phi}(k, s_\xi) + i\sqrt{\frac{1}{2\alpha(k)}}\hat{\pi}(k, s_\xi)|\Omega\rangle \\
&= \sqrt{\frac{\alpha(k)}{2}}e^{-f(k)}e^{-\frac{s_\xi}{2}}\langle\Omega|\hat{\phi}(e^{-s_\xi}k)|\Omega\rangle + i\sqrt{\frac{1}{2\alpha(k)}}e^{f(k)}e^{-\frac{s_\xi}{2}}\langle\Omega|\hat{\pi}(e^{-s_\xi}k)|\Omega\rangle \\
&= \left[\sqrt{\frac{\alpha(k)}{2}}e^{-f(k)} - \Delta\sqrt{\frac{1}{2\alpha(k)}}e^{f(k)}\right]e^{-\frac{s_\xi}{2}}\langle\Omega|\hat{\phi}(e^{-s_\xi}k)|\Omega\rangle \\
&= 0
\end{aligned} \tag{2.34}$$

finally yielding that:

$$\alpha(k) = \Delta e^{2f(k)} = \begin{cases} \Delta\left(\frac{|k|}{\Lambda}\right)^{2\chi} & |k| \leq \Lambda \\ \Delta & |k| > \Lambda \end{cases} \tag{2.35}$$

Since the cMERA state should resemble the CFT ground state for $|k| \leq \Lambda$, obvious choices for the parameters are $\chi = \frac{1}{2}$ and $\Delta = \Lambda$. Indeed, in this case the cMERA states correspond to the target states below the cut-off while above the cut-off a product state structure is found. This is illustrated in Figure 2.2.

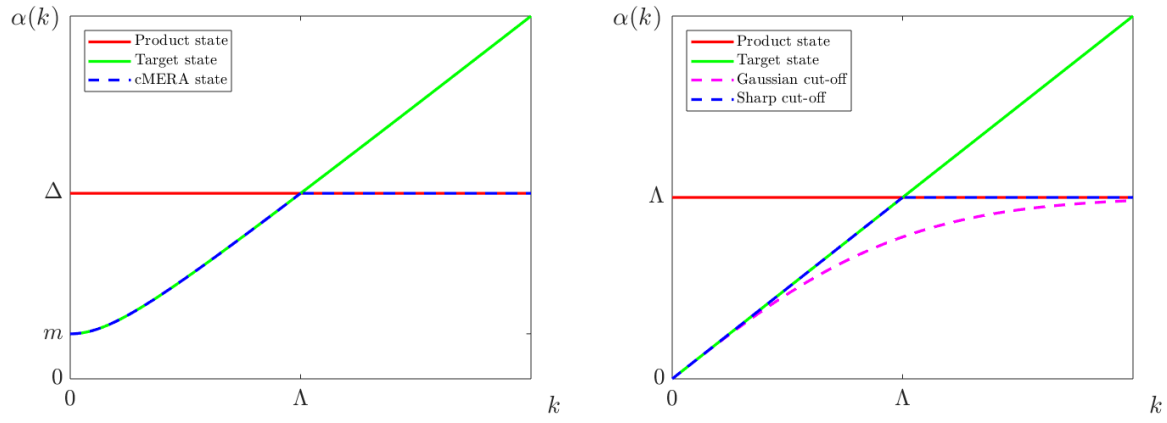

Figure 2.2: Comparison between $\alpha(k)$ functions of the product, target and cMERA states for Klein-Gordon bosons in the massless (left) and massive (right) case.

2.2.2 Massive Bosons and Sharp Cut-off Function

For massive bosons, the entangling generator $K(s)$ is not scale-invariant. As a result, one obtains $g(k,s) = \chi(s)\Gamma(k)$ when only considering the lowest-order polynomial contribution to the $g(k,s)$ function. Only the $\chi(s)$ function and Δ are left to be determined variationally and to do so, the energy functional is rather expressed in function of $\chi(s)$ than in function of the Bogoliubov angle. Consequently, the problem to be solved is:

$$\begin{aligned}\frac{\delta}{\delta\chi(s)}e[\chi] &= \int \frac{dk}{2\pi}\left(\frac{\partial}{\partial f(k)}\frac{1}{4}\left[e^{2f(k)}\Delta + \frac{k^2+m^2}{\Delta}e^{-2f(k)}\right]\frac{\delta f(k)}{\delta\chi(s)}\right) \\ &= \int \frac{dk}{2\pi}\left(\frac{1}{2}\left[e^{2f(k)}\Delta - \frac{k^2+m^2}{\Delta}e^{-2f(k)}\right]\Gamma(e^{-s}k)\right) = 0 \qquad \forall s \in]-\infty, 0]\end{aligned} \tag{2.36}$$

For a sharp cut-off function, this comes down to the requirement that:

$$\left[e^{2f(k)}\Delta - \frac{k^2+m^2}{\Delta}e^{-2f(k)}\right] = 0 \quad \Longleftrightarrow \quad f(k) = \frac{1}{2}\ln\left(\frac{\sqrt{k^2+m^2}}{\Delta}\right) \qquad |k| \leq \Lambda \tag{2.37}$$

yielding the following equation for $\chi(s)$:

$$\frac{1}{2}\ln\left(\frac{\sqrt{k^2+m^2}}{\Delta}\right) = -\int_1^{+\infty} \chi(-\ln z)\mathbb{H}\left(1-\frac{|zk|}{\Lambda}\right)\frac{1}{z}dz = -\int_1^{\frac{\Lambda}{|k|}} \frac{\chi(-\ln z)}{z}dz \tag{2.38}$$

where again the limit $s \to s_\xi$ was taken. Deriving this equation to k, one obtains:

$$\frac{|k|}{2(k^2+m^2)} = \frac{\chi(-\ln\frac{\Lambda}{|k|})}{|k|} \qquad \Rightarrow \qquad \chi(s) = \frac{1}{2}\frac{1}{1+\left(\frac{m}{\Lambda}e^{-s}\right)^2} \tag{2.39}$$

confirming that the $g(k,s)$ function quickly decreases for $s < s_\xi$. Indeed, since for massive bosons $\xi \approx m^{-1}$, implying that $s_\xi \approx \ln\frac{m}{\Lambda}$, $\chi(s)$ quickly decreases for $s < s_\xi$. The integral equation for $\chi(s)$ (2.38) was solved by derivation and therefore, equality between both sides should also be checked in a certain point. In $k = \Lambda$ the right-hand side equals zero. The only way the left-hand side equals zero for $k = \Lambda$, is if $\Delta = \sqrt{k^2+m^2}$. All variational parameters have thus

been determined. Again, product, target and cMERA state are all Gaussian and can hence be specified by means of family of annihilation operators as in equation (2.33). The specific $\alpha(k)$ functions are now given by:

$$\alpha(k) = \begin{cases} \Delta = \sqrt{\Lambda^2 + m^2} & \text{for } |\Omega\rangle \\ \omega(k) = \sqrt{k^2 + m^2} & \text{for } |\Psi\rangle \\ \begin{cases} \Delta & k \leq \Lambda \\ \omega(k) & k > \Lambda \end{cases} & \text{for } |\Psi^\Lambda\rangle \end{cases} \tag{2.40}$$

also displayed in Figure 2.2. One immediately observes that the massless cMERA is reproduced exactly by taking the limit $m \to 0$.

2.2.3 Massless Bosons and Gaussian Cut-off Function

Finally, the case of massless Klein-Gordon bosons in combination with a Gaussian cut-off function will be treated. Since the QFT reduces to a CFT, $K(s)$ is s-independent. The Gaussian cut-off function in equation (2.23) will be altered slightly, allowing a different width, in order to improve the correspondence with the target state. The entangling generator is hence specified by:

$$g(k, s) = \chi e^{-\frac{k^2}{\sigma\Lambda^2}} \tag{2.41}$$

yielding the following Bogoliubov angle:

$$\begin{aligned} f(k) &= -\int_1^{+\infty} \frac{1}{z} \chi e^{-\frac{z^2 k^2}{\sigma\Lambda^2}} dz \\ &= -\frac{\chi}{2} \int_{\frac{k^2}{\sigma\Lambda^2}}^{+\infty} \frac{e^{-t}}{t} dt = \frac{\chi}{2} \mathrm{Ei}\left(-\frac{k^2}{\sigma\Lambda^2}\right) \end{aligned} \tag{2.42}$$

where the exponential integral function was introduced, defined by $\mathrm{Ei}(x) = -\int_{-x}^{+\infty} \frac{e^{-t}}{t} dt$. As was the case for the massless bosons with a sharp cut-off, the remaining parameters will be determined via inspection of the annihilator operators. For the cMERA state, these are now specified by:

$$\alpha(k) = \Delta e^{\chi \mathrm{Ei}\left(-\frac{k^2}{\sigma\Lambda^2}\right)} \tag{2.43}$$

For small negative arguments, the exponential integral function can be approximated by $\mathrm{Ei}(x) \approx \gamma - \ln x$ with γ the Euler-Mascheroni constant, implying that:

$$\alpha(k) \approx \Delta e^{\chi \ln\left(e^\gamma \frac{k^2}{\sigma\Lambda^2}\right)} = \Delta \left(e^\gamma \frac{k^2}{\sigma\Lambda^2}\right)^\chi \qquad \text{if } k \ll \Lambda \tag{2.44}$$

This is in correspondence with the CFT ground state if $\chi = \frac{1}{2}$ and if $\frac{\Delta}{\Lambda}\sqrt{\frac{e^\gamma}{\sigma}} = 1$. In accordance with the sharp cut-off function, Δ is chosen equal to Λ while $\sigma = e^\gamma$. For $k \gg \Lambda$ the exponential integral becomes very small and thus $\alpha(k) \approx \Delta = \Lambda$, corresponding to the product state limit, as confirmed in Figure 2.2.

2.3 cMERA for Dirac Fermions

The intricacies of fermions in the cMERA framework will be illustrated by a free Dirac field in (1+1) dimensions with mass m and two fermion flavors. The Hamiltonian of this theory is given by:

$$H = \int dx \left[\psi^\dagger(x)\gamma^0\left(-i\gamma^1\frac{d}{dx} + m\right)\psi(x)\right] \tag{2.45}$$

where $\psi(x) = (\psi_0(x) \quad \psi_1(x))^T$ is a Dirac spinor satisfying the canonical anticommutation relations $\{\psi_\mu(x), \psi^\dagger_\nu(y)\} = \delta_{\mu\nu}\delta(x-y)$ or equivalently in Fourier space $\{\hat{\psi}_\mu(k), \hat{\psi}^\dagger_\nu(q)\} = \delta_{\mu\nu}\delta(k-q)$ (anticommutators between identical fields vanish). γ^0 and γ^1 are Dirac matrices satisfying $\gamma^\mu\gamma^\nu + \gamma^\nu\gamma^\mu = 2g^{\mu\nu}I$ with I the 2×2 unit matrix and $g^{\mu\nu}$ the Minkowski metric tensor with signature $(+,-)$. Throughout this work, the following representation will be utilized:

$$\gamma^0 = \begin{pmatrix} 1 & 0 \\ 0 & -1 \end{pmatrix} \qquad \gamma^1 = \begin{pmatrix} 0 & 1 \\ -1 & 0 \end{pmatrix} \tag{2.46}$$

The Hamiltonian can hence be expanded as:

$$\begin{aligned} H &= \int dx \left[-i\psi_0^\dagger(x)\frac{d}{dx}\psi_1(x) - i\psi_1^\dagger(x)\frac{d}{dx}\psi_0(x) + m\psi_0^\dagger(x)\psi_0(x) - m\psi_1^\dagger(x)\psi_1(x)\right] \\ &= \int dk \left[k\hat{\psi}_0^\dagger(k)\hat{\psi}_1(k) + k\hat{\psi}_1^\dagger(k)\hat{\psi}_0(k) + m\hat{\psi}_0^\dagger(k)\hat{\psi}_0(k) - m\hat{\psi}_1^\dagger(k)\hat{\psi}_1(k)\right] \end{aligned} \tag{2.47}$$

Again, finding a proper reference state constitutes the first step of the cMERA construction process. A simple factorized Guassian state is found by the prescription:

$$\hat{\psi}_0(k)|\Omega\rangle = 0 \qquad \wedge \qquad \hat{\psi}_1^\dagger(k)|\Omega\rangle = 0 \qquad \forall k \in \mathbb{R} \tag{2.48}$$

corresponding to the interpretation of $\hat{\psi}_0(k)$ as an annihilator of particles and $\hat{\psi}_1^\dagger(k)$ as an annihilator of anti-particles, both with momentum k. For the scaling generator the following form was proposed:

$$\begin{aligned} L &= -\frac{i}{2}\int dx \left[x\psi^\dagger(x)\frac{d\psi}{dx}(x) - x\frac{d\psi^\dagger}{dx}(x)\psi(x)\right] \\ &= -\frac{i}{2}\int dx \left[x\psi_0^\dagger(x)\frac{d\psi_0}{dx}(x) - x\frac{d\psi_0^\dagger}{dx}(x)\psi_0(x) + x\psi_1^\dagger(x)\frac{d\psi_1}{dx}(x) - x\frac{d\psi_1^\dagger}{dx}(x)\psi_1(x)\right] \\ &= \frac{i}{2}\int dk \left[k\hat{\psi}^\dagger(k)\frac{d\hat{\psi}}{dk}(k) - k\frac{d\hat{\psi}^\dagger}{dk}(k)\hat{\psi}(k)\right] \end{aligned} \tag{2.49}$$

The validity of this operator as a scaling generator is checked via the RG flow equations with $K(s) = 0$ and thus $L = U(0,s)^\dagger L U(0,s)$. The main difference with bosonic calculations lies in the fact that now anticommutation relations of the fields have to be applied instead of commutation relations. One obtains that:

$$\frac{\partial}{\partial s}\psi(x,s) = -i[L, \psi(x,s)] = x\frac{\partial}{\partial x}\psi(x,s) + \frac{1}{2}\psi(x,s) \tag{2.50}$$

yielding the following solutions for the field operator:

$$\psi(x,s) = e^{\frac{s}{2}}\psi(e^s x) \tag{2.51}$$

and an identical scaling behavior for its complex conjugate. In momentum-space this corresponds to:

$$\hat{\psi}(k,s) = e^{-\frac{s}{2}}\hat{\psi}(e^{-s}k) \tag{2.52}$$

The scaler thus clearly generates a correct scaling behavior for both the fields and their arguments. Furthermore, scaling leaves the reference state invariant, thus implying that L satisfies all necessary criteria.

As was the case for the Klein-Gordon bosons, a generator for Bogoliubov transformations is proposed for the entangler $K(s)$. However, a Bogoliubov mixing between the spinor fields and their adjoints is prohibited by the $U(1)$ invariance of the Dirac Hamiltonian. Therefore, only the different components of $\psi(x)$ will be mixed according to:

$$K(s) = i\int dk \left[g(k,s)\hat{\psi}_0^\dagger(k)\hat{\psi}_1(k) - \overline{g(k,s)}\hat{\psi}_0(k)\hat{\psi}_1^\dagger(k)\right] \tag{2.53}$$

To check the validity of this operator as an entanglement generator of the Bogoliubov type, one considers the RG flow equations of the spinor components with $L = 0$ and thus $K(s) = U(0,s)^\dagger K(s) U(0,s)$:

$$\begin{aligned}\frac{\partial}{\partial s}\hat{\psi}_0(k,s) &= -i[K(s),\hat{\psi}_0(k,s)] = -g(k,s)\hat{\psi}_1(k,s)\\ \frac{\partial}{\partial s}\hat{\psi}_1(k,s) &= -i[K(s),\hat{\psi}_1(k,s)] = \overline{g(k,s)}\hat{\psi}_0(k,s)\end{aligned} \tag{2.54}$$

The easiest way to integrate these, is to consider a scale-invariant theory and thus a $g(k,s)$ solely depending on k. In this case, the RG equations are solved by:

$$\begin{aligned}\hat{\psi}_0(k,s) &= \cos(|g(k)|s)\hat{\psi}_0(k) - \frac{g(k)}{|g(k)|}\sin(|g(k)|s)\hat{\psi}_1(k)\\ \hat{\psi}_1(k,s) &= \cos(|g(k)|s)\hat{\psi}_1(k) + \frac{g(k)}{|g(k)|}\sin(|g(k)|s)\hat{\psi}_0(k)\end{aligned} \tag{2.55}$$

clearly illustrating that $K(s)$ generates a Bogoliubov transformation. As was the case for the Klein-Gordon bosons in the previous section, $g(k,s)$ is analytical in its first argument but due to locality reasons it is reduced to a polynomial function in k. Furthermore, $g(k,s)$ can be chosen real-valued and odd in k and again higher-order terms essentially introduce no new physics. Therefore, the simplest form for $g(k,s)$ is given by:

$$g(k,s) = \chi(s)\frac{k}{\Lambda}\Gamma(k) \tag{2.56}$$

where $\Gamma(k)$ is a cut-off function and the factor Λ^{-1} was introduced to make $g(k,s)$ dimensionless.

The evolution of the spinor components under the combined effect of scaling and entangling is found by solving the RG equations taking both L and $K(s)$ into account. Based on the previous results, an ansatz for the solution is proposed:

$$\begin{aligned}\hat{\psi}_0(k,s) &= \cos(f(k,s))e^{-\frac{s}{2}}\hat{\psi}_0(e^{-s}k) - \sin(f(k,s))e^{-\frac{s}{2}}\hat{\psi}_1(e^{-s}k)\\ \hat{\psi}_1(k,s) &= \cos(f(k,s))e^{-\frac{s}{2}}\hat{\psi}_1(e^{-s}k) + \sin(f(k,s))e^{-\frac{s}{2}}\hat{\psi}_0(e^{-s}k)\end{aligned} \tag{2.57}$$

with $f(k,s)$ the Bogoliubov angle. Substitution in the RG equations yields a solution if:

$$\frac{\partial f}{\partial s}(k,s) = g(e^{-s}k,s) \iff f(k,s) = \int_0^s g(e^{-w}k,w)dw = -\int_1^{e^{-s}} g(zk,-\ln z)\frac{1}{z}dz \tag{2.58}$$

where again the initial condition $f(k,0)=0$ was used. All the remaining freedom in $g(k,s)$ (or equivalently $f(k,s)$) is eliminated via the variational minimization of the energy in the cMERA state. Therefore, the energy density functional is constructed:

$$\begin{aligned} e[f] &= \frac{1}{\int dx}\langle\Psi^\Lambda|H|\Psi^\Lambda\rangle = \frac{1}{\int dx}\langle\Omega|H(s_\xi)|\Omega\rangle \\ &= -\int \frac{dk}{2\pi}\left[k\sin(2f(k)) + m\cos(2f(k))\right] \end{aligned} \tag{2.59}$$

where $f(k)$ is the Bogoliubov angle at $s=s_\xi$. Below, the variational procedure is carried out for three specific cases, similar to those treated for the Klein-Gordon bosons.

2.3.1 Massless Fermions and Sharp Cut-off Function

For massless fermions, the Dirac model constitutes a CFT and as a result also $K(s)$ does not depend on s. In this case, the Bogoliubov angle for the cMERA can be inferred directly from the $g(k)$ function. Using a sharp cut-off function, one obtains:

$$f(k) = -\int_1^{+\infty} \frac{1}{z}\chi\frac{zk}{\Lambda}\mathbb{H}\left(1-\frac{|zk|}{\Lambda}\right)dz = \begin{cases} \chi\left(\frac{k}{\Lambda}-\text{sign}(k)\right) & |k|\leq\Lambda \\ 0 & |k|>\Lambda \end{cases} \tag{2.60}$$

illustrating that the Bogoliubov angle is an odd function of k. The only parameter left to be determined is χ. An optimal value is found by considering the annihilation operators, $\tilde{\psi}_0(k)$ and $\tilde{\psi}_1^\dagger(k)$, defining the relevant Gaussian states. For the reference state, these are simply given by $\hat{\psi}_0(k)$ and $\hat{\psi}_1^\dagger(k)$ while for the target state canonical quantization yields:

$$\begin{pmatrix}\tilde{\psi}_0(k)\\ \tilde{\psi}_1(k)\end{pmatrix} = \begin{pmatrix}\frac{2}{\sqrt{2}} & \frac{2}{\sqrt{2}}\text{sign}(k)\\ -\frac{2}{\sqrt{2}}\text{sign}(k) & \frac{2}{\sqrt{2}}\end{pmatrix}\begin{pmatrix}\hat{\psi}_0(k)\\ \hat{\psi}_1(k)\end{pmatrix} \tag{2.61}$$

As in the bosonic case, a common form can be recognized:

$$\begin{pmatrix}\tilde{\psi}_0(k)\\ \tilde{\psi}_1(k)\end{pmatrix} = \begin{pmatrix}\cos\theta(k) & \text{sign}(k)\sin\theta(k)\\ -\text{sign}(k)\sin\theta(k) & \cos\theta(k)\end{pmatrix}\begin{pmatrix}\hat{\psi}_0(k)\\ \hat{\psi}_1(k)\end{pmatrix} \tag{2.62}$$

where the angle $\theta(k)$ is zero for the product state and $\frac{\pi}{4}$ for the target state. For the cMERA state, the following relation between the Bogoliubov angle and $\theta(k)$ is found:

$$\text{sign}(k)\sin\theta(k)\cos f(k) = \cos\theta(k)\sin f(k) \tag{2.63}$$

which is equivalent to $\theta(k) = f(k)\text{sign}(k)$. The angle $\theta(k)$ hence is the even version of the Bogoliubov angle. For the massless fermions considered here, one obtains:

$$\theta(k) = \begin{cases} -\chi\left(1-\frac{|k|}{\Lambda}\right) & |k|\leq\Lambda \\ 0 & |k|>\Lambda \end{cases} \tag{2.64}$$

$\theta(k)$ thus drops down linearly from $-\chi$ at $k = 0$ to zero at $k = \Lambda$. In order to at least obtain correspondence with the reference state for $k = 0$, the best choice for χ is $-\frac{\pi}{4}$. However, the linear profile does not correspond to what one expects from a quality cMERA (reproducing the reference $\theta(k)$ up to $k \approx \Lambda$, then going to the product state $\theta(k)$). A better profile is found when the order of the $g(k)$ function is increased. Indeed, using the following $g(k)$ function:

$$g(k) = \chi_{2n+1} \left(\frac{k}{\Lambda}\right)^{2n+1} \mathbb{H}\left(1 - \frac{|k|}{\Lambda}\right) \tag{2.65}$$

the $\theta(k)$ angle is given by:

$$\theta(k) = \begin{cases} -\chi_{2n+1}\left(1 - \left(\frac{|k|}{\Lambda}\right)^{2n+1}\right) & |k| \leq \Lambda \\ 0 & |k| > \Lambda \end{cases} \tag{2.66}$$

where $\chi_{2n+1} = -\frac{\pi}{4}$ corresponds to the correct reference state limit. Increasing the order of $g(k)$ thus reduces the deviations between the exact reference $\theta(k)$ and the cMERA approximation from $\mathcal{O}\left(\frac{k}{\Lambda}\right)$ to $\mathcal{O}\left(\left(\frac{k}{\Lambda}\right)^{2n+1}\right)$. This effect is also illustrated in Figure 2.3. A perfect correspondence is found when $n \to +\infty$ but as was mentioned before, this implies a non-local entangling operation.

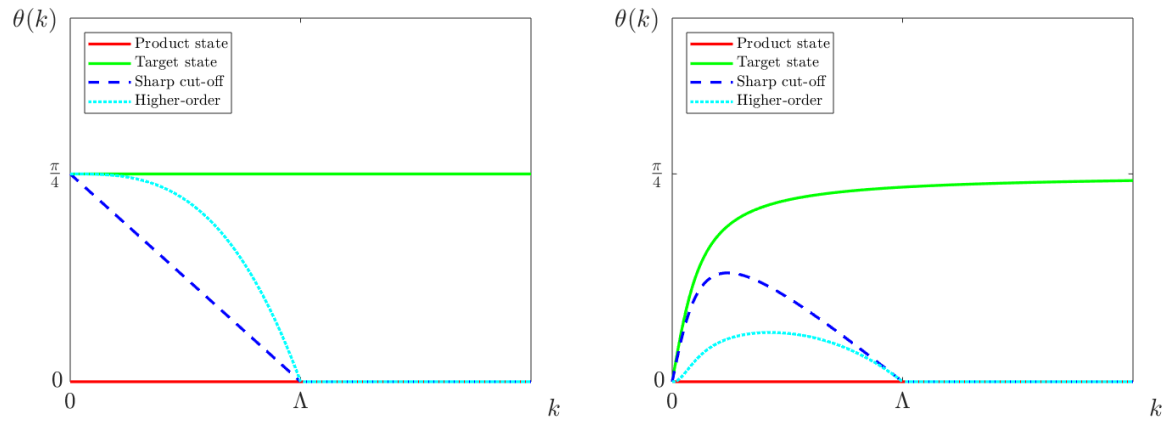

Figure 2.3: Comparison between $\theta(k)$ functions of the product, target and cMERA states for Dirac fermions in the massless (left) and massive (right) case both with sharp cut-off functions and higher-order terms ($n = 1$).

2.3.2 Massive Fermions and Sharp Cut-off Function

For massive fermions, $K(s)$ does depend on s and as a result, the variational procedure has to be carried out unabridged. Since all variational freedom is contained in $\chi(s)$, this function will be used in the energy minimization rather than the Bogoliubov angle. Taking the functional derivative of the energy functional then yields:

$$\begin{aligned} \frac{\delta}{\delta\chi(s)} e[\chi] &= -\int \frac{dk}{2\pi} \frac{\partial}{\partial f(k)} \left[k \sin(2f(k)) + m\cos(2f(k))\right] \frac{\delta f(k)}{\delta\chi(s)} \\ &= \int \frac{dk}{2\pi} 2\left[m\sin(2f(k)) - k\cos(2f(k))\right] e^{-s} \frac{k}{\Lambda} \Gamma\left(e^{-s}|k|\right) = 0 \qquad \forall s \in]-\infty, 0] \end{aligned} \tag{2.67}$$

The only way this is true, is if the term between parentheses equals zero for all momenta below the cut-off, *i.e.* if:

$$f(k) = \text{sign}(k) \arcsin\left(\sqrt{\frac{1}{2} - \frac{1}{2}\sqrt{\frac{m^2}{k^2+m^2}}}\right) \qquad |k| \leq \Lambda \tag{2.68}$$

One thus has to solve the following equation for $\chi(s)$:

$$\begin{aligned} \text{sign}(k) \arcsin\left(\sqrt{\frac{1}{2} - \frac{1}{2}\sqrt{\frac{m^2}{k^2+m^2}}}\right) &= -\int_1^{+\infty} \chi(-\ln z)\frac{zk}{\Lambda}\mathbb{H}\left(1 - \frac{|zk|}{\Lambda}\right)\frac{1}{z}dz \\ &= -\frac{k}{\Lambda}\int_1^{\frac{\Lambda}{|k|}} \chi(-\ln z)dz \qquad |k| \leq \Lambda \end{aligned} \tag{2.69}$$

This is done by differentiating this equation, yielding:

$$\chi(s) = \left[\kappa^2 \frac{d}{d\kappa}\left(\frac{1}{\kappa}\arcsin\left(\sqrt{\frac{1}{2} - \frac{1}{2}\sqrt{\frac{\left(\frac{m}{\Lambda}\right)^2}{\kappa^2 + \left(\frac{m}{\Lambda}\right)^2}}}\right)\right)\right]_{\kappa = e^s} \tag{2.70}$$

Since this result was found by differentiation, equality has to be checked in a certain k point for this solution to be correct. However, in contrast to the bosonic case, there is a difference between both sides of equation (2.69). On the right, $k = \Lambda$ yields 0, while substitution of this k value in the left-hand side gives:

$$\arcsin\left(\sqrt{\frac{1}{2} - \frac{1}{2}\sqrt{\frac{m^2}{\Lambda^2+m^2}}}\right) \tag{2.71}$$

Therefore, the only way complete correspondence is reached, is if $\Lambda \to +\infty$, *i.e.* in the CFT ground state. For all other Λ values, the difference in equation (2.71) results in a deviation of cMERA from the exact reference state Bogoliubov angle for $|k| \leq \Lambda$. In contrast to the massless case, this deviation is amplified when the order of $g(k,s)$ increases, as illustrated in Figure 2.3. The linear deviation, obtained in the massless case now also has a clear origin: it is a direct consequence of the observed difference in equation (2.71). Note that in Figure, $\theta(k)$ is displayed, rather than the Bogoliubov angle. These are still related via $\theta(k) = \text{sign}(k)f(k)$.

2.3.3 Massless Fermions and Gaussian Cut-off Function

$K(s)$ can once again be assumed s-independent due to the scale-invariance of the massless theory. In case of a Gaussian cut-off function, $g(k)$ is hence given by:

$$g(k) = \chi_{2n+1}\left(\frac{k}{\Lambda}\right)^{2n+1} e^{-\left(\frac{k}{\Lambda}\right)^2} \tag{2.72}$$

where the possibility of higher k orders was already included. For the cut-off function, the simple form of equation (2.23) was used. The Bogoliubov angle is calculated via:

$$\begin{aligned} f(k) &= -\int_1^{+\infty} \frac{1}{z}\chi_{2n+1}\left(\frac{zk}{\Lambda}\right)^{2n+1} e^{-\left(\frac{zk}{\Lambda}\right)^2} dz \\ &= -\chi_{2n+1}\text{sign}(k)\int_{\frac{|k|}{\Lambda}}^{+\infty} u^{2n}e^{-u^2}du \\ &= -\frac{\chi_{2n+1}}{2}\text{sign}(k)\int_{\left(\frac{k}{\Lambda}\right)^2}^{+\infty} z^{n-\frac{1}{2}}e^{-z}dz = -\frac{\chi_{2n+1}}{2}\text{sign}(k)\Gamma\left(n+\frac{1}{2},\left(\frac{k}{\Lambda}\right)^2\right) \end{aligned} \tag{2.73}$$

where $\Gamma(s,k)$ is the upper incomplete Gamma function defined by $\Gamma(s,k) = \int_k^{+\infty} z^{s-1}e^{-z}dz$. Finally, χ_{2n+1} is determined by requiring that $\theta(0) = \lim_{k\to 0^+} f(k) = \frac{\pi}{4}$. This is the case when:

$$\chi_{2n+1} = -\frac{\pi}{4}\frac{2}{\Gamma\left(n+\frac{1}{2},0\right)} = -\frac{\pi}{2}\frac{1}{\Gamma\left(n+\frac{1}{2}\right)} = -\frac{2^{n-1}\sqrt{\pi}}{(2n-1)!!} \tag{2.74}$$

where the $\Gamma\left(n+\frac{1}{2}\right)$ after the second equality signifies the Gamma function (and thus not the cut-off function). With this choice, the $\theta(k)$ indeed corresponds to its CFT value for $k=0$ after which it drops down to reach the product state value near $k=\Lambda$. As was the case for massless fermions with a sharp cut-off, better approximations of the reference state are found when n is increased, as depicted in Figure 2.4.

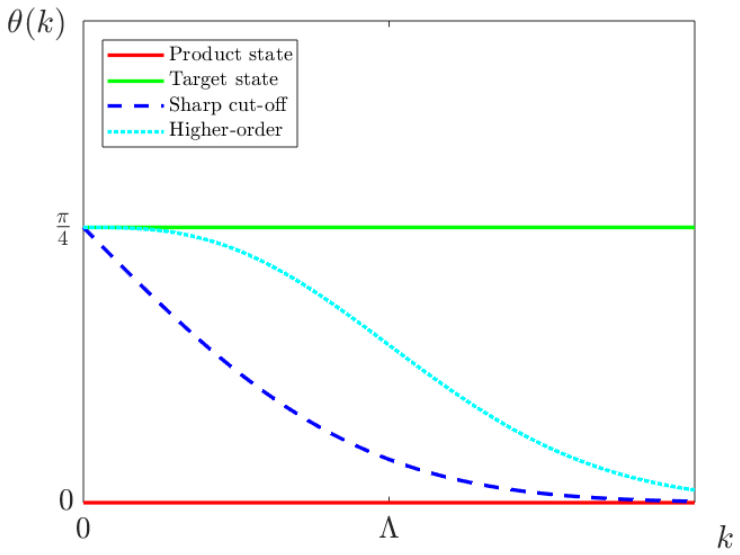

Figure 2.4: Comparison between $\theta(k)$ functions of the product, target and cMERA states for massless Dirac fermions with a Gaussian cut-off function. A cMERA with a higher-order $g(k)$ ($n=1$) was included as well.

Chapter 3

Klein-Gordon Theory in (1+1) Dimensions

The entanglement structure of cMERA and other Gaussian QFT states can be studied once their two-point correlators are known. Casini and Huerta reviewed this procedure[23] and successfully applied it to QFT ground states.[24] Vidal *et al.*[47] on the other hand, used the method to study the entanglement entropy in cMERA states of CFTs. In a way, this and the following chapter are a continuation of both these papers. Not only will Rényi entanglement entropies be calculated for cMERA states of both massless and massive QFTs, but also the entanglement Hamiltonian of these states will be constructed. The first part of this chapter will therefore introduce the followed methodology while in the second part, results of numerical simulations will be discussed as well as their correspondence to analytical approximations.

3.1 Methodology

3.1.1 Discrete Field Theory

How to determine the entanglement Hamiltonian and entropy of Gaussian states, will be introduced in a discrete setting. A generalization directly in the continuum follows in the next section. Consider therefore a 1d lattice with lattice points at $x_i = ia$ where a is the lattice spacing and $i \in \mathbb{Z}$. Corresponding to the Klein-Gordon theory we eventually wish to study, bosonic field operators ϕ_i and their conjugate momenta π_i are introduced on each lattice site. These Hermitian operators obey the canonical commutation relations $[\phi_i, \pi_j] = i\delta_{ij}$ and $[\phi_i, \phi_j] = [\pi_i, \pi_j] = 0$. As stated earlier, this work will only treat Gaussian states satisfying Wick's theorem. *I.e.* all non-zero correlators are obtained from two-point correlators by the prescription:

$$\langle f_1 f_2 ... f_{2k} \rangle = \frac{1}{2^k k!} \sum_\sigma \langle \mathcal{O} f_{\sigma(1)} f_{\sigma(2)} \rangle ... \langle \mathcal{O} f_{\sigma(2k-1)} f_{\sigma(2k)} \rangle \tag{3.1}$$

where the sum runs over all the permutations σ of the indices, where the f_i can be any of the scalar fields or conjugate momenta and where $\mathcal{O}$ orders the operators according to their ordering in the left-hand side of the equation. Furthermore, one assumes that $\langle \phi_i \rangle = \langle \pi_i \rangle = 0$. Due to Wick's theorem, all other combinations of an odd number of operators then also have expectation values equal to zero. The two-point correlators of such Gaussian states are given by:

$$\begin{aligned} \langle \phi_i \phi_j \rangle &= X_{ij} \qquad \langle \pi_i \pi_j \rangle = P_{ij} \\ \langle \phi_i \pi_j \rangle &= \langle \pi_j \phi_i \rangle^* = \frac{i}{2}\delta_{ij} + D_{ij} \end{aligned} \tag{3.2}$$

where X and P are real, Hermitian and positive and where D_{ij} is real. One also has that $\sum_{l=-\infty}^{+\infty} X_{il}P_{lj} = \frac{1}{4}\delta_{ij}$ and as $A_{lm} = \langle (\phi_l + i\lambda_{lk}\pi_k)(\phi_m + i\lambda^*_{ms}\pi_s) \rangle$ constitutes a Gram matrix, A is positive-definite for all matrices λ so that choosing $\lambda = -2X$ yields $XP \geq \frac{1}{4}$. Finally, D vanishes for the states considered in this work due to time inversion symmetry.

To study its entanglement properties, a state ρ is typically reduced to a physical interval L yielding the reduced density operator $\rho_L = \mathrm{tr}_{L^c}\rho$. In the discrete lattice setting considered here, this corresponds to tracing out all degrees of freedom out of the interval L, maintaining only the n consecutive lattice points $\{x_i\}_{i=1,...,n}$ within L. One then defines the correlation matrix C by $C_{ij} = \frac{1}{2}\langle \{R_i, R_j\} \rangle$, with R the vector containing all remaining scalar fields and conjugate momenta: $R = (\phi_1 \, ... \, \phi_n \, \pi_1 \, ... \, \pi_n)^T$. For Gaussian states with the aforementioned properties, this matrix is given by:

$$C = \left(\begin{array}{c|c} X & 0 \\ \hline 0 & P \end{array} \right) \tag{3.3}$$

As both X and P are real and positive-definite, C also is real and positive-definite, allowing the application of Williamson's theorem.[49,50]

Williamson's theorem

For a positive-definite matrix $C \in \mathbb{R}^{2n\times 2n}$, there exists a real symplectic matrix $S \in Sp(2n, \mathbb{R})$[1], so that:

$$S^T C S = \left(\begin{array}{c|c} \Omega & 0 \\ \hline 0 & \Omega \end{array} \right) \tag{3.4}$$

with $\Omega = \mathrm{diag}(\omega_1, ..., \omega_n)$, the diagonal matrix containing the so-called symplectic eigenvalues of C. These occur in the spectrum of JC as $\{\pm i\omega_l\}_{l=1,...,n}$. The columns of the symplectic matrix S are given by $\left\{\sqrt{\omega_l} f_l, \sqrt{\omega_l} e_l\right\}$ where $\{f_l, e_l\}$ is orthonormal w.r.t. the scalar product defined by C: $\langle \, . \, , \, . \, \rangle_C = \langle \, . \, , \, C \, . \, \rangle$ and where $\{e_l \pm i f_l\}$ are the eigenvectors of JC with eigenvalues $\pm i\omega_l$.

The implications of Williamson's theorem become clear when considering a linear transformation of the fields: $\tilde{R}_i = A_{ij}R_j$. When A is a so-called canonical field transformation, it preserves the canonical commutation relations of the fields and therefore has to be an element of the real symplectic group $Sp(2n, \mathbb{R})$. The correlation matrix is also affected by such a canonical transformation:

$$\tilde{C}_{ij} = \frac{1}{2}\langle \{\tilde{R}_i, \tilde{R}_j\} \rangle = \frac{1}{2}\langle \{A_{ik}R_k, A_{jl}R_l\} \rangle = A_{ik}C_{kl}A_{jl} \tag{3.5}$$

[1] A matrix $S \in \mathbb{R}^{2n\times 2n}$ belongs to $Sp(2n, \mathbb{R})$ when $S^T J S = J$, where J is the standard symplectic matrix given by $J = \left(\begin{array}{c|c} 0 & I \\ \hline -I & 0 \end{array} \right)$.

or equivalently $\tilde{C} = ACA^T$ with A symplectic. As the transpose of a symplectic matrix is also symplectic, Williamson's theorem thus essentially allows one to find a canonical field transformation A, bringing the C matrix in a diagonal form. This A is related to the symplectic matrix S in Williamson's theorem via $A = S^T$.

As was mentioned in the introductory chapter, a proper ansatz for the Gaussian reduced density operator ρ_L is given by:

$$\rho_L = Ke^{-\mathcal{H}} \tag{3.6}$$

where K is a normalization constant and where $\mathcal{H}$ is the entanglement Hamiltonian, given by:

$$\mathcal{H} = \sum_l \epsilon_l a_l^\dagger a_l \tag{3.7}$$

with $a_l^\dagger$ and a_l bosonic creation and annihilation operators satisfying $[a_l, a_{l'}^\dagger] = \delta_{ll'}$. K is hence determined by:

$$K = \prod_l (1 - e^{-\epsilon_l}) \tag{3.8}$$

As ρ_L is supposed to be a Gaussian state, the creation and annihilation operators should be related linearly to the fields $\{\tilde{R}_i\}$, *i.e.*:

$$\left(\begin{array}{c} \tilde{\phi} \\ \hline \tilde{\pi} \end{array}\right) = \left(\begin{array}{c|c} A & B \\ \hline C & D \end{array}\right) \left(\begin{array}{c} a^\dagger \\ \hline a \end{array}\right) \tag{3.9}$$

where $\tilde{\phi}$ and $\tilde{\pi}$ are column vectors containing the various fields and similar for $a^\dagger$ and a. Due to the fact that the fields are Hermitian, one immediately obtains that $B = A^*$ and $D = C^*$. In accordance to the paper of Casini and Huerta,[23] we therefore choose $A = \alpha^*$, $B = \alpha$, $C = -i\beta^*$ and $D = i\beta$. The commutation relations between fields and conjugate momenta then yield:

$$\alpha\beta^\dagger + \alpha^*\beta^T = -I \tag{3.10}$$

Furthermore, the following must apply:

$$\begin{aligned}
\Omega_{ij} = \langle \frac{1}{2}\{\tilde{\phi}_i, \tilde{\phi}_j\}\rangle = \mathrm{tr}(\rho_L \tilde{\phi}_i \tilde{\phi}_j) \quad &\Rightarrow \quad \Omega = \alpha^* \langle n \rangle \alpha^T + \alpha(\langle n \rangle + 1)\alpha^\dagger \\
\Omega_{ij} = \langle \frac{1}{2}\{\tilde{\pi}_i, \tilde{\pi}_j\}\rangle = \mathrm{tr}(\rho_L \tilde{\pi}_i \tilde{\pi}_j) \quad &\Rightarrow \quad \Omega = \beta^* \langle n \rangle \beta^T + \beta(\langle n \rangle + 1)\beta^\dagger \\
0 = \langle \frac{1}{2}\{\tilde{\phi}_i, \tilde{\pi}_j\}\rangle = \mathrm{tr}(\rho_L \frac{1}{2}\{\tilde{\phi}_i, \tilde{\pi}_j\}) \quad &\Rightarrow \quad \frac{1}{2}\alpha^*(2\langle n \rangle + 1)\beta^T = \frac{1}{2}\alpha(2\langle n \rangle + 1)\beta^\dagger
\end{aligned} \tag{3.11}$$

where $\langle n \rangle$ is a diagonal matrix containing the expectation values of the occupation numbers, *i.e.*:

$$\langle n \rangle_{ll} = \langle a_l^\dagger a_l \rangle = (e^{\epsilon_l} - 1)^{-1} \tag{3.12}$$

As a result, $\alpha = \tilde{\alpha}U$ and $\beta = \tilde{\beta}U$ with U unitary and diagonal, and $\tilde{\alpha}$ and $\tilde{\beta}$ real. The matrix of phases U can be absorbed in the definition of the annihilators so that one can choose α and β real. Equation (3.10) then gives $\alpha = -\frac{1}{2}\left(\beta^T\right)^{-1}$ while the third equation in (3.11) is automatically satisfied. The other two equations reduce to:

$$\begin{aligned}
\Omega &= \alpha(2\langle n \rangle + 1)\alpha^T \\
\Omega &= \beta(2\langle n \rangle + 1)\beta^T
\end{aligned} \tag{3.13}$$

Multiplying these then yields:

$$\Omega^2 = \alpha(2\langle n\rangle + 1)^2\alpha^{-1} \tag{3.14}$$

The entanglement energies are hence related to the symplectic eigenvalues of C via:

$$\omega_l = \frac{1}{2}\coth\frac{\epsilon_l}{2} \tag{3.15}$$

and α should be diagonal. Combining this with (3.13) implies that $\alpha = \frac{1}{\sqrt{2}}I$ and $\beta = -\frac{1}{\sqrt{2}}I$ and thus that:

$$a_l = \frac{1}{\sqrt{2}}(\tilde{\phi}_l + i\tilde{\pi}_l) \tag{3.16}$$

allowing to rewrite the entanglement Hamiltonian as:

$$\begin{aligned}
\mathcal{H} &= \sum_l \epsilon_l a_l^\dagger a_l \\
&= \sum_l \frac{\epsilon_l}{2}(\tilde{\phi_l}^2 + \tilde{\pi}_l^2) - \sum_l \frac{\epsilon_l}{2} \\
&= \begin{pmatrix} \tilde{\phi} \\ \hline \tilde{\pi} \end{pmatrix}^T \left(\begin{array}{c|c} \frac{\epsilon}{2} & 0 \\ \hline 0 & \frac{\epsilon}{2} \end{array}\right) \begin{pmatrix} \tilde{\phi} \\ \hline \tilde{\pi} \end{pmatrix} \\
&= \begin{pmatrix} \tilde{\phi} \\ \hline \tilde{\pi} \end{pmatrix}^T \left(\begin{array}{c|c} \frac{1}{2}\ln\left(\frac{\Omega+\frac{1}{2}}{\Omega-\frac{1}{2}}\right) & 0 \\ \hline 0 & \frac{1}{2}\ln\left(\frac{\Omega+\frac{1}{2}}{\Omega-\frac{1}{2}}\right) \end{array}\right) \begin{pmatrix} \tilde{\phi} \\ \hline \tilde{\pi} \end{pmatrix} \\
&= \begin{pmatrix} \phi \\ \hline \pi \end{pmatrix}^T S \left(\begin{array}{c|c} \frac{1}{2}\ln\left(\frac{\Omega+\frac{1}{2}}{\Omega-\frac{1}{2}}\right) & 0 \\ \hline 0 & \frac{1}{2}\ln\left(\frac{\Omega+\frac{1}{2}}{\Omega-\frac{1}{2}}\right) \end{array}\right) S^T \begin{pmatrix} \phi \\ \hline \pi \end{pmatrix}
\end{aligned} \tag{3.17}$$

where ϵ is the diagonal matrix containing the entanglement energies and where going from the second to the third line, the second term was absorbed in the K factor of the reduced density operator. In the last line, the symplectic matrix S from Williamson's theorem was introduced. Furthermore, the entanglement entropy can be derived from the entanglement Hamiltionan as follows:

$$\begin{aligned}
S &= -\mathrm{tr}(\rho_L \ln \rho_L) \\
&= -\ln K + K\mathrm{tr}(e^{-\mathcal{H}}\mathcal{H}) \\
&= \sum_l \left(-\ln(1-e^{-\epsilon_l}) + \frac{\epsilon_l e^{-\epsilon_l}}{1-e^{-\epsilon_l}}\right) \\
&= \sum_l \left[\left(\omega_l + \frac{1}{2}\right)\ln\left(\omega_l + \frac{1}{2}\right) - \left(\omega_l - \frac{1}{2}\right)\ln\left(\omega_l - \frac{1}{2}\right)\right]
\end{aligned} \tag{3.18}$$

One thus concludes that for Gaussian states on a lattice, the entanglement entropy and entanglement Hamiltonian can be calculated relatively easily once the Williamson decomposition of the C matrix is found.

For the states treated in this work, the derivation of entanglement properties can be simplified to some extent as the correlation matrix has a block-diagonal form. Indeed, the S and Ω matrix

are calculated by considering the eigenvalue problem of JC, whose eigenvalues are determined by:

$$\det(JC - \lambda I) = \det\left(\begin{array}{c|c} -\lambda I & P \\ \hline -X & -\lambda I \end{array}\right) = \det(\lambda^2 I + PX) \tag{3.19}$$

implying that the symplectic eigenvalues are given by the (positive) eigenvalues of $\sqrt{PX}$ and/or $\sqrt{XP}$. Furthermore, the eigenvectors of JC occur in pairs $e_l \pm i f_l$ for the eigenvalues $\lambda_l = \pm i\omega_l$, implying that:

$$JC(e_l \pm i f_l) = \pm i\omega_l (e_l \pm i f_l) \quad \Rightarrow \quad \begin{array}{l} JCe_l = -\omega_l f_l \\ JCf_l = \omega_l e_l \end{array} \quad \Rightarrow \quad \begin{array}{l} (JC)^2 e_l = -\omega_l^2 e_l \\ (JC)^2 f_l = -\omega_l^2 f_l \end{array} \tag{3.20}$$

Since $(JC)^2$ is given by:

$$(JC)^2 = \left(\begin{array}{c|c} -PX & 0 \\ \hline 0 & -XP \end{array}\right) \tag{3.21}$$

the e_l vectors are hence composed of the $\mathbb{R}^n$ eigenvectors of PX completed with n zeros while the f_l vectors consist of n zeros completed by the $\mathbb{R}^n$ eigenvectors of XP. As was stated in Williamson's theorem, these eigenvectors should also be orthonormal w.r.t. $\langle\,.\,,\,.\,\rangle_C = \langle\,.\,,\,C\,.\,\rangle$, implying that:

$$\begin{array}{ll} \left(E^T \,|\, 0\right) \left(\begin{array}{c|c} X & 0 \\ \hline 0 & P \end{array}\right) \left(\begin{array}{c} E \\ \hline 0 \end{array}\right) = \left(\begin{array}{c|c} I & 0 \\ \hline 0 & I \end{array}\right) & \Rightarrow \quad E^T X E = I \\ \left(0 \,|\, F^T\right) \left(\begin{array}{c|c} X & 0 \\ \hline 0 & P \end{array}\right) \left(\begin{array}{c} 0 \\ \hline F \end{array}\right) = \left(\begin{array}{c|c} I & 0 \\ \hline 0 & I \end{array}\right) & \Rightarrow \quad F^T P F = I \end{array} \tag{3.22}$$

where E and F are matrices with $\{e_l\}$ respectively $\{f_l\}$ as columns. The matrix S can thus be constructed by determining a complete set of eigenvectors for both XP and PX, orthogonalizing these so that equation (3.22) holds (e.g. by a Gram-Schmidt procedure), after which S is given by:

$$S = \left(\begin{array}{c|c} 0 & E\sqrt{\Omega} \\ \hline F\sqrt{\Omega} & 0 \end{array}\right) \tag{3.23}$$

where Ω can be constructed via the eigenvalues of XP and/or PX. One verifies that S is the correct matrix as follows:

$$S^T C S = \left(\begin{array}{c|c} \sqrt{\Omega} E^T X E \sqrt{\Omega} & 0 \\ \hline 0 & \sqrt{\Omega} F^T P F \sqrt{\Omega} \end{array}\right) = \left(\begin{array}{c|c} \Omega & 0 \\ \hline 0 & \Omega \end{array}\right) \tag{3.24}$$

That S is symplectic, comes down to the following requirement:

$$S^T J S = \left(\begin{array}{c|c} 0 & -\sqrt{\Omega} F^T E \sqrt{\Omega} \\ \hline \sqrt{\Omega} E^T F \sqrt{\Omega} & 0 \end{array}\right) = \left(\begin{array}{c|c} 0 & I \\ \hline -I & 0 \end{array}\right) \quad \Rightarrow \quad F^T E = E^T F = -\Omega^{-1} \tag{3.25}$$

This condition is met since $PXE = E\Omega^2$ implies that E^T are the left eigenvectors of XP while $XPF = F\Omega^2$ implies that F^T are the left eigenvectors of PX. As a result, $F^T E = E^T F$ is a diagonal matrix and thus:

$$E^T F \Omega^2 = E^T X P F = E^{-1} F^{-1^T} \quad \Rightarrow \quad F^T E = E^T F = \pm \Omega^{-1} \tag{3.26}$$

With the construction described above, one thus simply has to choose the minus sign. A straightforward implication is that:

$$\begin{aligned} XE &= -F\Omega \\ PF &= -E\Omega \end{aligned} \tag{3.27}$$

Although seemingly contradicting equation (3.20), this comes down to the fact that F should be built up by the $\{-f_l\}$ vectors rather than $\{f_l\}$. This technicality hence poses no problem if one simply chooses the sign convention $F^TE = E^TF = -\Omega^{-1}$.

With the method discussed above, one can construct the S and Ω matrices from Williamson's theorem by diagonalizing XP and PX. The entanglement entropy is then found via the eigenvalues and the entanglement Hamiltonian is given by:

$$\begin{aligned} \mathcal{H} &= \left(\frac{\phi}{\pi}\right)^T \left(\begin{array}{c|c} 0 & E\sqrt{\Omega} \\ \hline F\sqrt{\Omega} & 0 \end{array}\right) \left(\begin{array}{c|c} \frac{1}{2}\ln\left(\frac{\Omega+\frac{1}{2}}{\Omega-\frac{1}{2}}\right) & 0 \\ \hline 0 & \frac{1}{2}\ln\left(\frac{\Omega+\frac{1}{2}}{\Omega-\frac{1}{2}}\right) \end{array}\right) \left(\begin{array}{c|c} 0 & \sqrt{\Omega}F^T \\ \hline \sqrt{\Omega}E^T & 0 \end{array}\right) \left(\frac{\phi}{\pi}\right) \\ &= \phi^T E \left[\frac{1}{2}\Omega \ln\left(\frac{\Omega+\frac{1}{2}}{\Omega-\frac{1}{2}}\right)\right] E^T\phi + \pi^T F \left[\frac{1}{2}\Omega \ln\left(\frac{\Omega+\frac{1}{2}}{\Omega-\frac{1}{2}}\right)\right] F^T\pi \\ &= \phi^T M\phi + \pi^T N\pi \end{aligned} \tag{3.28}$$

where the prefactor matrices M and N are defined as:

$$\begin{aligned} M &= E\left[\frac{1}{2}\Omega \ln\left(\frac{\Omega+\frac{1}{2}}{\Omega-\frac{1}{2}}\right)\right] E^T = P\frac{1}{2\sqrt{XP}}\ln\left(\frac{\sqrt{XP}+\frac{1}{2}}{\sqrt{XP}-\frac{1}{2}}\right) \\ N &= F\left[\frac{1}{2}\Omega \ln\left(\frac{\Omega+\frac{1}{2}}{\Omega-\frac{1}{2}}\right)\right] F^T = \frac{1}{2\sqrt{XP}}\ln\left(\frac{\sqrt{XP}+\frac{1}{2}}{\sqrt{XP}-\frac{1}{2}}\right) X \end{aligned} \tag{3.29}$$

A large downside of the proposed method in light of computational calculations, is the fact that both XP and PX are not symmetric. This problem can be solved relatively easily by considering $\sqrt{C}J\sqrt{C}$ instead of JC. Both have the same eigenvalues and their eigenvectors are related via $\tilde{U} = \sqrt{C}U$ with U containing the eigenvectors of JC and $\tilde{U}$ those of $\sqrt{C}J\sqrt{C}$, indeed:

$$\sqrt{C}J\sqrt{C}\tilde{U} = \sqrt{C}JCU = \sqrt{C}UD = \tilde{U}D \tag{3.30}$$

where D is the diagonal matrix containing the eigenvalues of JC. Rather than diagonalizing JC, we can thus diagonalize $\sqrt{C}J\sqrt{C}$:

$$\sqrt{C}J\sqrt{C} = \left(\begin{array}{c|c} 0 & \sqrt{XP} \\ \hline -\sqrt{PX} & 0 \end{array}\right) \quad \Rightarrow \quad (\sqrt{C}J\sqrt{C})^2 = \left(\begin{array}{c|c} -\sqrt{X}P\sqrt{X} & 0 \\ \hline 0 & -\sqrt{P}X\sqrt{P} \end{array}\right) \tag{3.31}$$

For the diagonalization of this matrix, an analysis almost identical to that of JC applies. One can thus diagonalize $\sqrt{X}P\sqrt{X}$ and $\sqrt{P}X\sqrt{P}$ (both symmetric!) after which the square roots of the positive eigenvalues are placed in the diagonal matrix Ω. The eigenvectors make up the matrices $\tilde{E}$ and $\tilde{F}$, related to E and F via:

$$\left(\begin{array}{c|c} 0 & \tilde{E} \\ \hline \tilde{F} & 0 \end{array}\right) = \left(\begin{array}{c|c} \sqrt{X} & 0 \\ \hline 0 & \sqrt{P} \end{array}\right) \left(\begin{array}{c|c} 0 & E \\ \hline F & 0 \end{array}\right) \quad \Rightarrow \quad \begin{aligned} \tilde{E} &= \sqrt{X}E \\ \tilde{F} &= \sqrt{P}F \end{aligned} \tag{3.32}$$

so that the entanglement Hamiltonian prefactors are given by:

$$\begin{aligned} M &= X^{-\frac{1}{2}} E \left[\frac{1}{2} \Omega \ln \left(\frac{\Omega + \frac{1}{2}}{\Omega - \frac{1}{2}} \right) \right] E^T X^{-\frac{1}{2}} \\ N &= P^{-\frac{1}{2}} F \left[\frac{1}{2} \Omega \ln \left(\frac{\Omega + \frac{1}{2}}{\Omega - \frac{1}{2}} \right) \right] F^T P^{-\frac{1}{2}} \end{aligned} \tag{3.33}$$

A last note concerns the normalization of the eigenvectors in $\tilde{E}$ and $\tilde{F}$. The orthonormality requirement in equation (3.22) comes down to $\tilde{E}^T \tilde{E} = \tilde{F}^T \tilde{F} = I$, *i.e.* the eigenvectors should simply be orthonormal w.r.t. the standard scalar product.

3.1.2 Analytical Generalization

As cMERA states are defined directly in the continuum, an analytical generalization of the discrete analysis presented in the previous paragraph is desired. This can be realized by replacing all discrete quantities by their continuous variants (with correct physical dimensions), *i.e.* for instance:

$$\begin{aligned} \phi_i &\quad \leftrightarrow \quad \phi(x) \\ \frac{\pi_i}{a} &\quad \leftrightarrow \quad \pi(x) \\ F_{ij} = a \sum_{l=1}^{n} G_{il} H_{lj} &\quad \leftrightarrow \quad F(x,y) = \int_L G(x,w) H(w,y) dw \\ & \qquad \text{(if } G_{ij} \leftrightarrow G(x,y) \text{ and } H_{ij} \leftrightarrow H(x,y)) \end{aligned} \tag{3.34}$$

Consequently, the eigenvalue problems of XP and PX, or equivalently the left and right eigenvalue problems of XP, generalize to:

$$\begin{aligned} \int_L \int_L X(x,w) P(w,y) \kappa_l^R(y) dw dy &= \omega_l^2 \kappa_l^R(x) \\ \int_L \int_L \kappa_l^L(x) X(x,w) P(w,y) dw dx &= \omega_l^2 \kappa_l^L(y) \end{aligned} \tag{3.35}$$

where the upper indices are used to indicate left and right eigenvectors and where $X(x,y)$ and $P(x,y)$ now encode the two-point correlators of the fields as determined in Chapter 2:

$$\begin{aligned} X(x,y) &= \langle \phi(x) \phi(y) \rangle \\ &= \int_{-\infty}^{+\infty} \frac{dk}{\sqrt{2\pi}} \int_{-\infty}^{+\infty} \frac{dq}{\sqrt{2\pi}} e^{ikx} e^{iqy} \langle \phi(k) \phi(q) \rangle \\ &= \int_{-\infty}^{+\infty} \frac{dk}{\sqrt{2\pi}} \int_{-\infty}^{+\infty} \frac{dq}{\sqrt{2\pi}} e^{ikx} e^{iqy} \frac{1}{2\alpha(k)} \delta(k+q) \\ &= \int_{-\infty}^{+\infty} \frac{dk}{2\pi} e^{ik(x-y)} \frac{1}{2\alpha(k)} \\ &= \frac{1}{2\Delta} \delta(x-y) + \int_{-\infty}^{+\infty} \frac{dk}{2\pi} e^{ik(x-y)} \left(\frac{1}{2\alpha(k)} - \frac{1}{2\Delta} \right) \\ &= \frac{1}{2\Delta} \delta(x-y) + \int_{0}^{+\infty} \frac{dk}{2\pi} \cos(k(x-y)) \left(\frac{1}{\alpha(k)} - \frac{1}{\Delta} \right) \end{aligned} \tag{3.36}$$

$$\begin{aligned} P(x,y) &= \langle \pi(x)\pi(y) \rangle \\ &= \int_{-\infty}^{+\infty} \frac{dk}{2\pi} e^{ik(x-y)} \frac{\alpha(k)}{2} \\ &= \frac{\Delta}{2}\delta(x-y) + \int_{0}^{+\infty} \frac{dk}{2\pi} \cos(k(x-y)) \left(\alpha(k) - \Delta\right) \end{aligned} \tag{3.37}$$

In the massless case, the integrals for $X(x,y)$ are divergent due to a singularity in the integrands at $k = 0$. There are two ways to deal with this divergence. On the one hand, one could introduce a small IR regulator ζ, removing the interval $[-\zeta\Lambda, \zeta\Lambda]$ from the integration range. On the other hand, one could include a mass and by taking this mass to be small, the massless theory could be approximated. In both cases, the resulting correlators satisfy the continuous analogues of the matrix requirements mentioned in Section 3.1.1. As a result, the entanglement entropy can be calculated from the symplectic eigenvalues ω_l via:

$$S = \sum_l \left[\left(\omega_l + \frac{1}{2}\right) \ln\left(\omega_l + \frac{1}{2}\right) - \left(\omega_l - \frac{1}{2}\right) \ln\left(\omega_l - \frac{1}{2}\right) \right] \tag{3.38}$$

while the modular Hamiltonian is determined via the analytical generalization of equation (3.29):

$$\begin{aligned} M(x,y) &= \int_L P(x,w) \sum_l \frac{1}{2\omega_l} \ln\left(\frac{\omega_l + \frac{1}{2}}{\omega_l - \frac{1}{2}}\right) \kappa_l^L(w)\kappa_l^R(y) dw \\ &= \sum_l \psi(\omega_l) \left[\int_L P(x,w)\kappa_l^L(w) dw\right] \kappa_l^R(y) \\ N(x,y) &= \int_L \sum_l \frac{1}{2\omega_l} \ln\left(\frac{\omega_l + \frac{1}{2}}{\omega_l - \frac{1}{2}}\right) \kappa_l^L(x)\kappa_l^R(w) X(w,y) dw \\ &= \sum_l \psi(\omega_l)\kappa_l^L(x) \left[\int_L \kappa_l^R(w) X(w,y) dw\right] \end{aligned} \tag{3.39}$$

where everything is properly defined as long as $\omega_l > \frac{1}{2}$ and where the function $\psi(\omega)$ is given by:

$$\psi(\omega) = \frac{1}{2\omega} \ln\left(\frac{\omega + \frac{1}{2}}{\omega - \frac{1}{2}}\right) \tag{3.40}$$

Although generally valid, the eigenvalue problem in equation (3.35) can rarely be solved analytically. Yet it is possible to solve the equations in some specific cases. A product state reduced to the interval $\left[-\frac{L}{2}, \frac{L}{2}\right]$ for instance, has $\alpha(k) = \Delta$ for all $k \in \mathbb{R}$ and hence:

$$X(x,y) = \frac{1}{2\Delta}\delta(x-y) \qquad P(x,y) = \frac{\Delta}{2}\delta(x-y) \tag{3.41}$$

For these two-point correlator functions, the left and right eigenvalue problems are equivalent and yield:

$$0 = \left(\omega_l^2 - \frac{1}{4}\right) \kappa_l(x) \tag{3.42}$$

I.e. all symplectic eigenvalues are equal to $\frac{1}{2}$ and the corresponding eigenspace is the complete function space $L^2\left(\left[-\frac{L}{2}, \frac{L}{2}\right]\right)$. Consequently, the entanglement entropy of a product state is equal to zero (as it should be) and the entanglement Hamiltonian diverges. Indeed, $\psi\left(\frac{1}{2}\right) = +\infty$

and the contribution of each symplectic eigenvalue to $M(x,y)$ and $N(x,y)$ is hence divergent. Analytical calculations can also be carried out for cMERA states close to the product state, *i.e.* in the limit $\Lambda L \ll 1$. Indeed, in this case $X(x,y)$ and $P(x,y)$ only have to be evaluated in points where $k|x-y| \leq kL \ll k\Lambda^{-1}$, making it possible to approximate the cosines in equation (3.36) by one since the second factor in the integrands becomes very small (or zero) for $k > \Lambda$. One hence obtains the following two-point correlators:

$$\begin{aligned} X(x,y) &= \frac{1}{2\Delta}\delta(x-y) + \int_0^{+\infty} \frac{dk}{2\pi}\left(\frac{1}{\alpha(k)} - \frac{1}{\Delta}\right) = \frac{1}{2\Delta}\delta(x-y) + A \\ P(x,y) &= \frac{\Delta}{2}\delta(x-y) + \int_0^{+\infty} \frac{dk}{2\pi}\left(\alpha(k) - \Delta\right) = \frac{\Delta}{2}\delta(x-y) + B\Delta^2 \end{aligned} \tag{3.43}$$

where A and B are both dimensionless and do not depend on ΔL. Substituting this in equation (3.35), the eigenvalue problem is again symmetric and given by:

$$\int_L C(x,y)\kappa_l(y)dy = \left(\frac{\Delta}{2}A + \frac{\Delta}{2}B + AB\Delta^2 L\right)\int_{-\frac{L}{2}}^{\frac{L}{2}} \kappa_l(y)dy = \left(\omega_l^2 - \frac{1}{4}\right)\kappa_l(x) \tag{3.44}$$

The solutions of this equation consist on the one hand of all $L^2\left(\left[-\frac{L}{2},\frac{L}{2}\right]\right)$ functions, that integrate to zero on L, with eigenvalue $\omega_l = \frac{1}{2}$ and on the other hand of the constant functions with eigenvalue:

$$\omega_0 = \sqrt{\frac{1}{4} + \frac{\Delta L}{2}A + \frac{\Delta L}{2}B + (\Delta L)^2 AB} \geq \frac{1}{2} \tag{3.45}$$

We thus find that an infinite number of the eigenvalues remains $\frac{1}{2}$ (as in the product state) while one eigenvalue becomes larger than $\frac{1}{2}$. The former yield no contribution to the entanglement entropy and correspond to divergent contributions to the entanglement Hamiltonian. The latter on the other hand, yields an entanglement entropy larger than zero:

$$S = S(\omega_0) = \left(\omega_0 + \frac{1}{2}\right)\ln\left(\omega_0 + \frac{1}{2}\right) - \left(\omega_0 - \frac{1}{2}\right)\ln\left(\omega_0 - \frac{1}{2}\right) \tag{3.46}$$

Furthermore, the entanglement Hamiltonian receives a non-divergent and uniform contribution:

$$\begin{aligned} M_0(x,y) &= \psi(\omega_0)\left[\int_L P(x,w)\kappa^L dw\right]\kappa^R = -\frac{\Delta}{L}\ln\left[(A+B)\frac{\Delta L}{2}\right] \\ N_0(x,y) &= \psi(\omega_0)\kappa^L\left[\int_L \kappa^R X(w,y)dw\right] = \frac{-1}{\Delta L}\ln\left[(A+B)\frac{\Delta L}{2}\right] \end{aligned} \tag{3.47}$$

where $\kappa_0^L(x) = \kappa^L$ and $\kappa_0^R(x) = \kappa^R$ are both constant but should be normalized differently. Indeed, according to equation (3.22) one obtains:

$$\begin{aligned} \int_L dx \int_L dy \kappa^L X(x,y)\kappa^L = 1 \quad &\Rightarrow \quad \kappa^L = \left(\frac{L}{2\Delta} + AL^2\right)^{-\frac{1}{2}} \\ \int_L dx \int_L dy \kappa^R P(x,y)\kappa^R = 1 \quad &\Rightarrow \quad \kappa^R = \left(\frac{\Delta L}{2} + B(\Delta L)^2\right)^{-\frac{1}{2}} \end{aligned} \tag{3.48}$$

This approach can also be extended to higher-order Taylor approximations for the two-point correlators. The resulting eigenvalue problem will then amount to the diagonalization of higher-order matrices, yielding even more symplectic eigenvalues greater than $\frac{1}{2}$. These newly obtained

symplectic eigenvalues are typically smaller than those found via lower-order Taylor series. Increasing the approximation order towards infinity hence yields the picture of an array, decreasing to $\frac{1}{2}$, for the symplectic spectrum. As the analytical determination of eigenvalues is only possible up to 4×4 matrices, numerical diagonalization methods should be applied for their computation once the Taylor expansions contain more than 4 terms. However, the convergence of these Taylor series is very slow when $L\Lambda \gtrsim 1$. As a result, the Taylor approach is typically only applicable for $\Lambda L \ll 1$ where eigenvalues and eigenvectors can be calculated analytically. For higher ΛL, the encountered matrix eigenvalue problems are computationally intractable due to the elevated number of terms in the Taylor series required for convergence.

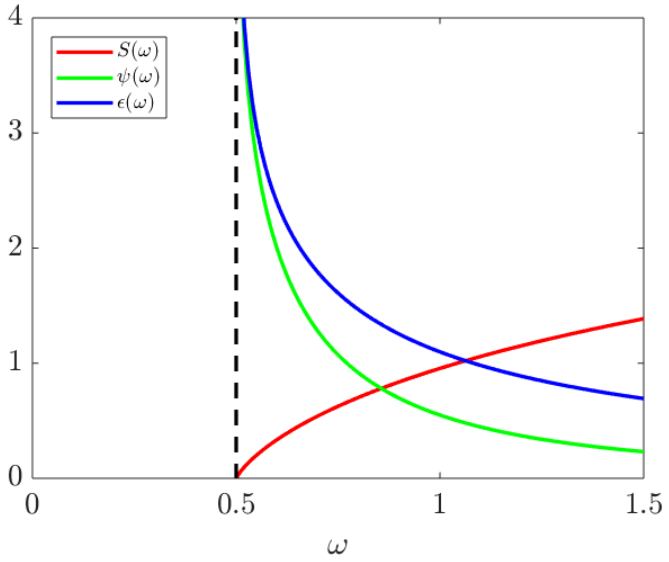

Figure 3.1: Comparison between the entanglement entropy contribution $S(\omega)$, the factor $\psi(\omega)$ and the entanglement energy $\epsilon(\omega)$ for symplectic eigenvalue ω.

In conclusion, one could say that even though the applicability of the continuous eigenvalue problem is relatively limited, it gives insight in how the symplectic eigenvalues (and thus the entanglement properties) change as function of the cMERA cut-off Λ. Indeed, for the product state ($\Lambda L = 0$), all symplectic eigenvalues are equal to $\frac{1}{2}$ so that the entanglement entropy is zero while all contributions to the entanglement Hamiltonian are divergent. Once $\Lambda L > 0$ on the other hand, the symplectic spectrum constitutes a decreasing array, converging to $\frac{1}{2}$. As a result, multiple eigenvalues contribute to the entanglement entropy. However, as Figure 3.1 illustrates, only the highest symplectic eigenvalues have a substantial influence. Increasing ΛL, the symplectic eigenvalues typically increase as well (*cfr.* equation (3.45)). By virtue of Figure 3.1, one therefore concludes that the entanglement entropy is a monotonically increasing function of ΛL. For the entanglement Hamiltonian $\mathcal{H}$ on the other hand, Figure 3.1 shows that the lowest symplectic eigenvalues have the largest influence. A decreasing symplectic spectrum thus leads to an array of increasing contributions for the entanglement Hamiltonian. However, this does not necessarily imply that $\mathcal{H}$ is divergent as for the product state. Indeed, in the next paragraph we will show that the modular Hamiltonian is non-divergent and purely local for CFT ground states. Casini *et al.* on the other hand found that even for such a CFT ground

state, the symplectic spectrum is an array quickly decreasing towards $\frac{1}{2}$.[24] Both results can be reconciled by the fact that the purely local entanglement Hamiltonian contains delta functions. The increasing $\mathcal{H}$ contributions thus pile up to approximate the delta functions without yielding a divergent entanglement Hamiltonian. For cMERA states, however, we expect this not to be the case. Indeed, as the unitary cMERA evolution only introduces fluctuations for length-scales larger than $\epsilon \approx \Lambda^{-1}$, the resulting state will still behave as a product state for length scales smaller than ϵ. We expect his "product state part" of the cMERA state to introduce symplectic values equal to $\frac{1}{2}$, thus making the entanglement Hamiltonian diverge. Note that a similar picture was also obtained via the lowest-order Taylor approach where only for the largest length scales (lowest Taylor order) a non-divergent contribution to the modular Hamiltonian was found while all other contributions (corresponding to smaller length scales) remained divergent. A proper way to deal with this divergent behavior will be discussed in the next section.

In the previous paragraph, it was mentioned that the entanglement Hamiltonian for CFT ground states, reduced to the interval L, is non-divergent and purely local. Here this will be proved together with some other useful analytical results, yielding approximations for both (Rényi) entanglement entropies and modular Hamiltonians in the high ΛL limit of cMERAs. First, we show that the entanglement Hamiltonian of a general CFT ground state reduced to the interval $[a, b]$ is given by:

$$\mathcal{H} = 2\pi \int_a^b dx \frac{(x-a)(b-x)}{(b-a)} \mathcal{T}_{00}(x) \tag{3.49}$$

where $\mathcal{T}_{00}(x)$ is the energy density of the CFT. The ground state CFT wave functional can be found by evolving a state in time from $t = -\infty$ to $t = 0$. Analogously, its conjugate is found by evolving from $t = +\infty$ to $t = 0$. In the complex Euclidean space-time plane (where the time t is replaced by the imaginary time $\tau = it$), this comes down to an evolution from the bottom ($z = x - i\infty$) up to $z = x$ and from the top ($z = x + i\infty$) down to $z = x$ for all $x \in \mathbb{R}$. Sewing these two functionals together along the real line then yields the trace of the corresponding density operator. However, for $\rho_{[a,b]}$ the trace should only be taken for the degrees of freedom outside $[a, b]$ and the wave functional and its conjugate are hence only sewed together outside of $[a, b]$. To calculate the remaining path integral, the following conformal transformation is applied:

$$w(z) = u(z) + iv(z) = \ln\left(\frac{z-a}{b-z}\right) \tag{3.50}$$

mapping the complex plane without $[a, b]$ to a cylinder. Indeed, the boundary points are transformed to $-\infty$ and $+\infty$ respectively. The interval $[a, b]$ approximated from above on the other hand, is mapped to $\{x + 0i \,|\, x \in \mathbb{R}\}$ while approximating from below yields $\{x + 2\pi i \,|\, x \in \mathbb{R}\}$. As Figure 3.2 shows, the resulting domain is an infinite rectangle with width 2π in the imaginary direction.

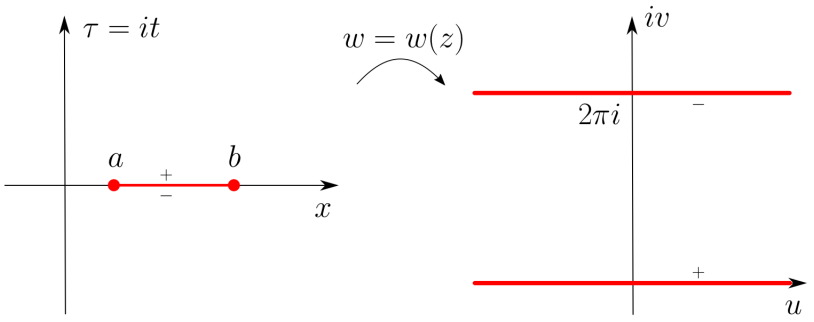

Figure 3.2: Illustration of the conformal transformation $w(z)$ mapping $\mathbb{C}\backslash[a,b]$ to a cylinder.

Within this setup, the path integral can easily be calculated:

$$\rho_{[a,b]} = K \exp\left[-2\pi \int_{\mathbb{R}} \mathcal{T}_{vv} du\right] \tag{3.51}$$

Invoking the fact that the reduced density operator for the CFT ground state is invariant under conformal transformations, the integration variable can be changed by inverting the conformal transformation:

$$\begin{aligned} \rho_{[a,b]} &= K \exp\left[-2\pi \int_{\mathbb{R}} \mathcal{T}_{vv}(u) du\right] \\ &= K \exp\left[-2\pi \int_a^b \frac{\mathcal{T}_{tt}(x)}{\left(\frac{du}{dx}\right)^2} \frac{du}{dx} dx\right] \\ &= K \exp\left[-2\pi \int_a^b \frac{(x-a)(b-x)}{(b-a)} \mathcal{T}_{00}(x) dx\right] \end{aligned} \tag{3.52}$$

This clearly agrees with the entanglement Hamiltonian in equation (3.49). For a massless Klein-Gordon theory in (1+1) dimensions, the modular Hamiltonian corresponding to the symmetric interval $\left[-\frac{L}{2}, \frac{L}{2}\right]$ thus reads:

$$\mathcal{H} = \int_{-\frac{L}{2}}^{\frac{L}{2}} dx \frac{\pi}{L} \left(\frac{L^2}{4} - x^2\right) \left(\pi^2(x) + \left(\frac{d}{dx}\phi(x)\right)^2\right) \tag{3.53}$$

Choosing the interval $[0, +\infty]$ on the other hand, the entanglement Hamiltonian is given by:

$$\mathcal{H} = 2\pi \int_0^{+\infty} x \mathcal{T}_{00}(x) dx \tag{3.54}$$

This result (also known as the Bisognano-Wichmann theorem) is more generally valid for massive field theories and also for higher dimensions due to analyticity properties originating from Lorentz invariance and positivity of energy. It is also tightly related to the CPT theorem.[51] As was mentioned by Cardy and Tonni in their paper concerning entanglement Hamiltonians in two-dimensional conformal field theory,[52] the bipartition of the complete Hilbert space into subspaces corresponding to sharp spatial regions is not legitimate. This is because local operators are distribution-valued and must be smeared spatially against test functions. A possible way to deal with this difficulty is by only considering states in the Hilbert space which are projected onto a common eigenstate of a locally complete set of commuting observables in a small spatial

region of thickness ϵ around the boundary points of the interval. For the Euclidean path integral, this has the effect of introducing small slits around the boundary points a and b with radius ϵ. As a result, the image under the conformal transformation now is a finite rectangle with boundaries $-\ln\left(\frac{|a|}{\epsilon}\right)$ and $\ln\left(\frac{|b|}{\epsilon}\right)$ on the real axis. Although this finite width has no influence on the calculated CFT modular Hamiltonian, it allows to calculate (Rényi) entanglement entropies:

$$S_\beta = \frac{c}{6}\left(1+\frac{1}{\beta}\right)\ln(\Lambda L) \tag{3.55}$$

where $\Lambda = \epsilon^{-1}$ now serves as a UV cut-off.

3.1.3 Discretization Approach

As the Taylor approach, based on the analytical generalization of Section 3.1.1, cannot be used when $\Lambda L \gg 1$ due to the slow convergence of the relevant Taylor series in this regime, a numerical method, applicable in all regimes, will be introduced here. The main idea is to restrict the continuous QFT to an equidistant lattice with spacing a after which discrete calculations on the lattice can be performed as in Section 3.1.1. Finally taking the limit $a \to 0$ then yields the entanglement properties in the continuum. The first step in this discretization procedure consists of putting the continuous theory on the lattice, *i.e.* discrete scalar fields ϕ_i and conjugate momenta π_i are placed on the lattice sites x_i with $[\phi_i, \pi_j] = i\delta_{ij}$ as well as $[\phi_i, \phi_j] = 0$ and $[\pi_i, \pi_j] = 0$. For the two-point correlators, the following matrices are chosen, based on the analogy $\phi_i \leftrightarrow \phi(ia)$ and $\pi_i \leftrightarrow a\pi(ia)$ and corresponding to the continuous cMERA case:

$$\begin{aligned}
X_{ij} &= \langle \phi_i \phi_j \rangle \\
&\equiv \langle \phi(ia)\phi(ja)\rangle \\
&= \frac{1}{2\Delta}\frac{\delta_{ij}}{a} + \int_0^{+\infty}\frac{dk}{2\pi}\cos(ka(i-j))\left(\frac{1}{\alpha(k)}-\frac{1}{\Delta}\right) \\
P_{ij} &= \langle \pi_i \pi_j \rangle \\
&\equiv a^2\langle \pi(ia)\pi(ja)\rangle \\
&= \frac{a\Delta}{2}\delta_{ij} + a^2\int_0^{+\infty}\frac{dk}{2\pi}\cos(ka(i-j))\left(\alpha(k)-\Delta\right) \\
\langle \phi_i \pi_j \rangle &\equiv \frac{i}{2}\delta_{ij} = \langle \pi_j \phi_i \rangle^*
\end{aligned} \tag{3.56}$$

In this way, X and P are clearly real, symmetric and positive and $XP \geq \frac{1}{4}$. However, it is generally not true that $\sum_{l=-\infty}^{+\infty} X_{il}P_{lj} = \frac{1}{4}\delta_{ij}$. Indeed, working out this sum yields:

$$\begin{aligned}
\sum_{l=-\infty}^{+\infty} X_{il}P_{lj} &= \frac{a^2}{4}\int_{-\infty}^{+\infty}\frac{dk}{2\pi}\int_{-\infty}^{+\infty}\frac{dq}{2\pi}\frac{\alpha(q)}{\alpha(k)}e^{ia(ki-qj)}\sum_{l=-\infty}^{+\infty}e^{ial(q-k)} \\
&= \frac{a}{4}\int_{-\infty}^{+\infty}\frac{dk}{2\pi}e^{iak(i-j)} \\
&= \frac{a}{4}\delta(a(i-j))
\end{aligned} \tag{3.57}$$

which is generally not equal to $\frac{1}{4}\delta_{ij}$. However, when $a \to 0$, this is the case and therefore the discretized version of the cMERA state corresponds to a Gaussian state on the lattice. As a

result, the method outlined in the second part of Section 3.1.1 (*i.e.* with symmetrization) can be applied to this state when small lattice spacings are considered. Solving the resulting discrete eigenvalue problem, then yields a finite spectrum of symplectic eigenvalues, approximating the infinite spectrum of the continuous cMERA state, as well as a discretized version of the entanglement Hamiltonian prefactors. The smaller a is chosen, the more symplectic eigenvalues are obtained and the closer they get to their continuous cMERA value. On the other hand, decreasing a increases the resolution with which the entanglement Hamiltonian prefactors are probed, thus improving the correspondence to their continuous analogues.

While the so-called "standard discretization method" introduced above seems directly implementable, both practical and theoretical difficulties were encountered. Using the Taylor approach for instance, it was argued that the symplectic spectrum of cMERA states constitutes an array decreasing to $\frac{1}{2}$. Casini *et al.*[24] reported that this decrease even has an exponentially decaying tail for CFT ground states. Numerical calculations within the standard discretization approach show that also for finite a and Λ values, the symplectic spectrum is rapidly decreasing to $\frac{1}{2}$. As a result, it is generally hard to determine the lowest symplectic eigenvalues correctly as they get extremely close to $\frac{1}{2}$. This problem also aggravates for lower a values because a smaller lattice spacing implies more lattice points and thus more (small) symplectic eigenvalues. The only way to overcome these numerical difficulties is by increasing the working precision. However, we did not have the time nor the resources to perform high-precision calculations for the symplectic spectrum within the scope of this work. Consequently, only the highest symplectic eigenvalues and their eigenvectors could be determined correctly. Luckily, this does not pose any problem for the calculation of entanglement entropies. Indeed, the entanglement entropy is dominated by the highest symplectic eigenvalues (Figure 3.1). A correct determination of the smaller eigenvalues is hence unneeded and one can simply use the standard working precision to determine symplectic spectra for low a. The highest (and correctly determined) eigenvalues should then be utilized to calculate the entanglement entropy while the lower (incorrect) eigenvalues should be discarded. For the entanglement Hamiltonian on the other hand, the situation is more involved. Indeed, Figure 3.1 shows that the lower symplectic eigenvalues have a dominant influence on the entanglement Hamiltonian. Being unable to determine the lower symplectic eigenvalues correctly thus seems to preclude a profound study of the modular Hamiltonian for cMERA states. However, this is not entirely true. As mentioned before, we expect the entanglement Hamiltonian for cMERA states to diverge due to its inherent product state part when $\Lambda < +\infty$. Based on this argument and based on the well-known spectral structure of product states and CFT ground states, the following ansatz was proposed for the symplectic spectrum of cMERA states within the standard discretization approach:

$$\omega_l = \frac{1}{2} + ze^{-\frac{c}{a\Lambda}l} \qquad \text{for} \quad l \gg 1 \tag{3.58}$$

where z and c are unknown multiplicative constants. Although this behavior seems reasonable and reproduces the constant spectrum (equal to $\frac{1}{2}$) for the continuous product state (*i.e.* for $a = 0$ and $\Lambda = 0$) as well as the simple exponential tail for the continuous CFT ground state (*i.e.* for $a = 0$ and $\Lambda = +\infty$), a decisive verification of this ansatz was not yet obtained due to the aforementioned computational difficulties. However, all of the results presented in the

following sections seem to be in agreement with the proposed spectral structure and we will therefore assume the validity of equation (3.58) throughout the rest of this work. An immediate consequence of this ansatz is that in the continuum limit ($a = 0$) the tail of the symplectic spectrum consists exclusively of eigenvalues equal to $\frac{1}{2}$. *I.e.* over a finite number of eigenvalues the symplectic spectrum of cMERA states (with $\Lambda < +\infty$ and $a = 0$) decreases to $\frac{1}{2}$ after which it stays equal to this value. The intuitive notion that the unentangled, small length scale degrees of freedom yield symplectic eigenvalues equal to $\frac{1}{2}$ is hence supported by more quantitative argumentation. We conclude that even though we were not able to prove it decisively yet, we have strong indications that the entanglement Hamiltonian for cMERA states is indeed divergent and that these divergences stem from the inherent product state part of cMERAs with $\Lambda < +\infty$.

It is worthwhile to study the causes of the divergent behavior for the cMERA entanglement Hamiltonian more precisely. Again, we start our analysis from the symplectic spectrum with the presumed exponential tail in equation (3.58). Combining this spectral structure with equation (3.29), one obtains that both the M and N prefactor matrices scale proportionally to $\frac{1}{a\Lambda}$. Indeed:

$$\begin{Bmatrix} M_{ij} \\ N_{ij} \end{Bmatrix} \quad \sim \quad \psi(\omega_l) = \frac{1}{2\omega_l} \ln\left(\frac{\omega_l + \frac{1}{2}}{\omega_l - \frac{1}{2}}\right) \approx -\ln\left(ze^{-\frac{c}{a\Lambda}l}\right) \sim \frac{1}{a\Lambda} \tag{3.59}$$

Now consider the continuous $N(x, y)$ prefactor, related to its discretized analogue via:

$$N(ia, ja) \leftrightarrow N_{ij} \tag{3.60}$$

as $N(x, y)$ is dimensionless. The inversely proportional scaling of N_{ij} with $a\Lambda$ implies that also $N(x, y)$ will diverge for $a \to 0$ when $\Lambda < +\infty$, once again confirming that the proposed spectral structure causes the entanglement Hamiltonian to diverge. It also possible that $N(x, y)$ contains purely local contributions in the form of $\delta(x-y)$ terms. These give rise to the following entanglement Hamiltonian contributions:

$$\int_{-\frac{L}{2}}^{\frac{L}{2}} dx \int_{-\frac{L}{2}}^{\frac{L}{2}} dy N(x)\delta(x-y)\pi(x)\pi(y) = \int_{-\frac{L}{2}}^{\frac{L}{2}} dx N(x)\pi^2(x) \tag{3.61}$$

and their discretized analogue is hence given by:

$$\int_{-\frac{L}{2}}^{\frac{L}{2}} dx N(x)\pi^2(x) \leftrightarrow a \sum_{i=-\lfloor \frac{n}{2} \rfloor}^{\lfloor \frac{n}{2} \rfloor} N_i a \left(\frac{\pi_i}{a}\right)^2 \tag{3.62}$$

Indeed, $N(x)$ must have a length dimension for the entanglement Hamiltonian to be dimensionless and is thus related to its discrete analogue via $N(ia) \leftrightarrow aN_i$.[2] An immediate consequence is that the N_i are proportional to $\frac{Z}{a}$ with Z a macroscopic length scale (typically L). However, the discrete N_i are also proportional to $\frac{1}{a\Lambda}$ as they are a part of the N matrix. Indeed, numerical calculations will yield a single N matrix containing both the local and the non-local contributions. The foregoing then shows that these contributions scale differently as a function of a: non-local parts are simply proportional to $\frac{1}{a\Lambda}$ while for the local parts an extra factor $\frac{Z}{a}$ should be taken

[2]The lattice points $x_i = ia$ are placed symmetrically around the origin, thus implying that an interval $\left[-\frac{L}{2}, \frac{L}{2}\right]$ contains an odd number n of lattice points and that i runs from $-\lfloor \frac{n}{2} \rfloor$ to $\lfloor \frac{n}{2} \rfloor$.

into account yielding a total proportionality to $\frac{Z}{\Lambda a^2}$. Furthermore, it is generally also possible for the entanglement Hamiltonian to contain contributions depending on spatial derivatives of the conjugate momenta and these will result in yet another scaling behavior for the corresponding part of the N matrix. Similar considerations also apply for the M prefactor matrix. One thus concludes that as the limit $a \to 0$ is considered, the numerically calculated prefactor matrices M and N will typically diverge. However, these divergences will follow different scaling laws for contributions originating from local, non-local and possibly even other terms in the entanglement Hamiltonian. Some terms may even result in a non-divergent behavior for the prefactor matrices. Exploiting these different scaling laws, the various contributions to the prefactor matrices can be separated, hence yielding a complete overview of how the entanglement Hamiltonian is structured for cMERA states and especially of how it diverges when $a \to 0$. In a way, this would be the entanglement Hamiltonian analogue of equation (3.55) for the entanglement entropies. An important remark in this context, is that to perform this scaling based decomposition, the M and N matrices will always have to be calculated for multiple a values. However, for the discrete calculations to work, a typically has to be small. M and N prefactors should thus be calculated for increasingly small a values and as was mentioned before, this requires additional working precision for the numerical calculations to yield consistent results. Indeed, Casini *et al.* successfully applied a similar scaling-based procedure to determine the local part of the entanglement Hamiltonian for QFT ground states.[24] However, they were also forced to increase the number of significant digits drastically. As we were not able to perform such high-precision calculations yet, another method was proposed to deal with the divergent entanglement Hamiltonian.

The divergences in the cMERA entanglement Hamiltonian originate from unentangled degrees of freedom on length scales smaller than $\epsilon = \frac{\pi}{\Lambda}$. If it were possible to somehow remove the influence of these small length scales, the divergences should automatically be avoided as well, allowing one to determine that part of the entanglement Hamiltonian that corresponds to the correlated degrees of freedom concentrated on larger length scales. The discretization method provides a natural way to find this non-divergent part of $\mathcal{H}$. Indeed, where the standard discretization approach takes the limit $a \to 0$, one could terminate this limiting process when $a = \epsilon$ is reached. In this way, correlations on length scales smaller than ϵ are not considered in the discrete calculations, thus excluding the product state part from the cMERA state. This should then allow to calculate a non-divergent modular Hamiltonian. Indeed, by this regularization the typical proportionality factor $\frac{1}{\Lambda a}$ is replaced by a constant, yielding no divergences at all for the calculated entanglement Hamiltonian. Furthermore, we also expect to retrieve the CFT entanglement Hamiltonian when $\Lambda L \to +\infty$ as $\frac{1}{\Lambda a}$ is a constant in this limit as well. However, for the discrete matrix calculations with $a = \epsilon$ to work, one should have that $\sum_{l=-\infty}^{+\infty} X_{il} P_{lj} = \frac{1}{4}\delta_{ij}$ and until now, this was only verified for $a \to 0$. Luckily, it also applies for a sharp cut-off function when $a = \frac{\pi}{\Lambda}$. In this case the two-point correlators are given by:

$$\begin{aligned} X_{ij} &= \frac{1}{2\Delta}\frac{\delta_{ij}}{a} + \int_0^{\frac{\pi}{a}} \frac{dk}{2\pi} \cos(ka(i-j)) \left(\frac{1}{\alpha(k)} - \frac{1}{\Delta}\right) \\ P_{ij} &= \frac{a\Delta}{2}\delta_{ij} + a^2 \int_0^{\frac{\pi}{a}} \frac{dk}{2\pi} \cos(ka(i-j)) \left(\alpha(k) - \Delta\right) \end{aligned} \tag{3.63}$$

On the other hand, one could also terminate the integrations in equation (3.36) at $\frac{\pi}{a}$, yielding:

$$\begin{aligned}\tilde{X}_{ij} &= \int_{-\frac{\pi}{a}}^{\frac{\pi}{a}} \frac{dk}{2\pi} e^{ika(i-j)} \frac{1}{2\alpha(k)} = \int_0^{\frac{\pi}{a}} \frac{dk}{2\pi} \cos(ka(i-j)) \frac{1}{\alpha(k)} \\ \tilde{P}_{ij} &= a^2 \int_{-\frac{\pi}{a}}^{\frac{\pi}{a}} \frac{dk}{2\pi} e^{ika(i-j)} \frac{\alpha(k)}{2} = a^2 \int_0^{\frac{\pi}{a}} \frac{dk}{2\pi} \cos(ka(i-j))\alpha(k)\end{aligned} \tag{3.64}$$

The resulting discrete correlator matrices are equal. Working out their difference, one obtains:

$$\begin{aligned}X_{ij} - \tilde{X}_{ij} &= \frac{1}{2\Delta a}\delta_{ij} - \frac{1}{\Delta}\int_0^{\frac{\pi}{a}} \frac{dk}{2\pi} \cos(ka(i-j)) \\ &= \frac{1}{2\Delta a}\delta_{ij} - \frac{1}{2\Delta a}\delta_{ij} - \frac{1}{2\pi\Delta}\frac{\sin(\pi(i-j))}{a(i-j)}(1-\delta_{ij}) = 0 \\ P_{ij} - \tilde{P}_{ij} &= \frac{a\Delta}{2}\delta_{ij} - a^2\Delta\int_0^{\frac{\pi}{a}} \frac{dk}{2\pi} \cos(ka(i-j)) \\ &= \frac{a\Delta}{2}\delta_{ij} - \frac{a\Delta}{2}\delta_{ij} - \frac{a^2\Delta}{2\pi}\frac{\sin(\pi(i-j))}{a(i-j)}(1-\delta_{ij}) = 0\end{aligned} \tag{3.65}$$

allowing to prove the necessary requirement via the $\tilde{X}$ and $\tilde{P}$ matrices:

$$\begin{aligned}\sum_{l=-\infty}^{+\infty} X_{il}P_{lj} = \sum_{l=-\infty}^{+\infty} \tilde{X}_{il}\tilde{P}_{lj} &= \frac{a^2}{4}\int_{-\frac{\pi}{a}}^{\frac{\pi}{a}} \frac{dk}{2\pi}\int_{-\frac{\pi}{a}}^{\frac{\pi}{a}} \frac{dq}{2\pi}\left(\frac{\alpha(q)}{\alpha(k)} e^{ia(kj-qn)} \sum_{l=-\infty}^{+\infty} e^{ial(q-k)}\right) \\ &= \frac{a}{4}\int_{-\frac{\pi}{a}}^{\frac{\pi}{a}} \frac{dk}{2\pi} e^{iak(j-n)} = \frac{1}{4}\delta_{ij}\end{aligned} \tag{3.66}$$

For a Gaussian cut-off however, this requirement is not met and the so-called "regularized discretization approach" should thus only be applied in combination with a sharp cut-off function. The non-divergent part of the entanglement Hamiltonian is then computed by setting $a = \epsilon$, determining the continuum-based two-point correlators X and P, after which the modular Hamiltonian prefactors M and N can be found via the symmetrized method of Section 3.1.1. Important is that $a = \epsilon$ also fixes the sampling resolution of both the correlators and the prefactors and that this resolution (*i.e.* $\frac{L}{a}$) linearly increases with ΛL. As a result, only a very limited resolution is obtained for small ΛL. However, this is no problem as the Taylor approach demonstrated that for small ΛL the prefactor profiles are relatively flat. One can thus safely interpolate between the numerically determined values in the M and N matrices to gain a complete image of (the non-divergent part of) the prefactors. The proposed regularization also deals with the problem of numerical accuracy. Indeed, as the matrices to be diagonalized are relatively small when $a = \epsilon$, the symplectic eigenvalues do not get too close to $\frac{1}{2}$ and can thus be calculated correctly. Only for large ΛL, additional working precision is required. Finally, note that the lattice spacing $a = \epsilon$ goes to zero when $\Lambda L \to +\infty$. In this case, the regularized and the standard discretization approach thus coincide. Indeed, in the CFT limit the modular Hamiltonian becomes non-divergent even if all length scale degrees of freedom are taken into account.

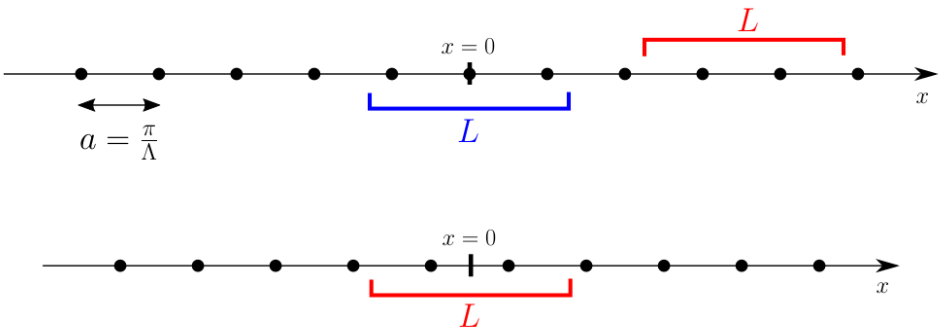

Figure 3.3: Illustration of the fact that L can contain an even and an odd number of lattice points when the regularized grid is used.

In the upper part of Figure 3.3 the 1d grid with lattice spacing $a = \frac{\pi}{\Lambda}$ is displayed together with the interval L symmetrically around $x = 0$. A displaced version of the interval was shown as well. Even though both have the same length, they contain a different number of lattice points, implying that different prefactors will be found for the entanglement Hamiltonian. However, the entanglement Hamiltonian should only depend on the length of the interval and not on its position. To resolve this discrepancy, an interpolation scheme was proposed. Sliding an interval of length L along the grid, this interval can contain two different numbers of lattice points, an even, $n_{even} = 2\left\lfloor \frac{L+a}{2a} \right\rfloor$, and an odd, $n_{odd} = 2\left\lfloor \frac{L}{2a} \right\rfloor + 1$. For a randomly placed interval, the probability to have $\min(n_{even}, n_{odd})$ lattice points is equal to $\left(\left\lceil \frac{\Lambda L}{\pi} \right\rceil - \frac{\Lambda L}{\pi}\right)$ while the probability of $\max(n_{even}, n_{odd})$ lattice points equals $\left(\frac{\Lambda L}{\pi} - \left\lfloor \frac{\Lambda L}{\pi} \right\rfloor\right)$. Therefore, any property $f(\Lambda L)$ should be interpolated between $f_{n_{even}}(\Lambda L)$ and $f_{n_{odd}}(\Lambda L)$ according to:

$$f(\Lambda L) = \left(\left\lceil \frac{\Lambda L}{\pi} \right\rceil - \frac{\Lambda L}{\pi}\right) f_{\min(n_{even},n_{odd})}(\Lambda L) + \left(\frac{\Lambda L}{\pi} - \left\lfloor \frac{\Lambda L}{\pi} \right\rfloor\right) f_{\max(n_{even},n_{odd})}(\Lambda L) \tag{3.67}$$

where $f_{n_{even}}(\Lambda L)$ is the property calculated via a grid as in the lower part of Figure 3.3. *I.e.* a grid where L contains n_{even} lattice points. For $f_{n_{odd}}(\Lambda L)$ on the other hand, the original grid should be applied. Applying this interpolation scheme, continuous profiles for the property $f(\Lambda L)$, independent of the location of L, are guaranteed.

3.2 Entanglement Properties

3.2.1 Entanglement Entropy

In order to allow comparison with analytical results, the entanglement entropy was first calculated for massless cMERA states. Indeed, for these states theoretical approximations exist when $\Lambda L \ll 1$ (equation (3.38)) and when $\Lambda L \gg 1$ (equation (3.55)). Utilizing the standard discretization approach (discarding all symplectic eigenvalues for which $\left|\omega - \frac{1}{2}\right| < 10^{-10}$) in combination with the $\alpha(k)$ functions determined in Chapter 2, entropy profiles were determined for massless cMERA states with both sharp and Gaussian cut-off functions. These are displayed in Figure 3.4 together with the analytical approximation of the entanglement entropy for small ΛL.

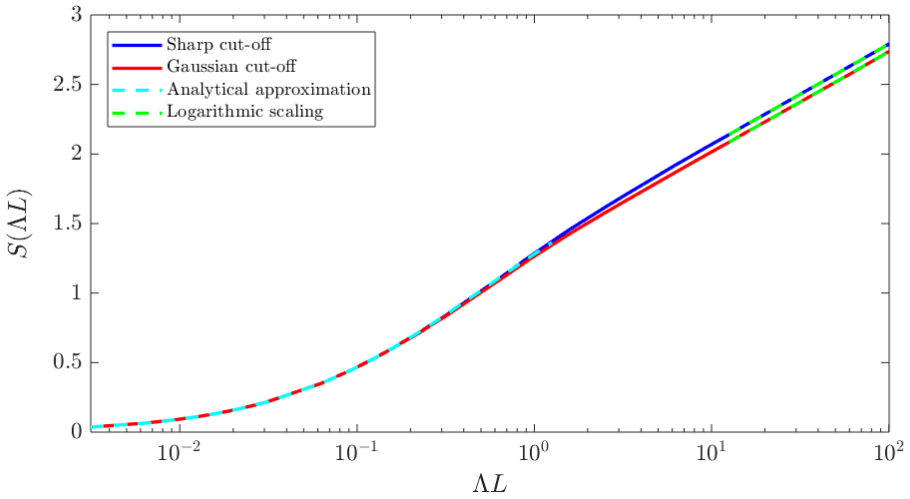

Figure 3.4: Numerically determined entropy profiles for free, massless Klein-Gordon cMERAs with sharp and Gaussian cut-off functions as well as the low ΛL approximation and linear fits for high ΛL.

For the numerical calculations, an IR regulator $\zeta = 10^{-11}$ was used together with $\Lambda a = 0.01$ for $\Lambda L < 10$ and $\Lambda a = 0.1$ for $\Lambda L > 10$ to yield converged entropy values. The numerical profiles clearly agree with the analytical approximation for small ΛL and a slightly larger entanglement entropy was found for the sharp cut-off function. Furthermore, linear fits were performed in the high ΛL region, matching both profiles to the well-known logarithmic CFT scaling law from equation (3.55). The following values were found for the central charge:

$$c_{\text{sharp}} = 0.940 \qquad c_{\text{Gaussian}} = 0.940 \tag{3.68}$$

confirming the correctness of the calculated entanglement entropies. The slight deviation from $c = 1$ is an artifact of the IR regulator. Indeed, we found that by lowering ζ the estimated central charges grew closer to one. The obtained results also correspond to those presented by Vidal *et al.*[47] In contrast to this paper however, cMERA states for massive QFTs were studied here as well. The resulting entropy profiles are displayed in Figure 3.5. As expected, adding a mass lowers the entanglement entropy. Indeed, a mass typically precludes the state from having fluctuations on length scales larger than the correlation length $\xi \approx m^{-1}$, thus lowering its entanglement entropy. Another interesting feature of Figure 3.5 is the equality of the slopes when $\Lambda L \gg 1$, indicating a universal behavior of the entanglement entropy in this regime. Furthermore, the offset near $mL = \Lambda L$ can be explained by the fact that a cMERA with cut-off Λ only introduces fluctuations on length scales larger than $\epsilon \approx \Lambda^{-1}$. However, as long as Λ is smaller than m, ϵ is larger than the correlation length ξ and thus all fluctuations introduced by the cMERA are suppressed by the mass. As a result, the entanglement entropy only starts to grow when $\epsilon \approx \xi$, *i.e.* when $\Lambda \approx m$. Finally we note that by taking the mass very small, massive cMERA states can be used to approximate massless cMERAs. Performing a linear fit in the region where $\Lambda L \gg 1$ then yields $c_{\text{massive}} = 1.003$. This value is even closer to one than those in (3.68) because the construction of the X and P matrices did not require an IR regulator now.

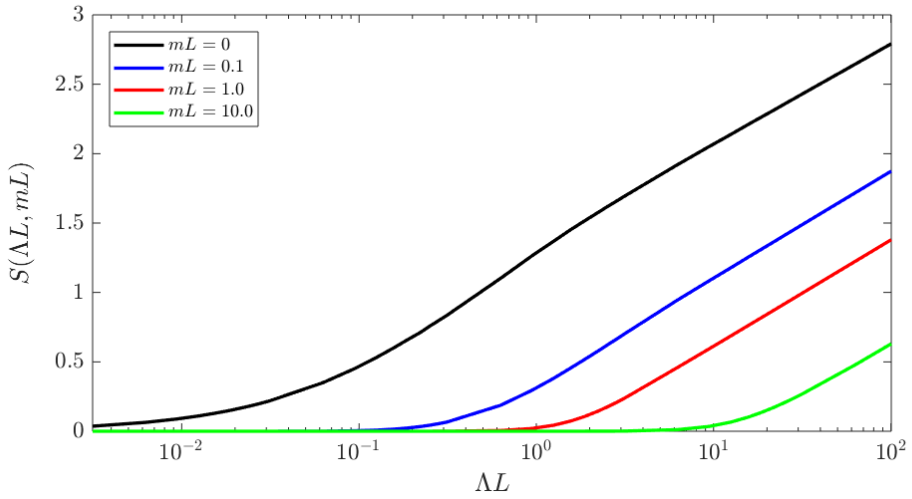

Figure 3.5: Numerically determined entropy profiles for both massless and massive cMERAs with a sharp cut-off function illustrating the influence of adding a mass to the Klein-Gordon field.

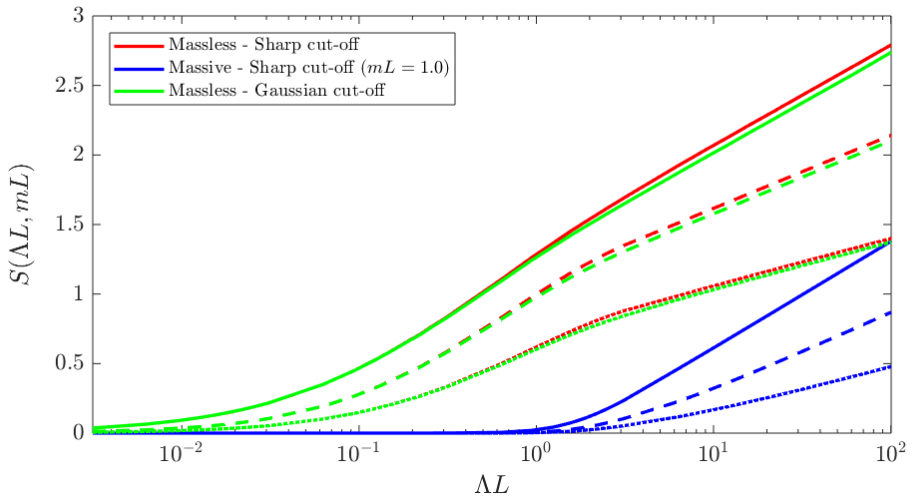

Figure 3.6: Rényi entropies for various cMERA states and for $\beta = 1$ (Von Neumann entropy, solid line), $\beta = 2$ (collision entropy, dashed line) and $\beta = +\infty$ (minimum entropy, dotted line).

β	Theoretical Slope	Massless Sharp cut-off	Massless Gaussian cut-off	Massive Sharp cut-off
1	$\frac{c}{3} \approx 0.333$	0.313	0.313	0.333
2	$\frac{c}{4} \approx 0.250$	0.228	0.228	0.240
$+\infty$	$\frac{c}{6} \approx 0.167$	0.148	0.148	0.139

Table 3.1: Comparison between theoretical slopes of the Rényi entanglement entropies and their fitted values ($mL = 1.0$ in the massive case).

It also interesting to study the Rényi entropies, S_β, for β values different from 1. Therefore, Figure 3.6 compares the traditional Von Neumann entropy ($\beta = 1$) to the collision entropy ($\beta = 2$) and the minimum entropy ($\beta = +\infty$). Both massless and massive cMERAs were treated and for the massless case, sharp and Gaussian cut-off functions were utilized. Similar profiles were found but as β increases, the entropies become smaller. Indeed, Rényi entropies decrease as function of β. As was the case for the Von Neumann entropies, all Rényi entropies follow a logarithmic scaling law in the CFT limit. However, the proportionality constant (and thus the slope in a logarithmic plot) depends on β according to equation (3.55). Estimates for the theoretical slopes (and thus for the central charge c) can therefore be found by performing linear fits to the numerically determined Rényi entropies in the large ΛL region. The results of this analysis were listed in Table 3.1. As mentioned in the previous paragraph, a massive cMERA yields the best results for the fit to the Von Neumann entropy. The same holds for the collision entropy. For $\beta = +\infty$ however, the massless models yield a better correspondence. This is due to the fact that the minimum entropy is not yet fully linear for the massive theory in the considered ΛL range.

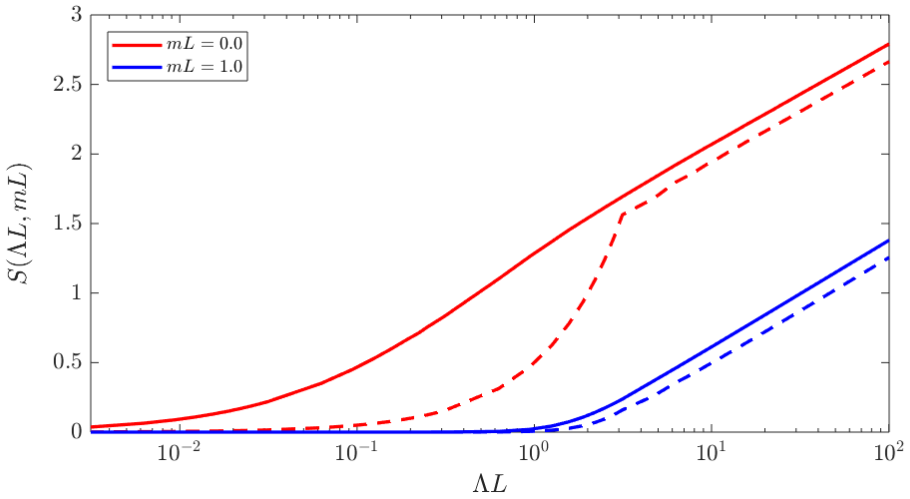

Figure 3.7: Comparison between fully converged (solid line) and regularized (dashed line) entanglement entropies in the massless and massive case (both with sharp cut-off function).

Finally, entanglement entropies can also be calculated following the regularized discretization approach. The resulting entropy profiles (utilizing the interpolation scheme from equation (3.67)) are compared to the saturated entropies in Figure 3.7. Again, a logarithmic scaling is found in the CFT limit but the regularized entropies are slightly smaller than their fully converged counterparts. A possible explanation could be that a small part of the total entanglement entropy is concentrated on length scales smaller than $\epsilon = \frac{\pi}{\Lambda}$. Indeed, even though a sharp cut-off was imposed at $k = \Lambda$ in momentum-space, this is not necessarily true in real-space, allowing for (a small amount of) fluctuations on length scales smaller than ϵ.

3.2.2 Entanglement Hamiltonian

Analogous to the entropy calculations, the cMERA modular Hamiltonian was initially determined for a massless Klein-Gordon theory, allowing for comparison with analytical CFT results. Indeed, for the CFT ground state, the entanglement Hamiltonian is given by:

$$\begin{aligned}\mathcal{H} &= \int_{-\frac{L}{2}}^{\frac{L}{2}} dx f(x) \left(\pi^2(x) + \left(\frac{d}{dx}\phi(x)\right)^2\right) \\ &= \int_{-\frac{L}{2}}^{\frac{L}{2}} dx \frac{\pi}{L}\left(\frac{L^2}{4} - x^2\right)\left(\pi^2(x) + \left(\frac{d}{dx}\phi(x)\right)^2\right)\end{aligned} \tag{3.69}$$

where the function $f(x)$ clearly has a length dimension. First, consider the term containing the conjugate momenta. Its discretized analogue is given by:

$$a\sum_i a f_i \left(\frac{\pi_i}{a}\right)^2 = \sum_i f_i \pi_i^2 \tag{3.70}$$

indicating that the f_i are proportional to $\frac{L}{a}$. As argued before, an additional proportionality factor $\frac{1}{a\Lambda}$ has to be taken into account for cMERA states with $\Lambda < +\infty$. Consequently, the local contribution to the entanglement Hamiltonian corresponds to that part of the numerically determined N matrix that scales as $\frac{L}{a^2\Lambda}$. Via similar considerations, one shows that non-local contributions in the conjugate momenta yield a proportionality to $\frac{1}{a\Lambda}$ for N. A term local in the derivatives of the $\pi(x)$ fields on the other hand, corresponds to the part of N scaling as $\frac{L^3}{a^4\Lambda}$. By determining the N matrix for various a values, one should hence be able to separate these differently scaling contributions, thus giving a complete picture of how the entanglement Hamiltonian is structured for the cMERA state. However, these calculations require additional working precision. Therefore we restricted ourselves to the determination of the non-divergent part of the entanglement Hamiltonian via the regularized discretization approach. In Figure 3.8 the resulting N prefactors are displayed for increasing ΛL. One observes that the profiles are non-local but become systematically more peaked, indicating a delta function behavior for large ΛL. Indeed, one expects to retrieve the purely local CFT profile from equation (3.69) when $\Lambda L \to +\infty$. For low ΛL on the other hand, the resolution diminishes and the profile becomes flat, corresponding to the predictions of the Taylor approach and Section 3.1.3. Applying the interpolation scheme from equation (3.67), one obtains that the uniform value of $N(x, y)$ linearly drops down to zero once $n_{even} = 0$ and $n_{odd} = 1$ (*i.e.* once $\Lambda L \leq \pi$). Indeed, for small ΛL, the cMERA state approximates the product state, making the modular Hamiltonian completely divergent. The non-divergent part of the entanglement Hamiltonian hence becomes simply equal to zero.

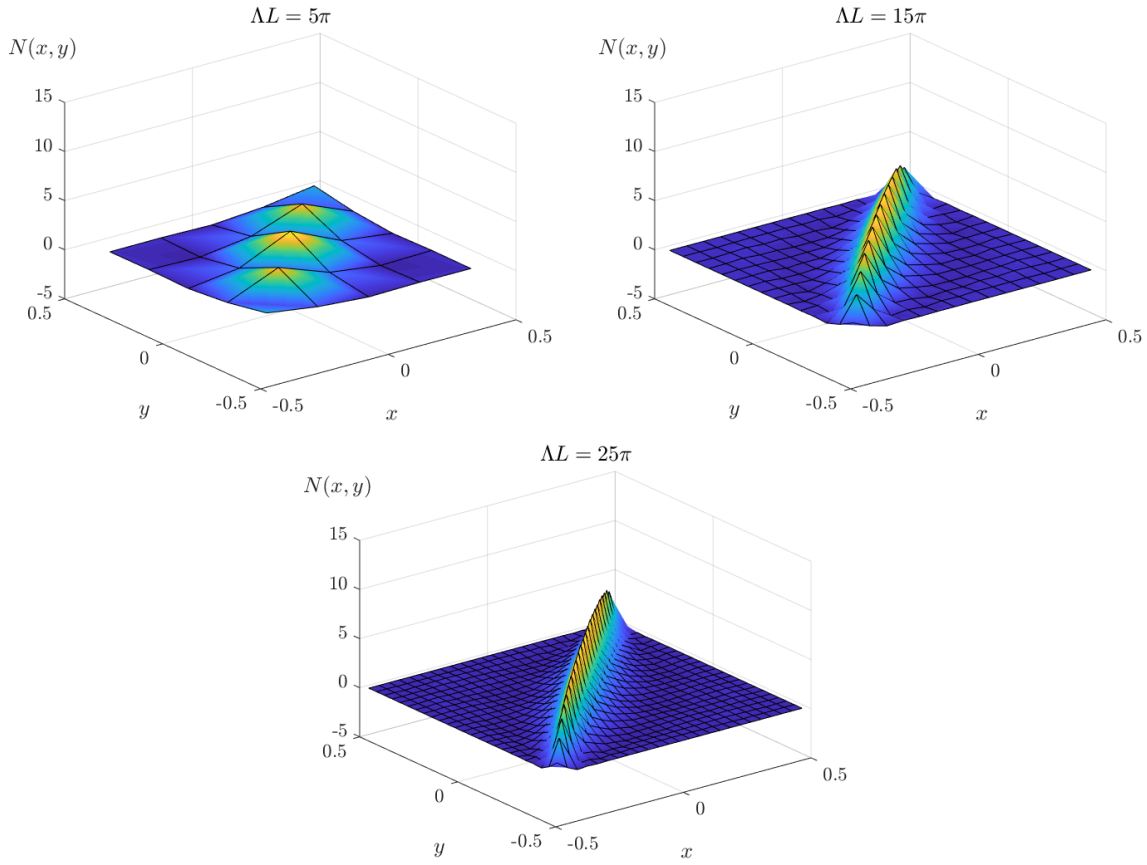

Figure 3.8: Regularized $N(x, y)$ prefactors of massless Klein-Gordon cMERAs for several ΛL values.

In the light of a further exploration of the correspondence with CFT results, it is useful to revisit the various scaling laws of the N matrix. For the terms of $\mathcal{H}$, local in the conjugate momenta, we obtained a scaling proportional to $\frac{L}{a^2\Lambda}$. In the regularized discretization approach ($\Lambda a = \pi$), this yields a contribution to the N matrix linearly increasing with ΛL. $\mathcal{H}$ terms, non-local in the conjugate momenta on the other hand, scale proportional to $\frac{1}{a\Lambda}$ and thus give rise to constant contributions for the N matrix. Finally, $\mathcal{H}$ terms containing derivatives of the conjugate momenta result in N contributions increasing even faster than linear as a function of ΛL. As a result, comparing the calculated N matrix to CFT results for large ΛL, we typically expect to retrieve only the $\mathcal{H}$ terms local in the conjugate momenta as only these terms appear in the CFT entanglement Hamiltonian. To compare these local terms directly to the CFT prefactor $f(x)$, a normalized version of the diagonal of N was compared to a normalized version of $f(x)$ for several ΛL values. Indeed, as the diagonal of N represents the most rudimentary approximation of the continuous delta function, one could expect that these profiles agree for large ΛL. However, as Figure 3.9 shows, this is not the case.

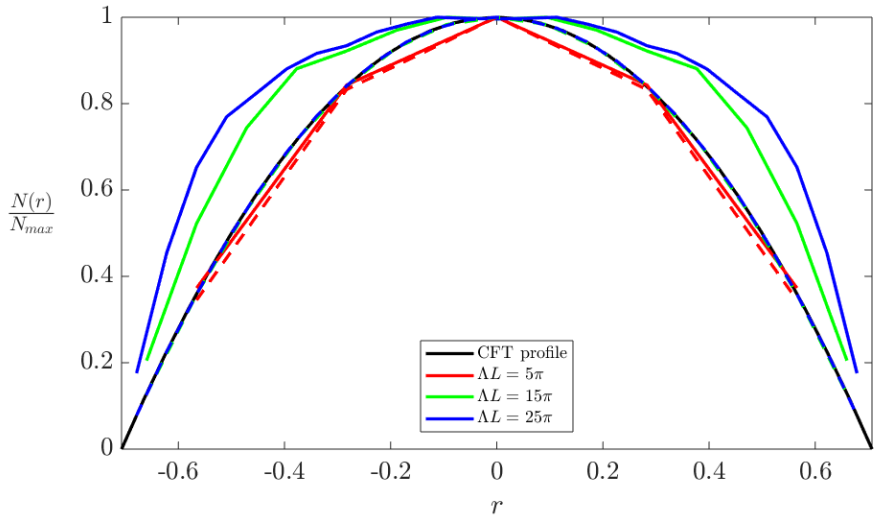

Figure 3.9: Comparison between the normalized diagonal of the regularized N matrix (solid lines), its summed out version placed back on the diagonal (dashed lines) and the normalized CFT profile, placed on the diagonal (*i.e.* as a function of $r = \sqrt{2}x$ instead of x), for several ΛL values and with $L = 1$.

This unsatisfactory agreement is explained by the fact that when $\Lambda L \gg 1$, $a = \frac{\pi}{\Lambda}$ becomes very small w.r.t. to system length L. As a result, the matrix elements of N closely neighboring the diagonal, will also contribute to possible delta functions. This becomes more apparent via the following:

$$\begin{aligned}
\int_L \int_L \pi(x) N(x,y) \pi(y) dx dy \quad \leftrightarrow \quad & a^2 \sum_i \sum_j \frac{\pi_i}{a} N_{ij} \frac{\pi_j}{a} = \\
& = a^2 \sum_i \sum_j \pi(ia) N_{ij} \pi(ja) \\
& = a^2 \sum_i \sum_{j=i-j_{max}}^{i+j_{max}} \pi(ia) N_{ij} \left(\pi(ia) + (j-i) a \pi'(ia) + \mathcal{O}(a^2) \right) \\
& = a \sum_i \pi(ia) \left(a \sum_{j=i-j_{max}}^{i+j_{max}} N_{ij} \right) \pi(ia) + \mathcal{O}(a^4) \\
& \approx \sum_i \pi_i \left(\sum_{j=i-j_{max}}^{i+j_{max}} N_{ij} \right) \pi_i
\end{aligned} \tag{3.71}$$

where going from the second to the third line a Taylor expansion for the continuous field was introduced and where simultaneously all contributions of N far from the diagonal were neglected by keeping $|i-j| < j_{max}$. Furthermore, all odd Taylor terms drop out due to the symmetry of N and going to the final line all higher-order Taylor contributions were neglected. This is possible because a becomes small compared to L for large ΛL and because we keep j close to i. Comparing the final line to equation (3.70) then yields a direct relation between the CFT prefactor $f(x)$ and a property that can be calculated from the matrix N:

$$f(ia) \leftrightarrow a f_i \approx a \sum_{j=i-j_{max}}^{i+j_{max}} N_{ij} \tag{3.72}$$

and indeed, this is done by summing the diagonal elements of N together with their neighbors. The results of this summing procedure are also displayed in Figure 3.9. In contrast to the pure diagonal, a satisfactory correspondence with the CFT profile is now obtained for large ΛL. As the elements of N become very small far from the diagonal, the value of j_{max} does not really matter and therefore it is typically set equal to the matrix dimensions of N.

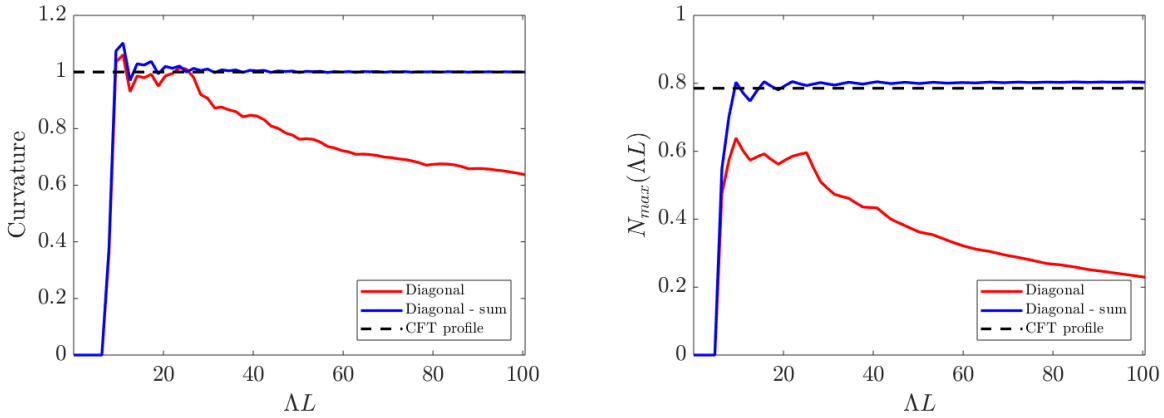

(a) Comparison between the curvature of parabolic fits to the diagonal of the N matrix, its summed out version $\sum_{j=i-j_{max}}^{i+j_{max}} N_{ij}$ and the parabolic CFT profile with $L = 1$.

(b) Comparison between the maximum of the diagonal of N (multiplied by a), its summed out version $a\sum_{j=i-j_{max}}^{i+j_{max}} N_{ij}$ and the maximum of the parabolic CFT profile with $L = 1$.

Figure 3.10: Detailed comparison between the regularized N matrix and the CFT prefactor for conjugate momenta.

To illustrate the obtained correspondence even more explicitly, parabolic profiles were fitted to the diagonal of N and its summed out version $\sum_{j=i-j_{max}}^{i+j_{max}} N_{ij}$. The curvature of these parabolas was then compared to the curvature of the CFT profile in Figure 3.10a. Where the summed out diagonal reproduces the curvature of the asymptotic CFT alsmost exactly, the fit to the pure diagonal underestimates the curvature. Due to the normalization of the profiles in Figure 3.9, only the correspondence between the shape of the cMERA and CFT prefactors could be verified. In order to check that the multiplicative factors of the parabolas agree as well, the maximum of the diagonal of N (multiplied by a to yield the correct dimensions), its summed out version and the maximum of the CFT prefactor were compared in Figure 3.10b. The maximum of the pure diagonal clearly underestimates the the CFT maximum. By summing out the near-diagonal elements however, a satisfactory correspondence was obtained. The slight overestimation of the CFT value in this case is again due to the IR regulator but as for the entanglement entropy this effect can be reduced by decreasing the IR regulator even further than 10^{-11}.

Finally, the influence of a mass on the $N(x, y)$ prefactor was studied. To do so, the regularized N matrices for massless and massive cMERA states were compared in Figure 3.11. An overall increase of the profile was found together with a slight broadening. Furthermore, one observes small side peaks along the counter-diagonal (see also Figure 3.11c). A (similar) non-local behavior was also documented by Casini *et al.* for the ground state QFT modular Hamiltonian.[24]

However, we argued before that non-local $\mathcal{H}$ terms typically correspond to constant N contributions as opposed to the local terms scaling proportional to ΛL. One therefore expects that to fully understand the (non-local) influence of a mass, high precision calculations will have to be utilized to separate the local and non-local N contributions. We also mention that as the massive N prefactor contains counter-diagonal contributions, one should not let j_{max} reach the matrix dimension in the summing procedure. Therefore, j_{max} was set equal to 15 for the massive case with $\Lambda L = 32\pi$ in Figure 3.11d. Note also that N prefactor matrices were only calculated for mL up to 1. Increasing the mass any further, the two-point correlators become so small that again additional working precision is necessary for a correct solution of the numerical eigenvalue problem.

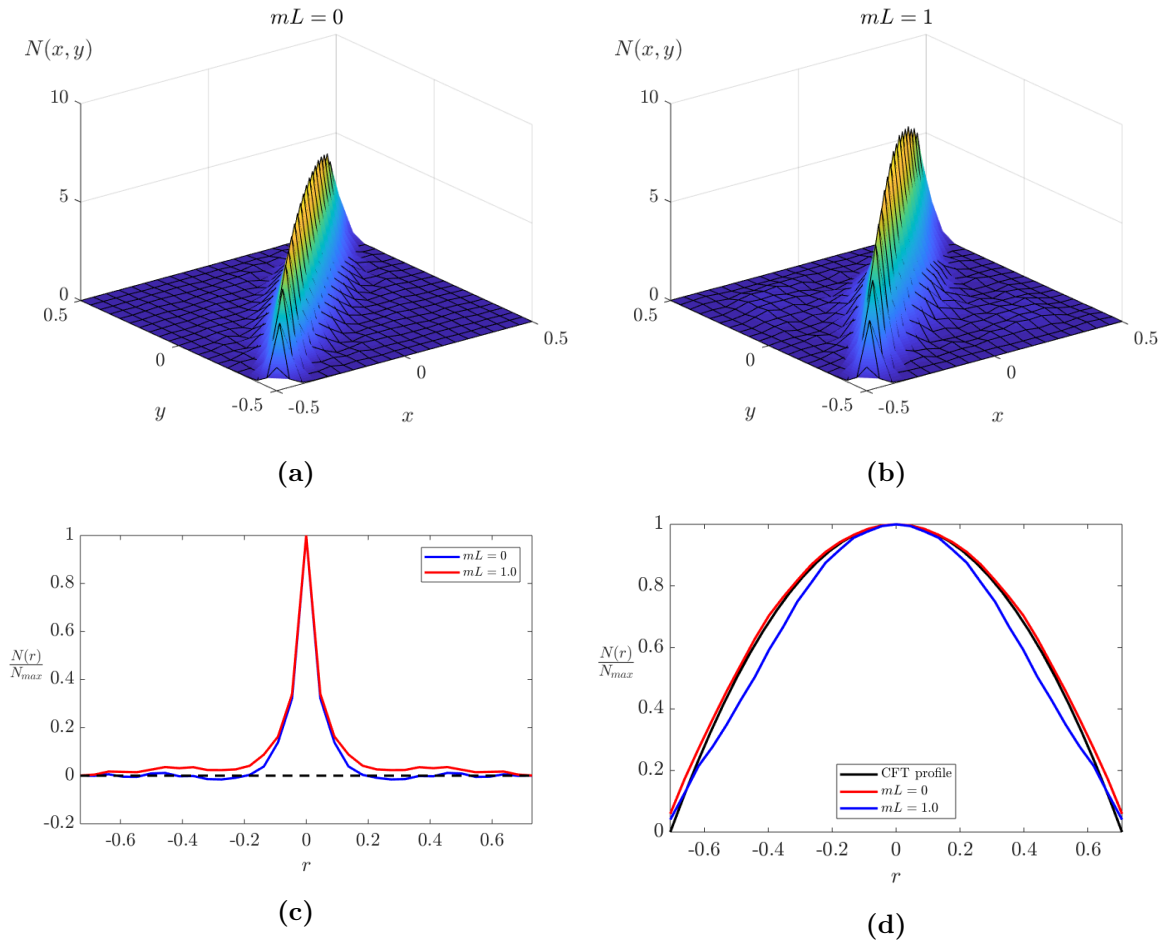

Figure 3.11: Influence of a mass on the regularized N prefactor.
(a) and (b) display the calculated N matrices for $mL = 0$ and $mL = 1$ with $\Lambda L = 32\pi$.
(c) compares the normalized counter-diagonals of these matrices and (d) the summed out diagonals.

Next, we turn to the $M(x,y)$ prefactor for the scalar fields in the entanglement Hamiltonian. For the CFT ground state, the term in $\mathcal{H}$ accompanying the scalar fields is given by:

$$\int_{-\frac{L}{2}}^{\frac{L}{2}} dx f(x)\left(\phi'(x)\right)^2 = -\int_{-\frac{L}{2}}^{\frac{L}{2}} f(x)\phi(x)\phi''(x)dx + \frac{1}{2}\int_{-\frac{L}{2}}^{\frac{L}{2}} f''(x)\phi^2(x)dx - \frac{1}{2}\left[f'(x)\phi^2(x)\right]_{-\frac{L}{2}}^{\frac{L}{2}} \tag{3.73}$$

where the apostrophe signifies the derivative w.r.t. x and where partial integration was applied to find the right-hand side. The discretized analogue hereof is:

$$-a\sum_i a f_i \phi_i \frac{\phi_i''}{a^2} + \frac{1}{2}a\sum_i \frac{f_i''}{a}\phi_i^2 - \frac{1}{2}f_{i_1}'\phi_{i_1}^2 + \frac{1}{2}f_{i_n}'\phi_{i_n}^2 \tag{3.74}$$

where i_1 is the index of the leftmost lattice point (and thus the lowest x_i) while i_n is the index corresponding to the rightmost lattice point. The f_i are proportional to $\frac{L}{a}$ (as seen before) whereas the f_i'' are proportional to $\frac{a}{L}$. The f_i' on the other hand do not receive a proportionality factor by the discretization procedure. Going from the CFT ground state to the cMERA, each of these contributions gains an additional proportionality to $\frac{1}{a\Lambda}$ as they are a part of the M matrix. Consequently, we expect $\mathcal{H}$ contributions local in the scalar fields and their second derivatives (and thus having the same form as the first term in the right-hand side of equation (3.73)) to yield a scaling proportional to $\frac{L}{a^2\Lambda}$ for M. $\mathcal{H}$ contributions corresponding to the second term in equation (3.73) on the other hand will result in a scaling proportional to $\frac{1}{\Lambda L}$ for M. Finally, the surface term will introduce M contributions scaling as $\frac{1}{a\Lambda}$. Again, we were not yet able to decompose the calculated M matrices in these various contributions as this requires high-precision calculations. However, utilizing the regularized discretization method, the non-divergent part of the M matrix was determined successfully. In this regularized M, the contributions originating from $\mathcal{H}$ terms local in the fields and their second derivatives, scale as ΛL and are therefore dominant for large ΛL. Indeed, the other contributions will scale sub-dominantly as $\frac{1}{\Lambda L}$ and as $\frac{1}{\pi}$. As a result, one only expects to retrieve the CFT terms local in the scalar fields and their second derivatives from the regularized M matrices when $\Lambda L \gg 1$.

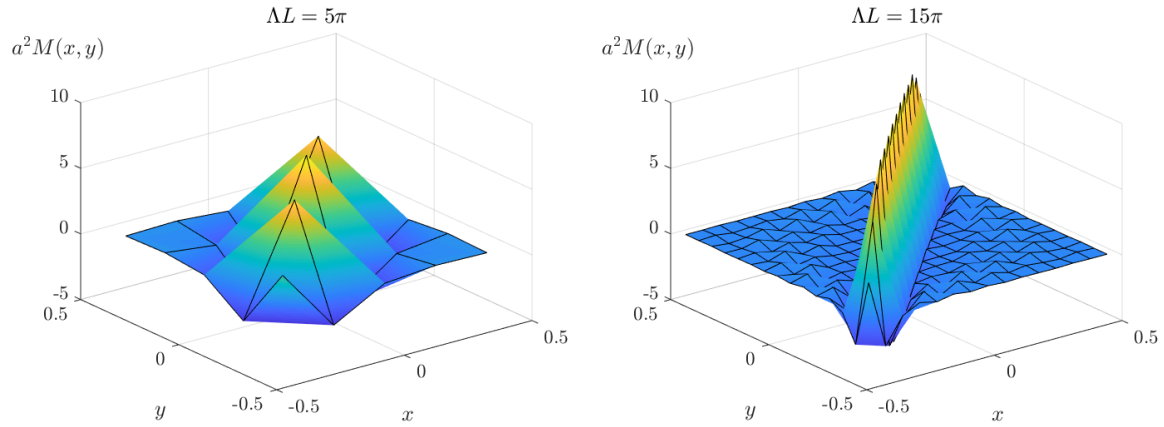

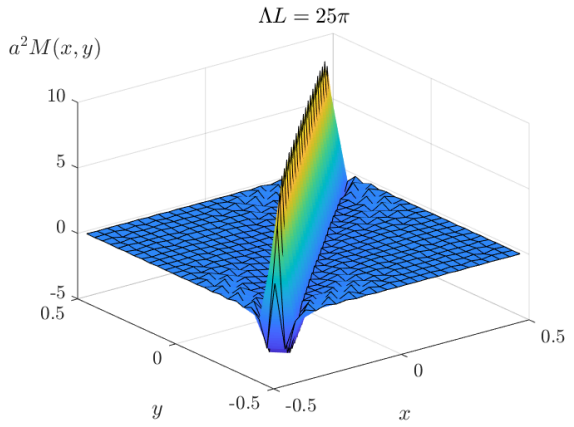

Figure 3.13: Regularized $a^2M(x,y) \leftrightarrow M_{ij}$ prefactors of massless Klein-Gordon cMERAs for several ΛL values.

To verify the hypotheses from the previous paragraph, the regularized discretization approach was used to calculate the (non-divergent part of the) M prefactors for a massless Klein-Gordon cMERA. In Figure 3.13, the resulting profiles are compared for increasing ΛL. Again, these are relatively flat for low ΛL but become significantly more peaked as ΛL increases, indicating a delta function behavior for large ΛL. However, in contrast to the profiles in Figure 3.8 for the N matrix, strongly negative side-peaks are now found next to the central positive peak. This shape corresponds to the intuitive notion of a discretized $\delta''(x-y)$ distribution. As a result, the calculated profiles seems to confirm that the M matrix is dominated by contributions corresponding to $\mathcal{H}$ terms local in the scalar fields and their second derivative. To verify this statement even more explicitly, we attempt to extract the parabolic CFT prefactor $f(x)$ from the calculated M matrix. To do so an argument similar to that in equation (3.71) is used:

$$\begin{aligned}
\int_L \int_L \phi(x) M(x,y) \phi(y) dx dy \quad &\leftrightarrow \quad a^2 \sum_i \sum_j \phi_i \frac{M_{ij}}{a^2} \phi_j = \\
&= \sum_i \sum_j \phi(ia) M_{ij} \phi(ja) \\
&= \sum_i \sum_{j=i-j_{max}}^{i+j_{max}} \phi(ia) M_{ij} \left(\phi(ia) + (j-i)a\phi'(ia) + \frac{(j-i)^2 a^2}{2} \phi''(ia) + \mathcal{O}(a^3) \right) \\
&= \sum_i \phi(ia) \left(\sum_{j=i-j_{max}}^{i+j_{max}} M_{ij} \right) \phi(ia) + \sum_i \phi(ia) \left(\frac{a^2}{2} \sum_{j=i-j_{max}}^{i+j_{max}} (j-i)^2 M_{ij} \right) \phi''(ia) + \mathcal{O}(a^4) \\
&\approx \sum_i \phi_i \left(\sum_{j=i-j_{max}}^{i+j_{max}} M_{ij} \right) \phi_i + \sum_i \phi_i \left(\frac{1}{2} \sum_{j=i-j_{max}}^{i+j_{max}} (j-i)^2 M_{ij} \right) \phi_i''
\end{aligned} \tag{3.75}$$

where now also the second order term was retained. Naively comparing this to equation (3.74), one would expect the following correspondences:

$$
\begin{aligned}
f(ia) \leftrightarrow a f_i &\approx -\frac{a}{2} \sum_{j=i-j_{max}}^{i+j_{max}} (j-i)^2 M_{ij} \\
f''(ia) \leftrightarrow \frac{f_i''}{a} &\approx \frac{2}{a} \sum_{j=i-j_{max}}^{i+j_{max}} M_{ij} \qquad\qquad i \neq i_1, i_n
\end{aligned}
\tag{3.76}
$$

with slight alterations for the second line when $i = i_1, i_n$ due to the surface terms. However, because the $\mathcal{H}$ contributions local in the scalar fields and their second derivatives correspond to the dominant M contribution, only the first correspondence will be obtained from the regularized M matrix. Indeed, as Figure 3.14 shows the normalized version of $-\frac{a}{2}\sum_{j=i-j_{max}}^{i+j_{max}}(j-i)^2 M_{ij}$ reproduces the analytical profile to a good degree for high ΛL.

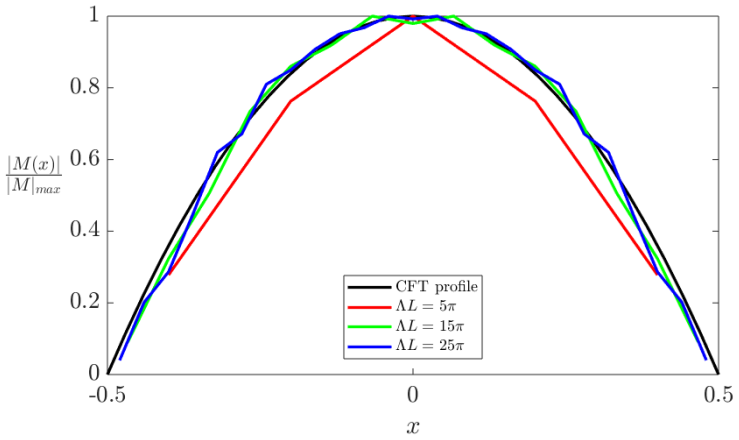

Figure 3.14: Comparison between the normalized version of $\sum_{j=i-j_{max}}^{i+j_{max}}(j-i)^2 M_{ij}$ and the normalized CFT profile for several ΛL values and with $L = 1$.

In order to study the correspondence between the dominant M contributions and the CFT predictions more comprehensively, parabolas were fitted to the numerically determined profiles. As Figure 3.15 shows, both the curvature and the minimum value of the analytical profiles are reproduced almost exactly. The slight overestimation of the curvature in Figure 3.15 can once again be attributed to the IR regulator.

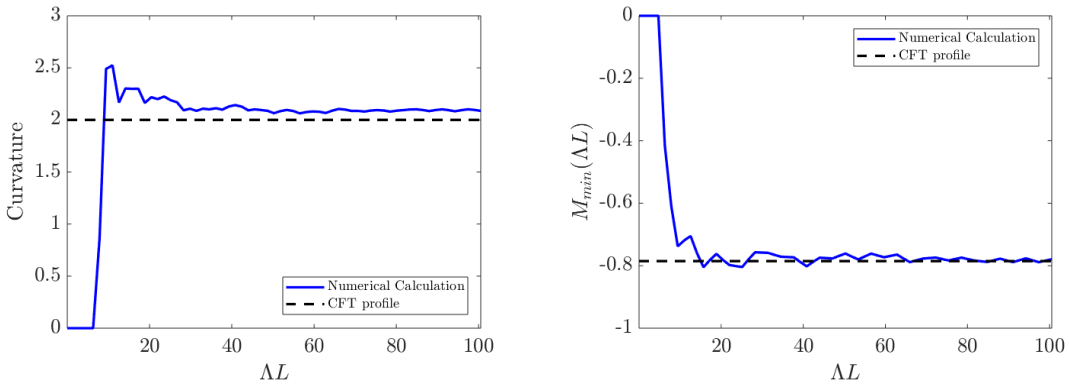

Figure 3.15: Detailed comparison between the CFT profile $-f(x)$ and $-\frac{a}{2}\sum_{j=i-j_{max}}^{i+j_{max}}(j-i)^2 M_{ij}$.

Finally, the influence of a mass on the regularized M prefactor was studied in Figure 3.16. Again an overall increase of the peaks was found. However, as masses typically introduce non-local terms (corresponding to sub-dominant M contributions), one should perform high-precision calculations to separate these non-local contributions from their local counterparts. Only in this way, it will be possible to fully understand the influence of a mass on the entanglement Hamiltonian of a cMERA state (e.g. making it possible to extract this mass from the calculated M matrices).

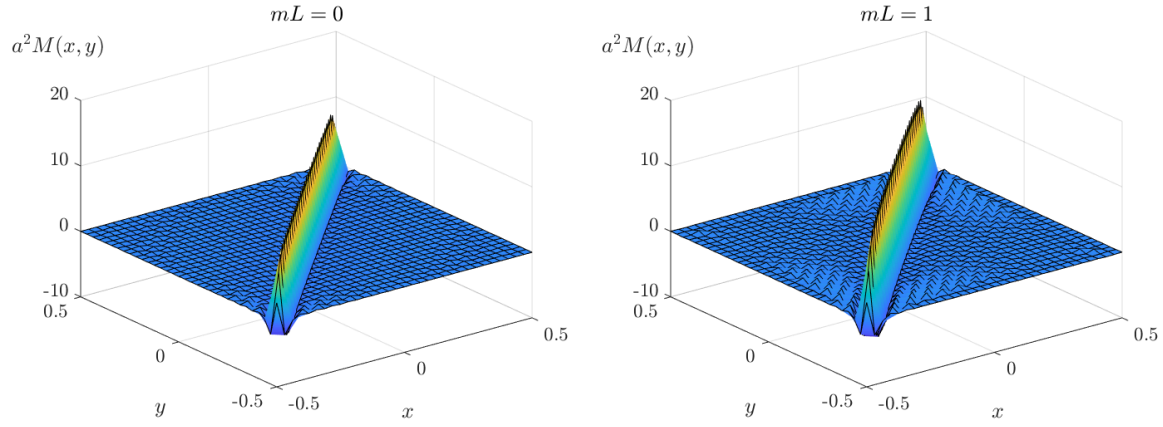

Figure 3.16: Influence of a mass on the regularized M prefactor in the cMERA entanglement Hamiltonian for $\Lambda L = 32\pi$.

Chapter 4

Dirac Theory in (1+1) Dimensions

As this chapter is the fermionic analogue of the previous, it has got a relatively similar structure: first, the followed methodology will be discussed after which the results of the corresponding numerical calculations will be presented. The main difference in methodology originates from the different canonical transformation groups for bosons and fermions: symplectic for the former and unitary for the latter. Entanglement properties on the other hand behave relatively similar for both theories.

4.1 Methodology

4.1.1 Discrete Field Theory

The procedure of inferring entanglement properties from the two-point correlators of Gaussian states is again introduced in a discrete setting by considering a 1d lattice with lattice points at $x_i = ia$ ($i \in \mathbb{Z}$ and lattice spacing a). Now however, fermionic field operators ψ_i are placed on all lattice sites, obeying the canonical anticommutation relations $\{\psi_i, \psi_j^\dagger\} = \delta_{ij}$ and $\{\psi_i, \psi_j\} = \{\psi_i^\dagger, \psi_j^\dagger\} = 0$. As for the bosonic case, all considered states are Gaussian and thus subjected to Wick's theorem. *I.e.* all non-zero multi-point correlators are obtained from two-point correlators by the prescription:

$$\langle \psi_{i_1} ... \psi_{i_k} \psi_{j_1}^\dagger ... \psi_{j_k}^\dagger \rangle = (-1)^{\frac{k(k-1)}{2}} \sum_\sigma \text{sign}(\sigma) \prod_{q=1}^{k} \langle \psi_{i_q} \psi_{j_{\sigma(q)}}^\dagger \rangle \tag{4.1}$$

where σ stands for all permutations of the indices. Furthermore, it is assumed that $\langle \psi_i \psi_j \rangle = \langle \psi_i^\dagger \psi_j^\dagger \rangle = 0$ so that all other multi-point correlators are equal to zero. The correlation matrix C is defined by $C_{ij} = \langle \psi_i \psi_j^\dagger \rangle$ and for the states treated here, this matrix thus determines all multi-point correlators. C is also Hermitian and positive. Moreover, using the anticommutation relations, one easily obtains that $\langle \psi_i^\dagger \psi_j \rangle = \delta_{ij} - C_{ji}$ is Hermitian and positive as well, implying that the eigenvalues of C are located in the interval $[0, 1]$. Finally, one also has that $\sum_{l=-\infty}^{+\infty} C_{il} C_{lj} = C_{ij}$, *i.e.* C is idempotent when considering the infinite lattice.

When the Gaussian state described in the previous paragraph is restricted to a finite interval L, all degrees of freedom outside this interval are traced out. As a result, only n consecutive lattice

sites remain. The corresponding C matrix is Hermitian and positive and can hence be diagonalized by a unitary transformation U: $U^\dagger C U = \Omega$ where Ω is the diagonal matrix containing the eigenvalues of C. The implications of this property become clear when considering an arbitrary linear transformation of the (separate) fields $\tilde{\psi}_i = A_{ij}\psi_j$. In order for the transformed fields to obey the canonical anticommutation relations, A should be unitary. The correlation matrix C is also affected by this unitary field transformation:

$$\tilde{C}_{ij} = \langle \tilde{\psi}_i \tilde{\psi}_j^\dagger \rangle = \langle A_{il}\psi_l \psi_k^\dagger A_{jk}^* \rangle = A_{il} C_{lk} A_{jk}^* \tag{4.2}$$

or equivalently $\tilde{C} = ACA^\dagger$. We thus conclude that the correlation matrix can always be diagonalized by a canonical field transformation where the necessary transformation matrix A is simply equal to the Hermitian conjugate of the unitary U diagonalizing C.

A proper ansatz for the reduced density operator of Gaussian states restricted to an interval L is given by:

$$\rho_L = K e^{-\mathcal{H}} = K e^{-\sum_l \epsilon_l a_l^\dagger a_l} \tag{4.3}$$

where $a_l^\dagger$ and a_l are creation and annihilation operators, obeying $\{a_l, a_{l'}^\dagger\} = \delta_{ll'}$ in case of fermions. The normalization factor K is then determined by:

$$K = \prod_l (1 + e^{-\epsilon_l})^{-1} \tag{4.4}$$

The creation and annihilation operators should also be linearly related to the fermionic fields. Here this transformation is trivial since the transformed fields $\{\tilde{\psi}_l\}$ are simply equal to the annihilation operators. Indeed, they obey the necessary anticommutation relations and also satisfy:

$$\begin{aligned} \Omega_{ij} &= \langle \tilde{\psi}_i \tilde{\psi}_j^\dagger \rangle = \mathrm{tr}(\rho_L \tilde{\psi}_i \tilde{\psi}_j^\dagger) \\ &= K \mathrm{tr}\left(e^{-\sum_l \epsilon_l \tilde{\psi}_l \tilde{\psi}_l^\dagger} \tilde{\psi}_i \tilde{\psi}_j^\dagger \right) = \langle n \rangle_{ij} \end{aligned} \tag{4.5}$$

where $\langle n \rangle$ is the diagonal matrix containing the expectation values of the occupation numbers:

$$\langle n \rangle_{ij} = \delta_{ij} \frac{1}{1 + e^{-\epsilon_i}} \tag{4.6}$$

The eigenvalues of C and the entanglement energies are hence related via:

$$\epsilon_l = \ln\left(\frac{\omega_l}{1 - \omega_l} \right) \tag{4.7}$$

Using the fact that the transformed fields are equal to the annihilation operators also allows to rewrite the entanglement Hamiltonian:

$$\begin{aligned} \mathcal{H} &= \sum_l \epsilon_l \tilde{\psi}_l^\dagger \tilde{\psi}_l \\ &= \left(\psi^\dagger \right)^T U \epsilon U^\dagger \left(\psi \right) \end{aligned} \tag{4.8}$$

where ϵ is the diagonal matrix containing all entanglement energies, where U is the unitary diagonalizing C and where all the fields were collected in column vectors. The entanglement

entropy can be derived from the entanglement Hamiltonian via:

$$\begin{aligned} S &= -\mathrm{tr}(\rho_L \ln \rho_L) \\ &= -\ln K + K\mathrm{tr}(e^{-\mathcal{H}}\mathcal{H}) \\ &= \sum_l \left(\ln(1+e^{-\epsilon_l}) + \frac{\epsilon_l e^{-\epsilon_l}}{1+e^{-\epsilon_l}} \right) \\ &= -\sum_l \left(\omega_l \ln(\omega_l) + (1-\omega_l)\ln(1-\omega_l) \right) \end{aligned} \tag{4.9}$$

Where until now only one flavor of fermionic operators was considered, the method can easily be extended to the case of multiple flavors as the canonical anticommutation relations still hold. To do so for two flavors, the definition of the C matrix is replaced by:

$$C = \left(\begin{array}{c|c} \langle \psi_{0_i} \psi^\dagger_{0_j} \rangle_{i,j=1,\ldots,n} & \langle \psi_{0_i} \psi^\dagger_{1_j} \rangle_{i,j=1,\ldots,n} \\ \hline \langle \psi_{1_i} \psi^\dagger_{0_j} \rangle_{i,j=1,\ldots,n} & \langle \psi_{1_i} \psi^\dagger_{1_j} \rangle_{i,j=1,\ldots,n} \end{array} \right) \tag{4.10}$$

which can again be diagonalized unitarily, yielding the entanglement Hamiltonian and entropy via the same prescriptions as before.

4.1.2 Analytical Generalization

The discrete field method discussed in the previous section can be extended to a continuous setting by replacing the vectors and matrices consisting of discrete quantities by continuous functions depending on one or more variables and having the correct physical dimensions. Specifically for the fermionic fields and the correlation matrix, this implies:

$$\begin{aligned} \psi_{\mu_i} &\quad\leftrightarrow\quad \sqrt{a}\psi_\mu(x) \\ C_{\mu_i\nu_j} = \langle \psi_{\mu_i} \psi^\dagger_{\nu_j} \rangle &\quad\leftrightarrow\quad a C_{\mu\nu}(x,y) = a\langle \psi_\mu(x) \psi^\dagger_\nu(y) \rangle \end{aligned} \tag{4.11}$$

so that the eigenvalue problem of C generalizes to:

$$\int_L C_{\mu\nu}(x,y)\kappa_{\nu_l}(y)dy = \omega_l \kappa_{\mu_l}(x) \tag{4.12}$$

For cMERA states, the continuous correlation matrix is determined by the $\theta(k)$ functions from Chapter 2:

$$\begin{aligned} C_{00}(x,y) &= \langle \psi_0(x)\psi_0^\dagger(y)\rangle \\ &= \int_{-\infty}^{+\infty} \frac{dk}{\sqrt{2\pi}} \int_{-\infty}^{+\infty} \frac{dq}{\sqrt{2\pi}} e^{i(kx-qy)} \langle \psi_0(k)\psi_0^\dagger(q)\rangle \\ &= \int_{-\infty}^{+\infty} \frac{dk}{\sqrt{2\pi}} \int_{-\infty}^{+\infty} \frac{dq}{\sqrt{2\pi}} e^{i(kx-qy)} \cos(\theta(k))\cos(\theta(q)) \langle \tilde{\psi}_0(k)\tilde{\psi}_0^\dagger(q)\rangle \\ &= \int_{-\infty}^{+\infty} \frac{dk}{2\pi} e^{ik(x-y)} \cos^2(\theta(k)) \\ &= \int_0^{+\infty} \frac{dk}{\pi} \cos(k(x-y)) \cos^2(\theta(k)) \end{aligned} \tag{4.13}$$

$$
\begin{aligned}
C_{01}(x,y) &= \langle \psi_0(x)\psi_1^\dagger(y)\rangle \\
&= \int_{-\infty}^{+\infty}\frac{dk}{\sqrt{2\pi}}\int_{-\infty}^{+\infty}\frac{dq}{\sqrt{2\pi}}e^{i(kx-qy)}\langle \psi_0(k)\psi_1^\dagger(q)\rangle \\
&= \int_{-\infty}^{+\infty}\frac{dk}{\sqrt{2\pi}}\int_{-\infty}^{+\infty}\frac{dq}{\sqrt{2\pi}}e^{i(kx-qy)}\cos\left(\theta(k)\right)\mathrm{sign}(q)\sin\left(\theta(q)\right)\langle \tilde{\psi}_0(k)\tilde{\psi}_0^\dagger(q)\rangle \\
&= \int_{-\infty}^{+\infty}\frac{dk}{4\pi}e^{ik(x-y)}\mathrm{sign}(k)\sin\left(2\theta(k)\right) \\
&= i\int_{0}^{+\infty}\frac{dk}{2\pi}\sin(k(x-y))\sin\left(2\theta(k)\right) \\
C_{10}(x,y) &= \langle \psi_1(x)\psi_0^\dagger(y)\rangle = \overline{\langle \psi_0(y)\psi_1^\dagger(x)\rangle} = i\int_{0}^{+\infty}\frac{dk}{2\pi}\sin(k(x-y))\sin\left(2\theta(k)\right) \\
C_{11}(x,y) &= \langle \psi_1(x)\psi_1^\dagger(y)\rangle \\
&= \int_{-\infty}^{+\infty}\frac{dk}{\sqrt{2\pi}}\int_{-\infty}^{+\infty}\frac{dq}{\sqrt{2\pi}}e^{i(kx-qy)}\langle \psi_1(k)\psi_1^\dagger(q)\rangle \\
&= \int_{-\infty}^{+\infty}\frac{dk}{2\pi}e^{ik(x-y)}\sin^2\left(\theta(k)\right) \\
&= \int_{0}^{+\infty}\frac{dk}{\pi}\cos(k(x-y))\sin^2\left(\theta(k)\right)
\end{aligned}
\tag{4.14}
$$

meeting the continuous version of all the requirements for C because the cMERA state is pure and Gaussian. As the integrands do not contain any singularities, there is no need to introduce an IR regulator for Dirac fermions. Furthermore, note that $C_{11}(x,y) = \delta(x-y) - C_{00}(x,y)$. Together with the specific structure of the off-diagonals of C, this implies that when ω is an eigenvalue with eigenfunction $(\kappa_0(x) \quad \kappa_1(x))^T$, $1-\omega$ also is an eigenvalue with eigenfunction $(-\kappa_1(x) \quad \kappa_0(x))^T$, indeed:

$$
\begin{aligned}
& \int \begin{pmatrix} C_{00}(x,y) & C_{01}(x,y) \\ C_{01}(x,y) & \delta(x-y)-C_{00}(x,y)\end{pmatrix}\begin{pmatrix}\kappa_0(y)\\ \kappa_1(y)\end{pmatrix}dy = \omega\begin{pmatrix}\kappa_0(x)\\ \kappa_1(x)\end{pmatrix} \\
\iff \quad & \begin{cases}\int\left(C_{00}(x,y)\kappa_0(y)+C_{01}(x,y)\kappa_1(y)\right)dy = \omega\kappa_0(x) \\ \int\left(C_{01}(x,y)\kappa_0(y)-C_{00}(x,y)\kappa_1(y)\right)dy = (\omega-1)\kappa_1(x)\end{cases} \\
\iff \quad & \int \begin{pmatrix} C_{00}(x,y) & C_{01}(x,y) \\ C_{01}(x,y) & \delta(x-y)-C_{00}(x,y)\end{pmatrix}\begin{pmatrix}-\kappa_1(y)\\ \kappa_0(y)\end{pmatrix}dy = (1-\omega)\begin{pmatrix}-\kappa_1(x)\\ \kappa_0(x)\end{pmatrix}
\end{aligned}
\tag{4.15}
$$

This is a consequence of the charge conjugation symmetry of the Dirac model and guarantees that the entanglement energies are symmetric around zero. Once the eigenvalue problem is solved, the entanglement entropy can be calculated via equation (4.9) while the entanglement Hamiltonian is given by the continuous generalization of equation (4.8):

$$
\begin{aligned}
\mathcal{H} &= \int_{-\frac{L}{2}}^{\frac{L}{2}}dx\int_{-\frac{L}{2}}^{\frac{L}{2}}dy\left[\psi^\dagger(x)\left(\sum_l \epsilon_l\kappa_l(x)\kappa_l^\dagger(y)\right)\psi(y)\right] \\
&= \int_{-\frac{L}{2}}^{\frac{L}{2}}dx\int_{-\frac{L}{2}}^{\frac{L}{2}}dy\begin{pmatrix}\psi_0^\dagger(x) & \psi_1^\dagger(x)\end{pmatrix}\left[\sum_l \epsilon_l\begin{pmatrix}\kappa_{0_l}(x)\kappa_{0_l}^*(y) & \kappa_{0_l}(x)\kappa_{1_l}^*(y)\\ \kappa_{1_l}(x)\kappa_{0_l}^*(y) & \kappa_{1_l}(x)\kappa_{1_l}^*(y)\end{pmatrix}\right]\begin{pmatrix}\psi_0(y)\\ \psi_1(y)\end{pmatrix}
\end{aligned}
\tag{4.16}
$$

As for the bosonic case, the eigenvalue problem in equation (4.12) can only be solved analytically for a product state and when $\Lambda L \ll 1$. First, the case of a product state on the interval $\left[-\frac{L}{2}, \frac{L}{2}\right]$ is treated. For this state, the correlation matrix becomes:

$$C(x,y) = \begin{pmatrix} \delta(x-y) & 0 \\ 0 & 0 \end{pmatrix} \tag{4.17}$$

The eigenfunctions are hence equal to 1 and 0 with eigenspaces $L^2\left(\left[-\frac{L}{2}, \frac{L}{2}\right]\right) \otimes \{0\}$, respectively $\{0\} \otimes L^2\left(\left[-\frac{L}{2}, \frac{L}{2}\right]\right)$. As a result, the entanglement entropy is equal to zero while every contribution to the entanglement Hamiltonian diverges. Indeed, the entanglement energy for eigenvalues equal to one and zero is infinite (see Figure 4.1). The eigenvalue problem can also be solved exactly for cMERA states with $\Lambda L \ll 1$. In this case, the correlation matrix can be approximated by:

$$C(x,y) = \begin{pmatrix} \delta(x-y) - A\Lambda & iB\Lambda^2(x-y) \\ iB\Lambda^2(x-y) & A\Lambda \end{pmatrix} \tag{4.18}$$

where A and B are dimensionless and do not depend on ΛL, resulting in the following eigenvalue problem:

$$\begin{aligned} -A\Lambda \int_{-\frac{L}{2}}^{\frac{L}{2}} \kappa_0(y)dy + iB\Lambda^2 \int_{-\frac{L}{2}}^{\frac{L}{2}} (x-y)\kappa_1(y)dy &= (\omega-1)\kappa_0(x) \\ iB\Lambda^2 \int_{-\frac{L}{2}}^{\frac{L}{2}} (x-y)\kappa_0(y)dy + A\Lambda \int_{-\frac{L}{2}}^{\frac{L}{2}} \kappa_1(y)dy &= \omega\kappa_1(x) \end{aligned} \tag{4.19}$$

The only way for the eigenvalue to be different from 0 and 1 is if the eigenfunctions are linear, *i.e.* if:

$$\kappa_0(x) = a + b\frac{x}{L} \qquad \kappa_1(x) = c + d\frac{x}{L} \tag{4.20}$$

Substituting this in in the previous equation, one obtains:

$$\begin{aligned} -A\Lambda La + iB\Lambda^2 Lcx - i\frac{B}{12}(\Lambda L)^2 d &= (\omega-1)(a + b\frac{x}{L}) \\ iB\Lambda^2 Lax - i\frac{B}{12}(\Lambda L)^2 b + A\Lambda Lc &= \omega(c + d\frac{x}{L}) \end{aligned} \tag{4.21}$$

yielding:

$$a(\omega - 1 + A\Lambda L) = 0 \qquad c(\omega - A\Lambda L) = 0 \qquad (\omega-1)b = \omega d = 0 \tag{4.22}$$

when only terms up to the first order in ΛL are withheld. Two pairs of solutions are found:

$$\begin{cases} \omega = A\Lambda L & c = 1 \quad a = b = d = 0 \\ \omega = 1 - A\Lambda L & a = 1 \quad b = c = d = 0 \end{cases} \qquad \begin{cases} \omega = 0 & d = 1 \quad a = b = c = 0 \\ \omega = 1 & b = 1 \quad a = c = d = 0 \end{cases} \tag{4.23}$$

implying that only the constant eigenfunctions contribute to the entanglement entropy:

$$S = -2\left[A\Lambda L \ln\left(A\Lambda L\right) + \left(1 - A\Lambda L\right)\ln\left(1 - A\Lambda L\right)\right] \tag{4.24}$$

while also yielding a non-divergent zeroth-order contribution to the entanglement Hamiltonian:

$$\mathcal{H} = \int_{-\frac{L}{2}}^{\frac{L}{2}} dx \int_{-\frac{L}{2}}^{\frac{L}{2}} dy \begin{pmatrix} \psi_0^\dagger(x) & \psi_1^\dagger(x) \end{pmatrix} \begin{pmatrix} \epsilon & 0 \\ 0 & -\epsilon \end{pmatrix} \begin{pmatrix} \psi_0(y) \\ \psi_1(y) \end{pmatrix} \tag{4.25}$$

where $\epsilon = \epsilon(1 - A\Lambda L) = \ln\left(\frac{1-A\Lambda L}{A\Lambda L}\right)$ is the positive entanglement energy corresponding to the eigenvalue $\omega = 1 - A\Lambda L$. Notice that the diagonal "blocks" in the entanglement Hamiltonian have an opposite sign while the off-diagonals are equal. This specific structure is a consequence of the $U(1)$ symmetry of the Dirac field and will therefore be found for all entanglement Hamiltonians. Indeed, by virtue of the generally valid result in equation (3.49), the entanglement Hamiltonian of the ground state (restricted to L) for a massless Dirac theory is given by:

$$\begin{aligned}\mathcal{H} &= \int_{-\frac{L}{2}}^{\frac{L}{2}} dx \frac{2\pi}{L}\left(\frac{L^2}{4} - x^2\right)\begin{pmatrix}\psi_0^\dagger(x) & \psi_1^\dagger(x)\end{pmatrix}\begin{pmatrix}0 & -i\frac{d}{dx}\\ -i\frac{d}{dx} & 0\end{pmatrix}\begin{pmatrix}\psi_0(x)\\ \psi_1(x)\end{pmatrix}\\ &= \int_{-\frac{L}{2}}^{\frac{L}{2}} dx f(x)\begin{pmatrix}\psi_0^\dagger(x) & \psi_1^\dagger(x)\end{pmatrix}\begin{pmatrix}0 & -i\frac{d}{dx}\\ -i\frac{d}{dx} & 0\end{pmatrix}\begin{pmatrix}\psi_0(x)\\ \psi_1(x)\end{pmatrix}\end{aligned} \tag{4.26}$$

having the same structure as before (though with zero diagonal blocks). In analogy with the bosonic case, the upper diagonal block will therefore be called $N(x, y)$ while the off-diagonals are given by $M(x, y)$. *I.e.*, the prefactors are defined by:

$$\mathcal{H} = \int_{-\frac{L}{2}}^{\frac{L}{2}} dx \int_{-\frac{L}{2}}^{\frac{L}{2}} dy \begin{pmatrix}\psi_0^\dagger(x) & \psi_1^\dagger(x)\end{pmatrix}\begin{pmatrix}N(x,y) & M(x,y)\\ M(x,y) & -N(x,y)\end{pmatrix}\begin{pmatrix}\psi_0(y)\\ \psi_1(y)\end{pmatrix} \tag{4.27}$$

Furthermore, the logarithmic scaling from equation (3.55) still applies for the Rényi entropies in the CFT regime.

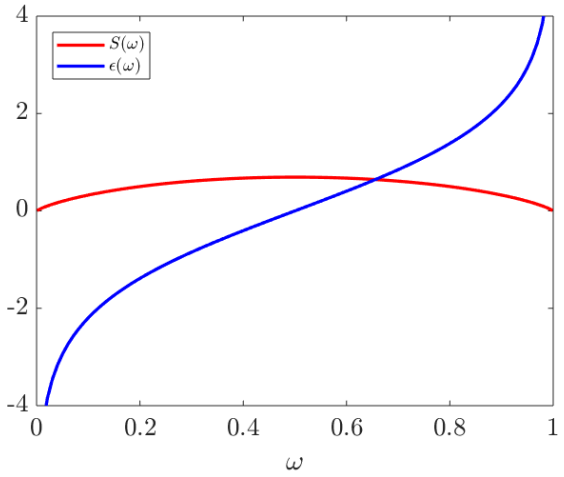

Figure 4.1: Comparison between the entanglement entropy contribution $S(\omega)$ and the entanglement energy $\epsilon(\omega)$ of an eigenvalue ω.

The analytical approach learns that the fermionic case is very similar to the bosonic. Indeed, for the product state ($\Lambda L = 0$), infinitely many eigenvalues are zero while equally many are equal to one. Therefore, all entanglement energies diverge, leading to a completely divergent entanglement Hamiltonian. The entanglement entropy on the other hand is zero. When ΛL becomes larger than zero, the Taylor method shows that the eigenvalues, originally equal to one, become slightly smaller, while the eigenvalues, that were equal to zero for the product state, increase. The resulting picture for the spectrum is one consisting of two arrays: an array increasing to one and another decreasing to zero. Both are related by the fact that all the

eigenvalues occur in pairs with a sum equal to one. As multiple eigenvalues are now located between zero and one, multiple eigenvalues contribute to the entanglement entropy. Figure 4.1 shows however that the entanglement entropy is mostly dominated by the eigenvalues close to $\frac{1}{2}$. Increasing ΛL, the eigenvalues are typically removed further from zero and one (*cfr.* equation (4.23)), yielding a larger entropy. Again, the entropy is thus a monotonically increasing function of ΛL. For the entanglement Hamiltonian on the other hand, Figure 4.1 shows that the largest contributions arise from eigenvalues close to zero and one. The structure of the spectrum thus leads to a series of increasing contributions for $\mathcal{H}$. As in the bosonic case, these increasing contributions pile up to delta functions (and their derivatives) when $\Lambda L = +\infty$, resulting in a non-divergent entanglement Hamiltonian. cMERAs with smaller ΛL on the other hand, still contain a product state part and we expect that this product state part (corresponding to unentangled degrees of freedom at length scales smaller than $\epsilon \approx \Lambda^{-1}$) will make the entanglement Hamiltonian diverge.

4.1.3 Discretization Approach

In order to calculate the (Rényi) entanglement entropies and the modular Hamiltonian for free Dirac cMERAs, the (regularized) discretization method has to be extended to a fermionic context. To do so, the fields are placed on an equidistant lattice according to $\psi_{\mu_i} \leftrightarrow \sqrt{a}\psi_\mu(ia)$ and with $\{\psi_i, \psi_j^\dagger\} = \delta_{ij}$ and $\{\psi_i, \psi_j\} = \{\psi_i^\dagger, \psi_j^\dagger\} = 0$. The correlation matrix is further chosen to be in correspondence with the continuous cMERA states:

$$\begin{aligned}
C_{11_{ij}} &= \langle \psi_{1_i} \psi_{1_j}^\dagger \rangle \\
&\equiv a\langle \psi_1(ia)\psi_1^\dagger(ja)\rangle \\
&= a\int_{-\infty}^{+\infty} \frac{dk}{2\pi} e^{ika(i-j)} \sin^2(\theta(k)) \\
&= a\int_{0}^{+\infty} \frac{dk}{\pi} \cos(ka(i-j)) \sin^2(\theta(k)) \\
C_{01_{ij}} &= \langle \psi_{0_i} \psi_{1_j}^\dagger \rangle \\
&\equiv a\langle \psi_0(ia)\psi_1^\dagger(ja)\rangle \\
&= a\int_{-\infty}^{+\infty} \frac{dk}{4\pi} e^{ika(i-j)} \mathrm{sign}(k) \sin(2\theta(k)) \\
&= ia\int_{0}^{+\infty} \frac{dk}{2\pi} \sin(ka(i-j)) \sin(2\theta(k)) \\
C_{10_{ij}} &= \langle \psi_{1_i} \psi_{0_j}^\dagger \rangle \\
&\equiv a\langle \psi_1(ia)\psi_0^\dagger(ja)\rangle = \overline{a\langle \psi_0(ja)\psi_1^\dagger(ia)\rangle} = C_{01_{ij}} \\
C_{00_{ij}} &= \langle \psi_{0_i} \psi_{0_j}^\dagger \rangle \\
&\equiv \delta_{ij} - C_{11_{ij}}
\end{aligned} \tag{4.28}$$

In order to apply the method from Section 4.1.1 to this discretized model, the states fixed by the correlation matrix above have to correspond to a Gaussian state on the lattice, thus meeting all the requirements mentioned in Section 4.1.1. It is trivial to see that C is Hermitian and positivity typically applies when a is not too large. Via the anticommutation relations, one

easily proves that $I - C$ is also Hermitian and positive in this case, yielding that the eigenvalues are contained in $[0, 1]$. As a result, only the condition that $\sum_{l=-\infty}^{+\infty} C_{il}C_{lj} = C_{ij}$ has yet to be verified. This is the case when the limit $a \to 0$ is considered. Indeed, working out the square of C_{11}, one obtains:

$$\begin{aligned}\sum_{l=-\infty}^{+\infty} C_{11_{il}}C_{11_{lj}} &= a^2 \sum_{l=-\infty}^{+\infty} \int_{-\infty}^{+\infty} \frac{dk}{2\pi} e^{ika(i-l)} \sin^2(\theta(k)) \int_{-\infty}^{+\infty} \frac{dq}{2\pi} e^{iqa(l-j)} \sin^2(\theta(q)) \\ &= a^2 \int_{-\infty}^{+\infty} \frac{dk}{2\pi} \int_{-\infty}^{+\infty} \frac{dq}{2\pi} \sin^2(\theta(k)) \sin^2(\theta(q)) e^{ia(ki-qj)} \sum_{l=-\infty}^{+\infty} e^{ial(q-k)} \\ &= a \int_{-\infty}^{+\infty} \frac{dk}{2\pi} e^{ika(i-j)} \sin^4(\theta(k))\end{aligned} \tag{4.29}$$

Completely analogous calculations also yield that:

$$\begin{aligned}\sum_{l=-\infty}^{+\infty} C_{01_{il}}C_{01_{lj}} &= a \int_{-\infty}^{+\infty} \frac{dk}{2\pi} e^{ika(i-j)} \cos^2(\theta(k)) \sin^2(\theta(k)) \\ \sum_{l=-\infty}^{+\infty} C_{11_{il}}C_{01_{lj}} &= \frac{a}{2} \int_{-\infty}^{+\infty} \frac{dk}{2\pi} e^{ika(i-j)} \sin^2(\theta(k)) \operatorname{sign}(k) \sin(2\theta(k)) = \sum_{l=-\infty}^{+\infty} C_{01_{il}}C_{11_{lj}}\end{aligned} \tag{4.30}$$

As a result, C^2 always reduces to:

$$\begin{aligned}\left(\begin{array}{c|c} C_{00} & C_{01} \\ \hline C_{01} & C_{11} \end{array}\right)^2 &= \left(\begin{array}{c|c} C_{00}^2 + C_{01}^2 & C_{01} - C_{11}C_{01} + C_{01}C_{11} \\ \hline C_{01} - C_{01}C_{11} + C_{11}C_{01} & C_{01}^2 + C_{11}^2 \end{array}\right) \\ &= \left(\begin{array}{c|c} C_{00}^2 + C_{01}^2 & C_{01} \\ \hline C_{01} & C_{11} \end{array}\right)\end{aligned} \tag{4.31}$$

To show that the upper diagonal block is equal to C_{00}, one has to exploit the fact that $a \to 0$:

$$\begin{aligned}C_{00_{ij}} &= \delta_{ij} - C_{11_{ij}} \\ &= a\delta(ia - ja) - a \int_{-\infty}^{+\infty} \frac{dk}{2\pi} e^{ika(i-j)} \sin^2(\theta(k)) = a \int_{-\infty}^{+\infty} \frac{dk}{2\pi} e^{ika(i-j)} \cos^2(\theta(k))\end{aligned} \tag{4.32}$$

so that:

$$\sum_{l=-\infty}^{+\infty} C_{00_{il}}C_{00_{lj}} = a \int_{-\infty}^{+\infty} \frac{dk}{2\pi} e^{ika(i-j)} \cos^4(\theta(k)) \quad \Rightarrow \quad C_{00}^2 + C_{01}^2 = C_{00} \tag{4.33}$$

completing the proof. The method to determine the entanglement properties from Section 4.1.1 can therefore safely be applied to the discretized fields with the continuum-based correlators from equation (4.28) when working with small lattice spacings. The resulting discrete eigenvalue problem will then yield a finite spectrum, approximating the infinite spectrum of the continuous cMERA state, as well as a discretized version of the entanglement Hamiltonian prefactors. The smaller a is chosen, the more eigenvalues are obtained and the closer they get to their continuous cMERA value. On the other hand, decreasing a, increases the resolution with which the entanglement Hamiltonian prefactors are probed, thus improving the correspondence to their continuous analogues.

The discretization method for fermions suffers from computational problems similar to those in the bosonic case. Indeed, for small lattice spacings, a large number of lattice points will be contained in the physical interval L. As a result, the discretized eigenvalue problem of C will have large dimensions and a lot of eigenvalues will have to be determined. However, these eigenvalues rapidly get close to zero and one, making it hard to determine them correctly by computational means. As for the Klein-Gordon bosons however, these computational difficulties can be circumvented for the entanglement entropy. Indeed, as Figure 4.1 shows, only the eigenvalues close to $\frac{1}{2}$ contribute substantially to the entanglement entropy. Therefore, only these eigenvalues should be determined correctly. One can thus simply solve the eigenvalue problem for a high-dimensional C with standard working precision, keep the highest (and correctly determined) eigenvalues to calculate the entanglement entropy and discard the lower (incorrectly determined) eigenvalues as they hardly have any influence on the entanglement entropy. In accordance to the bosonic case, all eigenvalues closer to one or zero than 10^{-10} were hence discarded. For the entanglement Hamiltonian on the other hand, the eigenvalues close to zero and one have a dominant influence, thus seemingly precluding a comprehensive study of $\mathcal{H}$. However, assume that the spectra obtained via the discretization approach again have an exponentially decaying tail, given by:

$$\omega_{\text{low}_l} = ze^{-\frac{c}{a\Lambda}l} \qquad \text{for} \quad l \gg 1 \tag{4.34}$$

where the "low" subscript indicates that these are the eigenvalues smaller than $\frac{1}{2}$ (their partners greater than $\frac{1}{2}$ are simply given by $\omega_{\text{high}_l} = 1 - \omega_{\text{low}_l}$). With this spectral structure, each continuum cMERA state has eigenvalues equal to zero and one when $\Lambda < +\infty$. Consequently, the entanglement Hamiltonian diverges. As in the bosonic case, we were not yet able to verify that the spectra indeed exhibit the aforementioned exponential tails. However, the proposed behavior is in agreement with the well-known spectral structure of the product and target states. Furthermore, the results presented in the following sections will support this ansatz. Therefore, the validity of equation (4.34) is assumed throughout the rest of this work. An immediate consequence hereof is the typical scaling factor $\frac{1}{a\Lambda}$ for the prefactor matrices M and N, indeed:

$$\begin{cases} M_{ij} \\ N_{ij} \end{cases} \sim \quad |\epsilon(\omega_{\text{low}_l})| = |\epsilon(\omega_{\text{high}_l})| = \ln\left(\frac{1 - ze^{-\frac{c}{a\Lambda}l}}{ze^{-\frac{c}{a\Lambda}l}}\right) \approx \ln\left(\frac{1}{z}e^{-\frac{c}{a\Lambda}l}\right) \sim \frac{1}{a\Lambda} \tag{4.35}$$

Together with the discretization procedure, this will yield specific scaling laws for the various contributions to the prefactor matrices. As in the bosonic case, high-precision calculations for increasingly small lattice spacing should be able to separate these differently scaling contributions in order to yield a complete description of the entanglement Hamiltonian. For now however, we restricted ourselves to the determination of the non-divergent part of the entanglement Hamiltonian by terminating the $a \to 0$ limit when $a = \epsilon = \frac{\pi}{\Lambda}$ is reached. Indeed, in this way, the unentangled, small length scale degrees of freedom, responsible for the product state part of the cMERA are removed, thus yielding a non-divergent entanglement Hamiltonian. However, as a is now equal to ϵ, it is not necessarily true anymore that $\sum_{l=-\infty}^{+\infty} C_{il}C_{lj} = C_{ij}$. Luckily, this

is still the case for cMERAs with a sharp cut-off function at $\Lambda = \frac{\pi}{a}$, indeed:

$$\begin{aligned} C_{00_{ij}} &= \delta_{ij} - C_{11_{ij}} \\ &= a\int_{-\frac{\pi}{a}}^{\frac{\pi}{a}} \frac{dk}{2\pi} e^{ika(i-j)} - a\int_{-\frac{\pi}{a}}^{\frac{\pi}{a}} \frac{dk}{2\pi} e^{ika(i-j)} \sin^2(\theta(k)) \\ &= a\int_{-\frac{\pi}{a}}^{\frac{\pi}{a}} \frac{dk}{2\pi} e^{ika(i-j)} \cos^2(\theta(k)) \end{aligned} \tag{4.36}$$

so that:

$$\sum_{l=-\infty}^{+\infty} C_{00_{il}} C_{00_{lj}} = a\int_{-\frac{\pi}{a}}^{\frac{\pi}{a}} \frac{dk}{2\pi} e^{ika(i-j)} \cos^4(\theta(k)) \quad \Rightarrow \quad C_{00}^2 + C_{01}^2 = C_{00} \tag{4.37}$$

while the requirement is generally valid for the other block matrices. To calculate the regularized entanglement Hamiltonian, the discrete field method from Section 4.1.1 can thus safely be applied to the discretized fields with the continuum-based correlators from equation (4.28) when working with $a = \frac{\pi}{\Lambda}$ and a sharp cut-off. For a Gaussian cut-off function on the other hand, the regularized discretization method is not applicable. As for the Klein-Gordon bosons, the condition $a = \frac{\pi}{\Lambda}$ fixes the resolution of the obtained prefactors while also circumventing computational difficulties. Only for large ΛL values, the working precision has to be increased. Finally, the interpolation scheme lined out at the end of Section 3.1.3 and in equation (3.67) should also be used for fermions in order for the calculated quantities to depend only on the length L of the physical interval and not on its position.

4.2 Entanglement Properties

4.2.1 Entanglement Entropy

The entanglement entropy was first calculated for free, massless Dirac cMERAs with sharp and Gaussian cut-off functions using the standard discretization method in combination with the $\theta(k)$ angles determined in Chapter 2. As Figure 4.2 shows, the obtained profiles are similar to those for Klein-Gordon bosons (Figure 3.4) with a correspondence to the analytical profile for small ΛL and a logarithmic scaling for large ΛL. Again, $\Lambda a = 0.01$ was used for $\Lambda L < 10$ while $\Lambda a = 0.1$ for $\Lambda L > 10$ in order to reach converged entropy values. In the large ΛL limit, linear fits were performed yielding the following estimates for the central charge of the theory:

$$c_{\text{sharp}} = 1.004 \qquad c_{\text{Gaussian}} = 1.001 \tag{4.38}$$

Comparing this with equation (3.68), the fermionic results agree better with the theoretical value $c = 1$. Indeed, since for Dirac fermions, no IR regulator has to be introduced, the correspondence between the estimated c and its theoretical value improves.

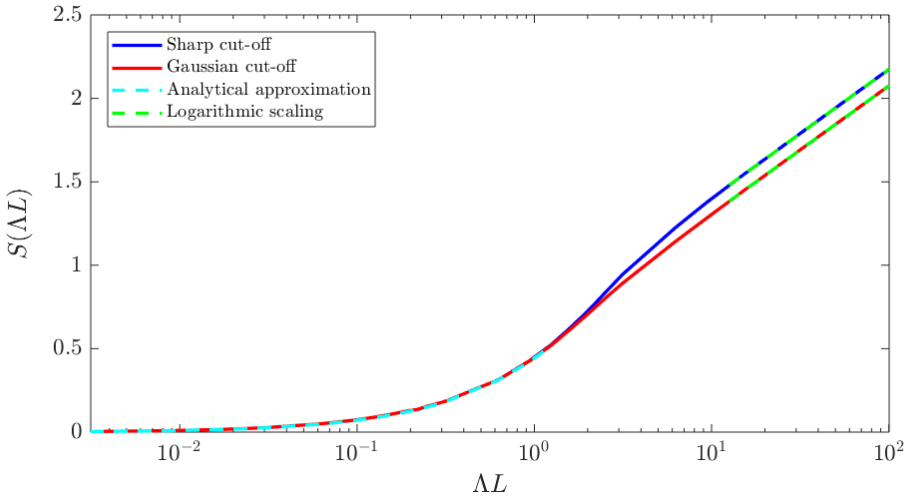

Figure 4.2: Numerically determined entropy profiles for free, massless Dirac cMERAs with sharp and Gaussian cut-off functions as well as the low ΛL approximation and linear fits for high ΛL.

Adding a mass to the field theory, the entropy decreases because the mass suppresses long-range fluctuations. This is illustrated by Figure 4.3. As for bosons, the slopes of the profiles are similar in the linear regime, confirming that in this limit the entanglement entropy displays a universal behavior. Also the typical offset near $\Lambda L = mL$ is found for the fermionic theory.

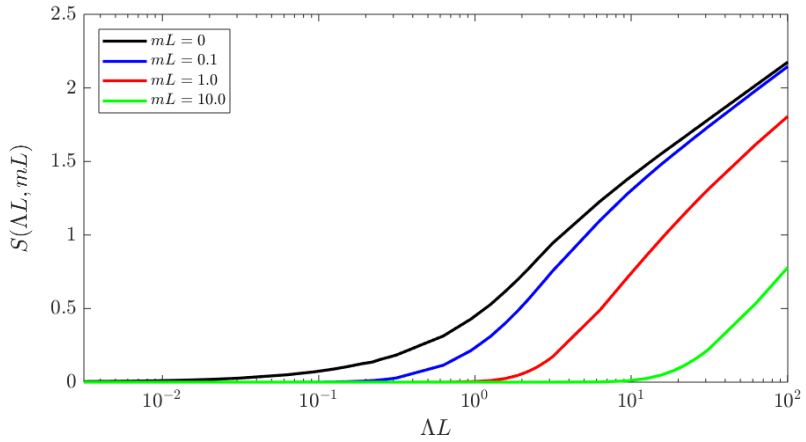

Figure 4.3: Numerically determined entropy profiles for both massless and massive cMERAs with a sharp cut-off function illustrating the influence of adding a mass to the Dirac field.

Besides the standard Von Neumann entanglement entropies, collision and minimum entropies were also calculated for the Dirac cMERAs. The results are collected in Figure 4.4. As for the Klein-Gordon bosons, the profiles behave similarly for the three cMERA types and the Rényi entropies decrease with increasing β. In the large ΛL region, linear fits were performed, yielding the estimates for the central charge displayed in Table 4.1. The best correspondence was obtained for a massless cMERA with a sharp cut-off function, slightly outperforming the variant with a Gaussian cut-off. For the massive cMERA on the other hand, the slope is typically overestimated but this is mainly due to the fact the profiles are not yet fully linear in the considered ΛL range.

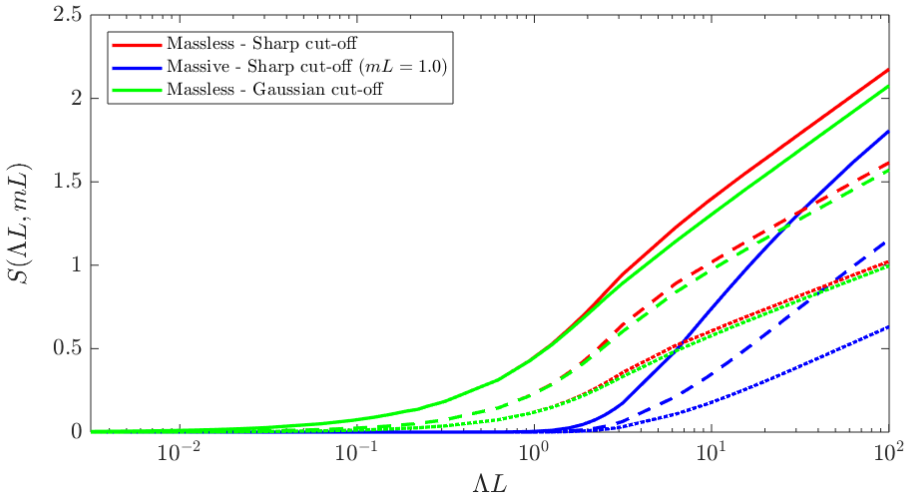

Figure 4.4: Rényi entropies for various cMERA states and for $\beta = 1$ (Von Neumann entropy, solid line), $\beta = 2$ (collision entropy, dashed line) and $\beta = +\infty$ (minimum entropy, dotted line).

β	Theoretical Slope	Massless Sharp cut-off	Massless Gaussian cut-off	Massive Sharp cut-off
1	$\frac{c}{3} \approx 0.333$	0.335	0.334	0.452
2	$\frac{c}{4} \approx 0.250$	0.256	0.257	0.354
$+\infty$	$\frac{c}{6} \approx 0.167$	0.179	0.180	0.200

Table 4.1: Comparison between theoretical slopes of the Rényi entanglement entropies and their fitted values ($mL = 1.0$ in the massive case).

Finally, entanglement entropies were also calculated following the regularized discretization approach. As in the bosonic case, slightly smaller entanglement entropies were found, indicating again that a small part of the complete entanglement entropy may be concentrated on length scales smaller than $\epsilon \approx \Lambda^{-1}$.

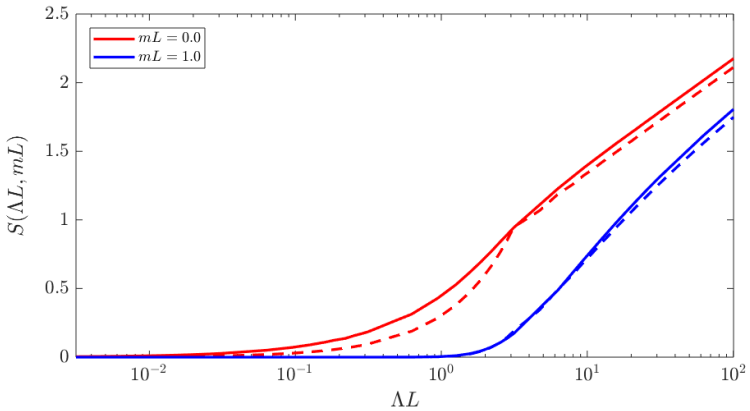

Figure 4.5: Comparison between saturated (solid line) and regularized (dashed line) entanglement entropies in the massless and massive case (both with sharp cut-off function).

4.2.2 Entanglement Hamiltonian

The non-divergent part of the entanglement Hamiltonian for massless Dirac cMERAs was determined by applying the regularized discretization approach. The resulting profiles for the M prefactor are displayed in Figure 4.6. Note that M is imaginary and becomes systematically more peaked for large ΛL. As in the bosonic case, this indicates a delta function-like behavior in the limit $\Lambda L \to +\infty$. Inspecting the profiles more carefully, one observes an upward and positive peak in combination with a downward negative peak. This corresponds to the intuitive notion of a discretized $\delta'(x-y)$ distribution. The M prefactor thus seems to approach the correct CFT limit. Indeed, the part of the CFT entanglement Hamiltonian corresponding to M is given by:

$$-i\int_{-\frac{L}{2}}^{\frac{L}{2}} dx f(x)\psi_0^\dagger(x)\frac{d}{dx}\psi_1(x) \quad \leftrightarrow \quad -i\sum_i f_i \psi_{0_i}^\dagger \psi'_{1_i} \tag{4.39}$$

containing a first derivative. As this is the only contribution to the entanglement Hamiltonian in the CFT limit, it scales dominantly. Therefore, we expect to retrieve the CFT parabola $f(x)$ from the M matrix.

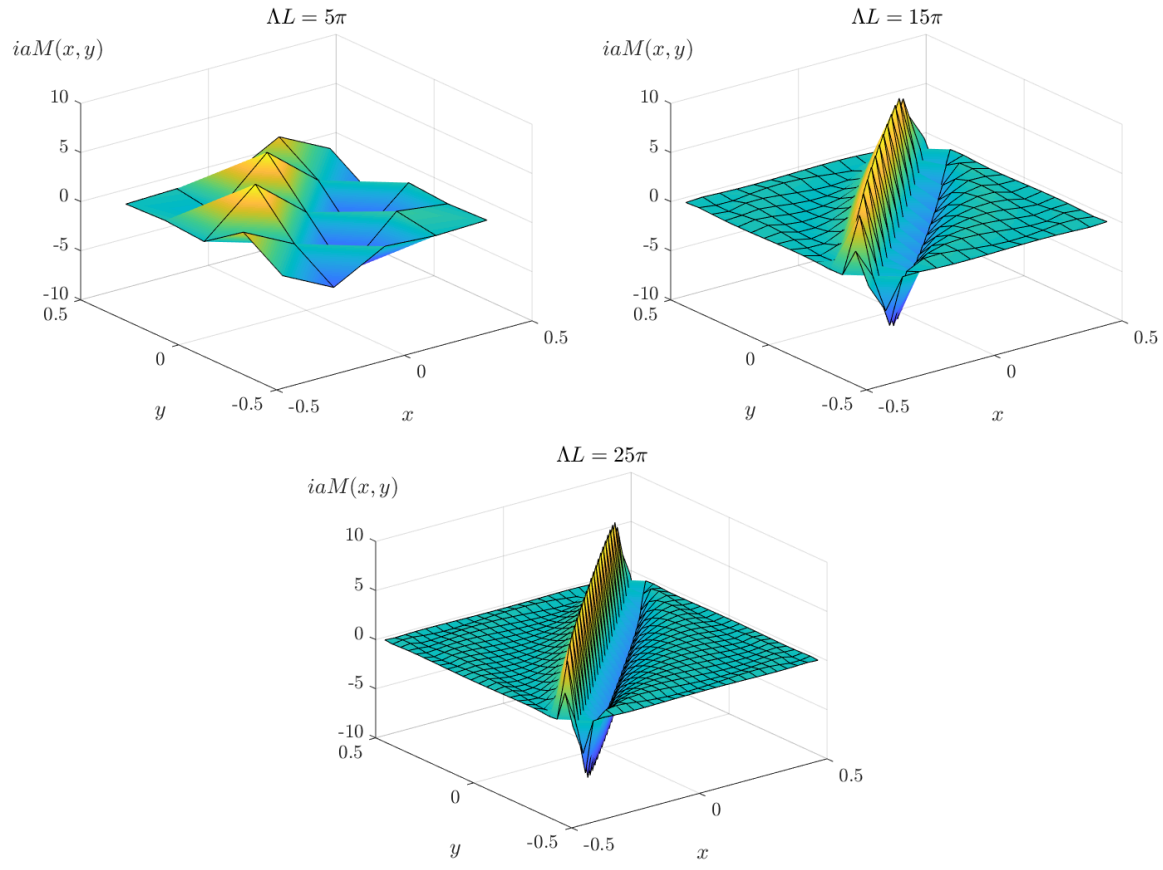

Figure 4.6: Regularized $iaM(x,y) \leftrightarrow iM_{ij}$ prefactors of massless Dirac cMERAs for several ΛL values.

To extract the CFT parabola $f(x)$ from the M matrix, we proceed as follows:

$$\begin{aligned}
&\int_L \int_L \psi_0^\dagger(x) M(x,y) \psi_1(y) dx dy \quad \leftrightarrow \quad a^2 \sum_i \sum_{j=1}^{n} \frac{\psi_{0_i}^\dagger}{\sqrt{a}} \frac{M_{ij}}{a} \frac{\psi_{1_j}}{\sqrt{a}} = \\
&= a \sum_i \sum_j \psi_0^\dagger(ia) M_{ij} \psi_1(ja) \\
&= a \sum_i \sum_{j=i-j_{max}}^{i+j_{max}} \psi_0^\dagger(ia) M_{ij} \left(\psi_1(ia) + (j-i)a\psi_1'(ia) + \mathcal{O}(a^2) \right) \\
&= a \sum_i \psi_0^\dagger(ia) \left(\sum_{j=i-j_{max}}^{i+j_{max}} M_{ij} \right) \psi_1(ia) + a \sum_i \psi_0^\dagger(ia) \left(a \sum_{j=i-j_{max}}^{i+j_{max}} (j-i) M_{ij} \right) \psi_1'(ia) + \mathcal{O}(a^3) \\
&\approx \sum_i \psi_{0_i}^\dagger \left(\sum_{j=i-j_{max}}^{i+j_{max}} M_{ij} \right) \psi_{1_i} + \sum_i \psi_{0_i}^\dagger \left(\sum_{j=i-j_{max}}^{i+j_{max}} (j-i) M_{ij} \right) \psi_{1_i}'
\end{aligned} \tag{4.40}$$

Comparing this to equation (4.39) the following correspondence is found:

$$f(ia) \leftrightarrow a f_i \approx ia \sum_{j=i-j_{max}}^{i+j_{max}} (j-i) M_{ij} \tag{4.41}$$

As Figure 4 illustrates, the correctly summed out version of M indeed corresponds to the CFT parabola. Both the curvature and the maximum are reproduced almost exactly.

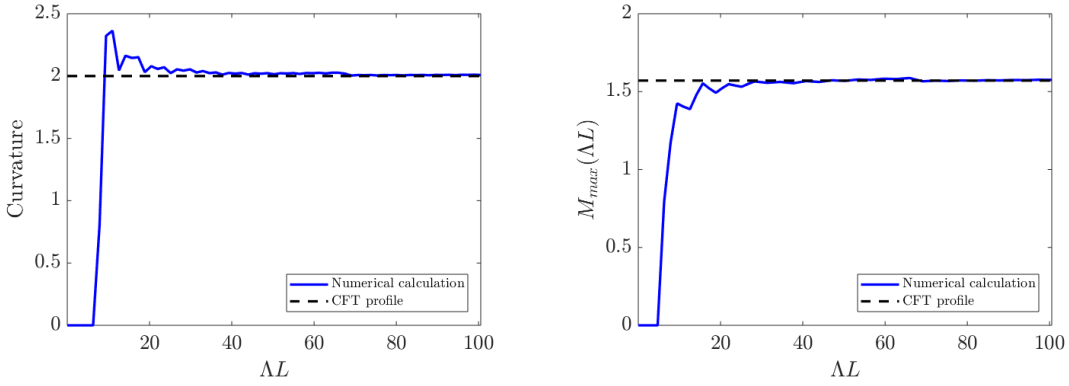

Figure 4.7: Detailed comparison between the CFT profile $f(x)$ and $ia \sum_{j=i-j_{max}}^{i+j_{max}} (j - i) M_{ij}$.

Next, the regularized N prefactor matrix was determined for the massless Dirac cMERA. The resulting profiles are displayed in Figure 4.8. Again, these profiles become systematically more peaked for larger ΛL, indicating a delta function behavior. In the CFT limit however, the $N(x,y)$ prefactor equals zero. As a result, the N matrix should approach a delta function multiplied by zero. To verify this, the same reasoning as in equation (4.40) can be followed, now leading to the following correspondence:

$$0 \leftrightarrow 0 \approx \sum_{j=i-j_{max}}^{i+j_{max}} N_{ij} \tag{4.42}$$

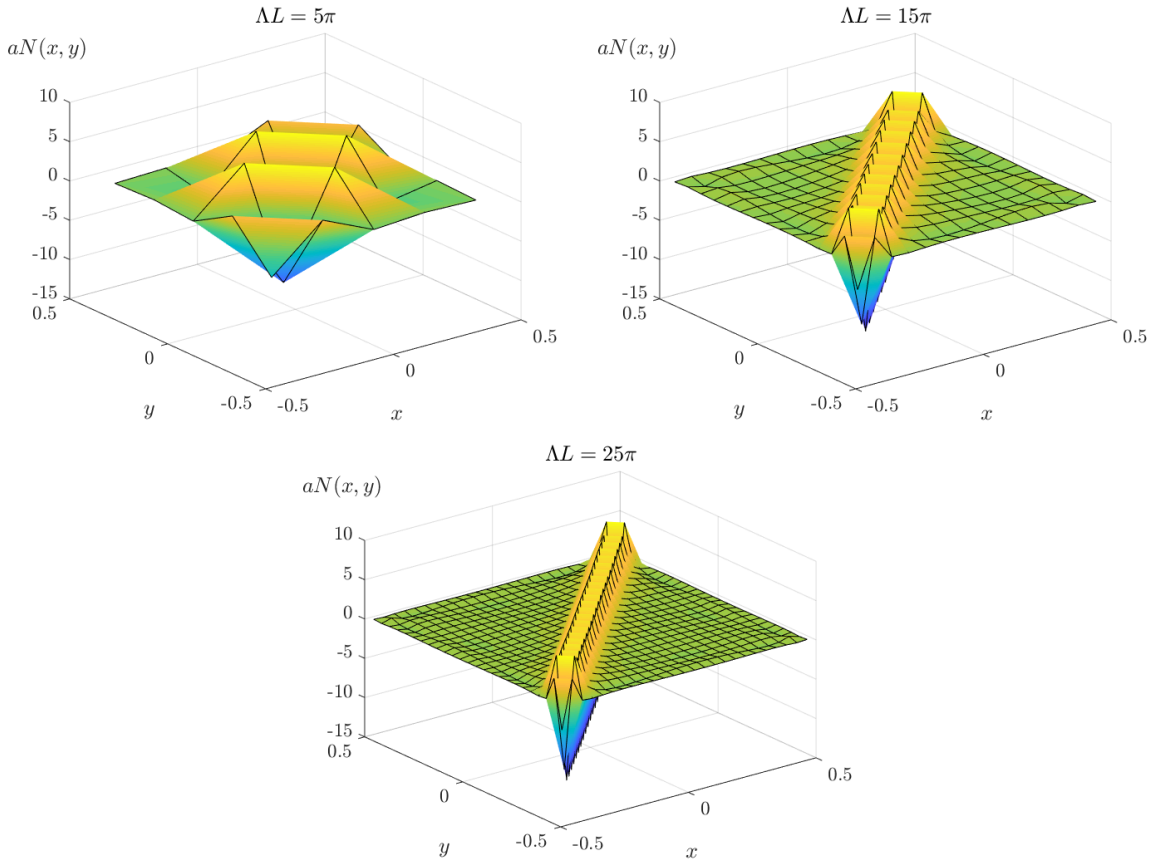

Figure 4.8: Regularized $aN(x,y) \leftrightarrow N_{ij}$ prefactors of massless Dirac cMERAs for several ΛL values.

In Figure 4.9, the maximum of this summed out version of N was displayed, confirming that in the limit $\Lambda L \to +\infty$, the N matrix corresponds to a delta function multiplied by zero.

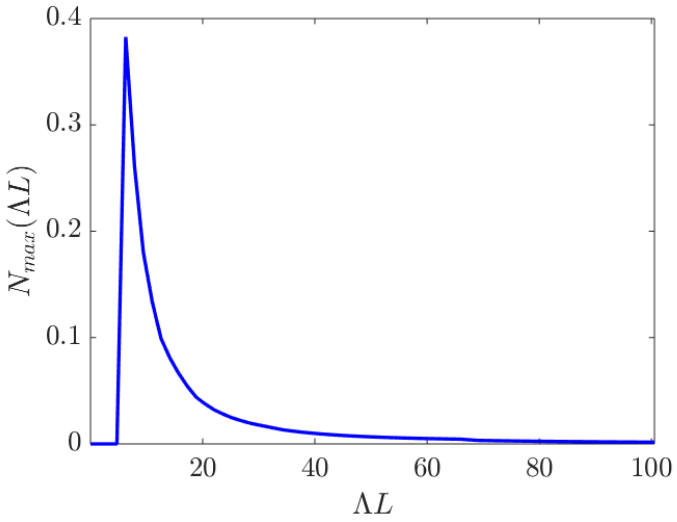

Figure 4.9: Maximum of the summed version of the regularized N matrix.

Chapter 5

Conclusion and Outlook

In this work, the entanglement properties of cMERA states for free quantum fields theories were studied. To this end, their entanglement entropy and modular Hamiltonian were determined. Where the former is an easily interpretable quantity, describing how much entanglement is present in a quantum state, the latter offers a more complete picture of how entanglement is structured and as such allows to derive all other entanglement properties. Furthermore, it provides a versatile tool in the study of universal behavior in extended quantum systems.

Before calculating any of these quantities, the cMERA state itself was discussed extensively in Chapter 2. Focusing on its interpretation as the continuous analogue of the MERA tensor network and on the important role of the energy cut-off Λ, the cMERA state was understood as a product state whereto correlations are added on increasingly large length scales via a unitary RG flow. The explicit construction of this unitary was performed for Klein-Gordon and Dirac field theories in (1+1) dimensions. Once constructed, the question remained: how to determine the (Rényi) entanglement entropies and the entanglement Hamiltonian for cMERA states? Pivotal in this context was the paper of Casini and Huerta reviewing how entanglement properties can be derived from the two-point correlators of Gaussian states.[23] Indeed, based on this procedure, Vidal *et al.* were able to calculate the entanglement entropy for cMERA states of massless CFTs,[47] while Casini *et al.* successfully applied the method to study the entanglement Hamiltonian for QFT ground states.[24] In this project, we wanted to apply the methodology to cMERA states with a two-fold goal: reproducing the findings of Vidal *et al.* for the entanglement entropy on the one hand, but on the other hand also elaborating on these results by considering massive field theories as well as (Rényi) entropies other than the standard Von Neumann entropy. Furthermore, the determination of the entanglement Hamiltonian for cMERA states was put forward as an objective.

In order to achieve these goals, the so-called discretization method was proposed. Herein, the quantum fields are discretized (*i.e.* placed on an equidistant lattice with lattice spacing a) and attributed two-point correlators corresponding to the continuous cMERA state. The entanglement properties of this discretized system can then be calculated by the method of Casini and Huerta, amounting to a matrix eigenvalue problem. Solving this and finally taking the limit $a \to 0$, the continuous entropy properties are found. Applying this procedure to CFT cMERAs,

a satisfactory correspondence was obtained between the calculated entanglement entropies and those determined by Vidal *et al.* Furthermore, the entropy profiles were found to agree with analytical approximations in both low and high Λ regions (e.g. the well-known logarithmic scaling law for high Λ was reproduced correctly). Considering massive quantum field theories on the other hand, an overall decrease of the entropy profiles was obtained together with a well-understood offset near $m = \Lambda$. Also collision and minimum entropies were determined for the various cMERAs. These too correspond to the expectations, for instance confirming that the Rényi entropy S_β is a non-increasing function of β. By performing linear fits to the entropies in the logarithmically scaling region, it was possible to retrieve the central charge of the theory numerically.

As the unitary cMERA evolution only introduces correlations on length scales larger than $\epsilon \approx \Lambda^{-1}$, the resulting state still behaves as a product state below ϵ. However, the entanglement Hamiltonian of a product state is completely divergent. Therefore, the modular Hamiltonian $\mathcal{H}$ of a cMERA state is also expected to diverge due to its inherent product state part. In the performed numerical calculations this was reflected by the fact that the discretized version of the entanglement Hamiltonian prefactors diverged as $a \to 0$. By dimensional arguments, based on the discretization procedure, we showed that these divergences follow different scaling laws for different $\mathcal{H}$ contributions (e.g. local scales differently than non-local). This allows for a scaling-based decomposition of the discretized entanglement Hamiltonian, yielding a complete description of how and why each part of $\mathcal{H}$ diverges. However, to perform such a decomposition, one needs enhanced computational accuracy to correctly solve the encountered matrix eigenvalue problems. As we did not have the time nor the resources to perform these calculation within the scope of this thesis, an alternative regularization scheme was proposed. This so-called regularized discretization approach is formally identical to the standard method but with $a = \epsilon$ instead of $a \to 0$. The aim of this modification is to remove the unentangled degrees of freedom on small length scales. In this way, the product state part of the cMERA is removed as well, yielding a non-divergent entanglement Hamiltonian corresponding to those degrees of freedom that were entangled by the cMERA unitary. An important consequence of this regularization is that in the limit for large Λ, only the dominant part of the calculated prefactors can be compared to CFT results. For this dominant part, a satisfactory correspondence with analytical results was obtained for both Klein-Gordon and Dirac theories. To study the sub-dominant parts of the entanglement Hamiltonian however (e.g. the influence of a mass is typically a sub-dominant effect), a scaling-based decomposition is indispensable. Therefore, the most obvious prospect of this thesis is the high-precision determination of cMERA entanglement Hamiltonians, allowing scaling-based decompositions.

In conclusion, one could say that the main goal of this work, to better understand the entanglement properties of cMERA states, was achieved successfully. Not only did we gain qualitative insight in the how the entanglement properties change as a function of relevant variables, we were also able to determine these properties quantitatively, reproducing theoretical results. Only for the entanglement Hamiltonian further research is required focusing on its sub-dominant contributions.

Bibliography

[1] Michael E. Peskin and Daniel V. Schroeder. *An Introduction to quantum field theory.* Addison-Wesley, Reading, USA, 1995.

[2] Hans A. Bethe. The electromagnetic shift of energy levels. *Physical Review*, 72:339–341, August 1947.

[3] Kenneth G. Wilson. Renormalization group and critical phenomena. 1. Renormalization group and the Kadanoff scaling picture. *Phys. Rev.*, B4:3174–3183, 1971.

[4] Kenneth G. Wilson. Renormalization group and critical phenomena. 2. Phase space cell analysis of critical behavior. *Phys. Rev.*, B4:3184–3205, 1971.

[5] Kenneth G. Wilson. The Renormalization Group: Critical Phenomena and the Kondo Problem. *Rev. Mod. Phys.*, 47:773, 1975.

[6] Leo P. Kadanoff. Scaling laws for Ising models near T(c). *Physics*, 2:263–272, 1966.

[7] Steven R. White. Density matrix formulation for quantum renormalization groups. *Phys. Rev. Lett.*, 69:2863–2866, November 1992.

[8] Tim R Morris. The exact renormalization group and approximate solutions. *International Journal of Modern Physics A*, 9(14):2411–2449, 1994.

[9] John R. Schrieffer and Peter A. Wolff. Relation between the Anderson and Kondo Hamiltonians. *Phys. Rev.*, 149:491–492, September 1966.

[10] Sergey Bravyi, David P. DiVincenzo, and Daniel Loss. Schrieffer-Wolff transformation for quantum many-body systems. *Annals of Physics*, 326:2793–2826, October 2011.

[11] V. P. Yurov and Alexander B. Zamolodchikov. Tuncated conformal space approach to scaling Lee-Yang model. *Int. J. Mod. Phys.*, A5:3221–3246, 1990.

[12] Dean Lee, Nathan Salwen, and Daniel Lee. The Diagonalization of quantum field Hamiltonians. *Phys. Lett.*, B503:223–235, 2001.

[13] Slava Rychkov and Lorenzo G. Vitale. Hamiltonian truncation study of the ϕ^4 theory in two dimensions. *Phys. Rev.*, D91:085011, 2015.

[14] Tibor Rakovszky, Márton Mestyán, Mario Collura, Márton Kormos, and Gábor Takács. Hamiltonian truncation approach to quenches in the Ising field theory. *Nucl. Phys.*, B911:805–845, 2016.

[15] Erwin Schrödinger. Die gegenwärtige situation in der quantenmechanik. *Naturwissenschaften*, 23:807–812, November 1935.

[16] Albert Einstein, Boris Podolsky, and Nathan Rosen. Can Quantum-Mechanical Description of Physical Reality Be Considered Complete? *Physical Review*, 47:777–780, May 1935.

[17] John S. Bell. On the Problem of Hidden Variables in Quantum Mechanics. *Rev. Mod. Phys.*, 38:447–452, July 1966.

[18] Schmidt Erhard. *Zur Theorie der linearen und nichtlinearen Integralgleichungen.* Mathematische Annalen, 1907.

[19] Ingo Peschel, Xiaoqun Wang, Matthias Kaulke, and Karen Hallberg. Density-matrix renormalization. *Lecture Notes in Physics*, 528, 1999.

[20] Mingee Chung and Ingo Peschel. Density-matrix spectra for two-dimensional quantum systems. *Phys. Rev. B*, 62:4191–4193, August 2000.

[21] Ingo Peschel. Calculation of reduced density matrices from correlation functions. *Journal of Physics A: Mathematical and General*, 36:L205, 2003.

[22] Michel Gaudin. *Nucl.Phys.*, 15, 1960.

[23] Horacio Casini and Marina Huerta. Entanglement entropy in free quantum field theory. *Journal of Physics A: Mathematical and Theoretical*, 42:504007, 2009.

[24] Rául E. Arias, David D. Blanco, Horacio Casini, and Marina Huerta. Local temperatures and local terms in modular hamiltonians. *Phys. Rev. D*, 95:065005, March 2017.

[25] Jan de Boer, Michal P. Heller, Robert C. Myers, and Yasha Neiman. Holographic de Sitter geometry from entanglement in conformal field theory. *Phys. Rev. Lett.*, 116:061602, February 2016.

[26] Frank Verstraete, Valentin Murg, and Juan I. Cirac. Matrix product states, projected entangled pair states, and variational renormalization group methods for quantum spin systems. *Advances in Physics*, 57:143–224, 2008.

[27] Frank Verstraete and Juan I. Cirac. Matrix product states represent ground states faithfully. *Phys. Rev. B*, 73:094423, March 2006.

[28] Mark Fannes, Bruno Nachtergaele, and Reinhard F Werner. Finitely correlated states on quantum spin chains. *Communications in mathematical physics*, 144(3):443–490, 1992.

[29] Ian Affleck, Tom Kennedy, Elliott H. Lieb, and Hal Tasaki. Rigorous results on valence-bond ground states in antiferromagnets. *Phys. Rev. Lett.*, 59:799–802, August 1987.

[30] Frank Verstraete and Juan I. Cirac. Renormalization algorithms for Quantum-Many Body Systems in two and higher dimensions. *eprint arXiv:cond-mat/0407066*, July 2004.

[31] Jacob Jordan, Roman Orús, Guifré Vidal, Frank Verstraete, and Juan I. Cirac. Classical simulation of infinite-size quantum lattice systems in two spatial dimensions. *Phys. Rev. Lett.*, 101:250602, December 2008.

[32] Laurens Vanderstraeten, Jutho Haegeman, Philippe Corboz, and Frank Verstraete. Gradient methods for variational optimization of projected entangled-pair states. *Phys. Rev. B*, 94(15):155123, October 2016.

[33] Philippe Corboz, Miklós Lajkó, Andreas M. Läuchli, Karlo Penc, and Frédéric Mila. Spin-orbital quantum liquid on the honeycomb lattice. *Phys. Rev. X*, 2:041013, November 2012.

[34] Frank Pollmann, Erez Berg, Ari M. Turner, and Masaki Oshikawa. Symmetry protection of topological phases in one-dimensional quantum spin systems. *Physical Review B*, 85(7):075125, 2012.

[35] Guifré Vidal. Entanglement renormalization. *Physical review letters*, 99(22):220405, 2007.

[36] Matthias Bal, Marek M. Rams, Valentin Zauner, Jutho Haegeman, and Frank Verstraete. Matrix product state renormalization. *Phys. Rev. B*, 94(20):205122, November 2016.

[37] Glen Evenbly and Guifré Vidal. Algorithms for entanglement renormalization. *Phys. Rev. B*, 79:144108, April 2009.

[38] P. Corboz, R. Orús, B. Bauer, and G. Vidal. Simulation of strongly correlated fermions in two spatial dimensions with fermionic projected entangled-pair states. *Phys. Rev. B*, 81(16):165104, April 2010.

[39] Carlos Pineda, Thomas Barthel, and Jens Eisert. Unitary circuits for strongly correlated fermions. *Phys. Rev. A*, 81:050303, May 2010.

[40] Guifré Vidal. Class of quantum many-body states that can be efficiently simulated. *Physical review letters*, 101(11):110501, 2008.

[41] Shinsei Ryu and Tadashi Takayanagi. Holographic Derivation of Entanglement Entropy from the anti de Sitter Space/Conformal Field Theory Correspondence. *Physical Review Letters*, 96(18):181602, May 2006.

[42] Brian Swingle. Entanglement renormalization and holography. *Physical Review D*, 86(6):065007, 2012.

[43] Thomas Hartman and Juan Maldacena. Time Evolution of Entanglement Entropy from Black Hole Interiors. *JHEP*, 05:014, 2013.

[44] Frank Verstraete and Juan I. Cirac. Continuous matrix product states for quantum fields. *Physical review letters*, 104(19):190405, 2010.

[45] Jutho Haegeman, Tobias J. Osborne, Henri Verschelde, and Frank Verstraete. Entanglement renormalization for quantum fields in real space. *Physical review letters*, 110(10):100402, 2013.

[46] Masahiro Nozaki, Shinsei Ryu, and Tadashi Takayanagi. Holographic geometry of entanglement renormalization in quantum field theories. *Journal of High Energy Physics*, 2012(10):1–40, 2012.

[47] Adrián Franco-Rubio and Guifré Vidal. Entanglement and correlations in the continuous multi-scale entanglement renormalization ansatz. *Journal of High Energy Physics*, 2017:129, December 2017.

[48] Qi Hu and Guifré Vidal. Spacetime symmetries and conformal data in the continuous multiscale entanglement renormalization ansatz. *Phys. Rev. Lett.*, 119:010603, July 2017.

[49] Williamson John. On the algebraic problem concerning the normal forms of linear dynamical systems. *Am. J. Math.*, 58:141–163, 1936.

[50] Maurice A. de Gosson. *Symplectic Geometry and Quantum Mechanics*. Birkhäuser Basel, 2006.

[51] Joseph J. Bisognano and Eyvind H. Wichmann. On the duality condition for quantum fields. *Journal of Mathematical Physics*, 17(3):303–321, 1976.

[52] John Cardy and Erik Tonni. Entanglement Hamiltonians in two-dimensional conformal field theory. *Journal of Statistical Mechanics: Theory and Experiment*, 2016(12):123103, 2016.